ABSTRACT

Title of Document: AN ANALYTICAL MODEL FOR DEVELOPING A CANARY DEVICE TO PREDICT SOLDER JOINT FATIGUE FAILURE UNDER THERMAL CYCLING CONDITIONS

Sony Mathew, Ph.D., 2015

Directed By: Professor Michael G. Pecht , Department of Mechanical Engineering

Solder joint fatigue failure is a prevalent failure mechanism for electronics subjected to thermal cycling loads. The failure is attributed to the thermo-mechanical stresses in the solder joints caused by differences in the coefficient of thermal expansion of the printed circuit board (PCB), electronic component, and solder. Physics of failure models incorporate the knowledge of a product's material properties, geometry, life-cycle loading and failure mechanisms to estimate the remaining useful life of the product. Engelmaier's model is widely used in the industry to estimate the fatigue life of electronics under thermal cycling conditions. However, for leadless electronic components, the Engelmaier strain metric does not consider the solder attachment area, the solder fillet thickness, and the thickness of the PCB.

In this research a first principles model to estimate the strain in the solder interconnects has been developed. This new model considers the solder attachment area, and the geometry and material properties of the solder, component and PCB respectively. The developed model is further calibrated based on the results of finite

element analysis. The calibrated model is validated by comparing its results with results of testing of test assemblies under different thermal cycling loading conditions.

Further, the calibrated first principles model is used to design reduced solder attachment areas for electronic components so that under the same loading conditions they fail faster than components with regular solder attachment areas. Such structures are called expendable Canary devices and can be used to predict the solder joint fatigue failure of regular electronic components in the actual field conditions. The feasibility of using a leadless chip resistor with reduced solder attachment area as a canary device to predict the failure of ball grid array (BGA) component has been proven based on testing data.

Further, a methodology for the developing and implementing canary device based prognostics has been developed in this research. Practical implementation issues, including estimating the number of canary devices required, determination of appropriate prognostic distance, and failure prediction schemes that may be used in the actual field conditions have also been addressed in this research.

AN ANALYTICAL MODEL FOR DEVELOPING A CANARY DEVICE TO PREDICT SOLDER JOINT FATIGUE FAILURE UNDER THERMAL CYCLING CONDITIONS

By

Sony Mathew

Dissertation submitted to the Faculty of the Graduate School of the
University of Maryland, College Park, in partial fulfillment
of the requirements for the degree of
Doctor of Philosophy
2015

Advisory Committee:

Professor Michael G. Pecht, Chair
Professor Abhijit Dasgupta
Professor Peter Sandborn
Professor Patrick McCluskey
Professor David Barbe
Senior Research Scientist Dr. Michael Osterman

© Copyright by
Sony Mathew
2015

Dedication

I dedicate my Ph. D., degree to my family including my loving mother Mrs. Annamma Mathai, who has relentlessly encouraged me to pursue higher academic goals, my father Mr. Samuel Mathai, who has lovingly supported all my efforts, my wife Mary for her love and support, and my wonderful children, Megan, my pride and joy, and Andrew, my new-born bundle of love. They have patiently endured with me in this journey.

Acknowledgements

I thank my Lord and Savior Jesus Christ for all the blessing that He has bestowed upon me. I thank God for giving me the strength to persevere, and the wisdom and knowledge to succeed in this effort.

I thank my adviser Prof. Michael Pecht for his guidance and support during the course of my degree. I thank Prof. Abjijit Dasgupta, my co-adviser, for his guidance and for the time and effort he has invested in helping me with my research. I thank Dr. Michael Osterman for his help and financial support for my degree. I thank the members of my committee including Prof. David Barbe, Prof. Peter Sandborn, and Prof. Patrick McCluskey, for their support in this effort.

I thank my sister Sonia Mathew, my brother in law Cmdr. Mathew Varghese, Caroline (niece), Jonathan (nephew) and my in-laws Mr. C.P. John and Mrs. Saramma John. Thanks to my cousin Ajay Abraham and his wife Babita Joy for their love and support. Special thanks to my friends, Saji Mathai, Oliver Mathias, Suresh Varghese, Blaze Mathew and their families for their love and support.

Thanks to the faculty, staff and my peers at CALCE including Dr. Diganta Das, Bhanu Sood, Joan Lee, Roy Arunkumar, Mark Zimmerman, Eli Dolev, Menahem Ratzker, Ranjith Kumar, Sandeep Menon, Elviz George, Swapnesh Patel, Anshul Shrivastava, Arvind Vasan, Nick Williard, Fei Chai, and Surya Kunche. Thank you to my friends and supporters in the Mechanical Engineering Department, at Mar Thoma Church of Greater Washington (especially Babu Varghese, Shibu Philipose and their families), and other social circles, for the love and encouragement during my studies.

Table of Contents

Dedication ii
Acknowledgements iii
Table of Contents iv
List of Tables vi
List of Figures vii
Chapter 1: Introduction 1
1.1 Prognostic Approaches 2
1.2 Canary Devices 4
1.3 Solder Interconnect Canary 8
1.4 Solder Joint Fatigue Failure 10
1.4.1 Engelmaier's Model 11
1.4.2 Preliminary Modification for Engelmaier's Model 13
1.5 Research Focus 14
Chapter 2: First Principles Model for Solder Strain 15
2.1 Simplification of solder interconnect geometry 16
2.2 Modeling the assembly as a system of springs 19
2.3 Comparison of strain estimates from models 24
2.4 Conclusions 25
Chapter 3: FEA and Model Calibration 26
3.1 Finite element modelling 26
3.2 Simulation results and analysis 30
3.2.1 Results for varying solder pad area 30
3.2.2 Relation between exponent and component geometry 36
3.2.3 Results for varying solder fillet thickness 37
3.3 Analytical model calibration 39
3.4 Conclusions 42
Chapter 4: Validation Testing 44
4.1 Test vehicles and testing 44
4.2 Test results and comparison 46
4.3 Conclusions 49
Chapter 5: Feasibility of Canary Design 50

5.1 PoF model estimates ... 50
5.2 Prototype testing ... 52
5.3 Results and comparison ... 55
5.4 Conclusions ... 57
Chapter 6: Methodology Development ... 59
6.1 Literature review on canary devices ... 59
6.2 Methodology for canary based prognostics ... 65
6.3 Conclusions ... 68
Chapter 7: Implementation of Canary Based Prognostics ... 69
7.1 Failure prediction scheme ... 69
7.2 Confidence in number of canary devices selected ... 74
7.2.1 Procedure ... 75
7.2.2 Calculating the probability of missing target system failure ... 77
7.2.3 Example case ... 78
7.3 Conclusions ... 83
Chapter 8: Dissertation Contributions ... 85
Chapter 9: Future Work ... 86
Appendix A: FEA – Graphs and Tables ... 87
Appendix B: External Patents on Canary Devices ... 101
Bibliography ... 104

List of Tables

Table 1: Comparison of strain range estimates 25
Table 2: Resistor types and dimensions 26
Table 3: Material properties for simulation 28
Table 4: Simulation test loads 28
Table 5: Percentage increase in strain range values 32
Table 6: Relation between component size and exponent 36
Table 7: Percentage change in strain range vs pad length and fillet thickness 37
Table 8: Percentage change in strain range values of FEA and models 39
Table 9: Strain range values for calibrated first principles model 41
Table 10: Validation test matrix 46
Table 11: Cycles to failure comparison 49
Table 12: PoF model estimates of cycles to failure for BGA 51
Table 13: PoF model estimates for cycles to failure for canaries 51
Table 14: Feasibility test matrix 54
Table 15: Cycles to failure for feasibility test vehicle 1 55
Table 16: Cycles to failure for feasibility test vehicle 2 55
Table 17: Prior experimental data 79
Table 18: Probability of missing target system failure 80
Table 19: FEA strain data for 2512 resistor 97
Table 20: FEA strain data for 1210 resistor 97
Table 21: FEA strain data for 1206 resistor 98
Table 22: FEA strain data for 0805 resistor 99
Table 23: Comparison strain estimates from FEA and Models ($\Delta T = 180^oC$) 99
Table 24: Comparison strain estimates from FEA and Models ($\Delta T = 140^oC$) 100

List of Figures

Figure 1: Prognostic distance between canary device and actual product [1] 6
Figure 2: Prognostic distance varying with load levels 6
Figure 3: Classification of canary devices [3] 7
Figure 4: Schematic representation of resistors with varying solder pad area 9
Figure 5: Schematic representation of expansion due to temperature 16
Figure 6: Simplification of solder attachment 17
Figure 7: Horizontal displacement.. 18
Figure 8: Board bending 19
Figure 9: Resistor-solder representation 20
Figure 10: Assembly representation 23
Figure 11: Resistor with regular solder pad width.. 27
Figure 12: Resistor with reduced solder pad width 27
Figure 13: Selected volume for strain range estimation 29
Figure 14: Solder fillet 30
Figure 15: $\Delta\gamma$ versus pad width for 2512 resistor (Test 1).. 33
Figure 16: $\Delta\gamma$ versus pad width for 1210 resistor (Test 1).. 33
Figure 17: $\Delta\gamma$ versus pad width for 1206 resistor (Test 1).. 34
Figure 18: $\Delta\gamma$ versus pad width for 0805 resistor (Test 1).. 34
Figure 19: Comparison of $\Delta\gamma$ vs pad width for 2512 Resistor.................................. 35
Figure 20: Comparison of $\Delta\gamma$ vs pad width for 1210 Resistor.................................. 35
Figure 21: Exponent vs component geometry 36
Figure 22: Strain range vs solder thickness for 2512 resistor 38
Figure 23: Strain range vs solder thickness for 1210 resistor 38
Figure 24: Comparison of strain range estimates for 2512 resistor 40
Figure 25: Comparison of strain range estimates for 1210 resistor 40
Figure 26: Validation test vehicle 1 45
Figure 27: Validation test vehicle 2 45
Figure 28: Validation test data (0^oC to 100^oC with 120 minute dwell) 47

Figure 29: Validation test data (0°C to 100°C with 10 minute dwell) 47
Figure 30: Validation test data (-55°C to 125°C with 15 minute dwell) 48
Figure 31: Feasibility test vehicle 1 53
Figure 32: Feasibility test vehicle 2 54
Figure 33: Results for feasibility test vehicle 1 56
Figure 34: Results for feasibility test vehicle 2 57
Figure 35: Methodology for canary-based prognostics 65
Figure 36: Multiple prognostic distances 70
Figure 37: Effect of changing η_C 75
Figure 38: Effect of changing β_C 75
Figure 39: Twenty Canaries vs target system (Run 1) 81
Figure 40: Five Canaries vs target system (Run 4) 82
Figure 41: Probability of Probability of Miss 82
Figure 42: Number of Canaries Vs Probability of Miss 83
Figure 43: Δγ versus pad width for 2512 resistor (Test 2) 87
Figure 44: Δγ versus pad width for 2512 resistor (Test 3) 87
Figure 45: Δγ versus pad width for 2512 resistor (Test 4) 88
Figure 46: Δγ versus pad width for 2512 resistor (Test 5) 88
Figure 47: Δγ versus pad width for 2512 resistor (Test 6) 89
Figure 48: Δγ versus pad width for 1210 resistor (Test 2) 89
Figure 49: Δγ versus pad width for 1210 resistor (Test 3) 90
Figure 50: Δγ versus pad width for 1210 resistor (Test 5) 90
Figure 51: Δγ versus pad width for 1210 resistor (Test 4) 91
Figure 52: Δγ versus pad width for 1210 resistor (Test 6) 91
Figure 53: Δγ versus pad width for 1206 resistor (Test 2) 92
Figure 54: Δγ versus pad width for 1206 resistor (Test 3) 92
Figure 55: Δγ versus pad width for 0805 resistor (Test 2) 93
Figure 56: Δγ versus pad width for 0805 resistor (Test 3) 93
Figure 57: Comparison of strain range with calibrated models for 2512 resistor 94
Figure 58: Strain comparisons for 2512 resistor 94
Figure 59: Comparison of strain range with calibrated models for 1206 resistor 95

Figure 60: Strain comparisons for 1210 resistor 95
Figure 61: Strain range vs pad length under fillet for 2512 resistor 96
Figure 62: Strain range vs pad length under fillet for 1210 resistor 96

Chapter 1: Introduction

The reliability of electronic products under usage conditions is a key issue for many companies and their customers. The reliability issue becomes vital in the case of electronics that perform critical functions, which if not performed could lead to failure of the product, lead to huge financial losses or pose life threatening consequences to the end user. While researchers and engineers have made great strides in building in safety and reliability features into the product in the design phase itself, there are many uncertainties associated with the product in actual usage conditions. Having scheduled maintenance for the product creates issues for the availability of the product and also increases the chances of human induced faults in the product. Current reliability techniques are not suitable for assessing the reliability of the product under fielded conditions. Prognostics is the approach that permits the reliability of a system to be evaluated and predicted in its actual application conditions [1].

Prognostics and health management (PHM) is an enabling discipline consisting of technologies and methods to assess the remaining useful life (RUL) of a product in its actual life cycle conditions to determine the advent of failure and mitigate system risk [1]. In recent years, prognostics and health management (PHM) has emerged as a key enabling technology to provide early warning of failure; forecast maintenance as needed; reduce maintenance cycles; assess the potential for life extensions; and improve future designs and qualification methods. There are three different approaches for conducting prognostics for a product: (1) the physics-of-failure (PoF)

based approach, which includes a) the monitoring of life cycle environment loading and modeling of stress and damage [2] and b) the use of canary devices to provide advance warning of failure [3]; (2) the data-driven approach, which involves the use of machine learning techniques to analyze current and historical data to estimate remaining useful life; and (3) the fusion approach, which combines the PoF and data-driven techniques to provide an accurate estimate of remaining useful life.

1.1 Prognostic Approaches

Physics of failure is an approach that utilizes knowledge of a product's life-cycle loading and failure mechanisms to assess product reliability. PoF methodology is based on the identification of potential failure mechanisms and failure sites for a device, product, or system. A failure mechanism is described by the relationship between the stresses and variability at potential failure sites. The methodology proactively assesses reliability by establishing a scientific basis for evaluating new materials, structures, and technologies. PoF-based prognosis permits the assessment and prediction of system reliability under its actual application conditions. It integrates sensor data with models that enable in-situ identification of the deviation or degradation of a product from its expected normal operating condition (i.e., the system's "health") and the prediction of the future state of reliability. Based on the collected operational and environmental data, the health status of the products can be assessed. The amount of damage can then be calculated from the PoF models to obtain the remaining life.

A data-driven approach for prognostics is preferred when models are not available or when monitoring loads and environmental conditions are not possible. This approach is primarily based on signal processing, pattern recognition, and state estimation. The prognosis is based on state awareness of the product based on the monitored performance parameters and forecasting total degradation and time-to failure based on the forecasted degradation. This methodology starts with functional evaluation of the system under consideration. After a feasibility study, data acquisition techniques are investigated to gather system performance information in real time. A number of features are looked at to represent system behavior based on sensor information. During this process, data cleaning and data normalization are performed on raw data to reduce the associated noise and remove the scaling effects.

Features can be extracted directly from routinely monitored product operating data or performance data. Machine learning techniques can be used to process the data features to establish the healthy state of the given product. These approaches are based on statistical and learning techniques from the theory of pattern recognition. This data is also used to identify performance deviation due to the presence of a fault. To be effective, it is necessary that the training data for the machine learning algorithms span the universe of system faults and operational conditions. A threshold limit on the data features are set to define the start of the performance degradation that will lead to operational failure. Trending of features to a defined failure criteria provides fault or damage progression over time. This information is used to estimate the remaining useful life of the product.

The fusion approach combines the benefits of the PoF and data-driven techniques to provide an estimate of remaining useful life. The fusion approach utilizes data-driven techniques for anomaly detection and classification to detect early degradation of a product. Understanding the physics of failure helps identify the parameters that are causing the anomaly. The faulty parameters are isolated by incorporating the results from the anomaly detection and the PoF information. Further, knowing the physics of failure helps narrow in on the possible root cause of product failure. After the critical parameters are isolated, the PoF models that use the isolated parameters as the primary inputs are selected. The PoF models are used independently to calculate the RUL of the product based on the environmental and parameter data along with information such as the material properties and product specifications. Knowledge of the product's physics of failure can be used to extract the failure thresholds for the measured product parameters, the failure modes, stages of degradation, and labels of healthy and unhealthy conditions.

Studies have been conducted on a variety of products using the PoF and data-driven approaches to prognostics. However, one prognostic approach that has not gained mainstream implementation is the use of canary devices to predict the failure of a given product. This dissertation presents a methodology to develop and implement a canary device to predict failure in electronic products.

1.2 Canary Devices

The concept of using a canary device to predict the failure of a system is derived from the use of canary bird in a coal mine to detect poisonous gases. Since canary

birds are more sensitive to hazardous gases than humans, they can experience the effects of these hazardous gases even when the quantity of the gas is low. The death or sickening of canary birds serves as an early warning to miners to take corrective action and exit the mine.

A canary for prognostics of systems is defined as, ***a device integrated with the target system, which senses a predefined system parameter as a function of the loading condition, and provides real time information of the instantaneous health of the system***. The canary device provides early warning of system degradation. The amount of degradation of the target system is a function of the sensitivity of the canary device to the environmental and operating loading condition. A canary may be created using a structure that is more sensitive to life cycle conditions than the target system [3]. Under the same environmental and operational loading conditions, the canary device fails faster than the target system.

Generally, the canary device is designed to fail by the same failure mechanism as the target system. But if there exists a clear mapping between the failures of the canary devices to the failure of the target system, then it does not matter if the mechanisms match. The canary device must also fail prior to the target system. The difference between the time to failure of the canary device and the actual product is referred to as prognostic distance. Figure 1 shows the concept of 'prognostic distance'. The prognostic distance will vary based on the failure probability density distributions for target systems and the corresponding canary devices. In many cases, many similar canary devices can be made in such a way that they each fail at different

times before the target system. Figure 2 illustrates the concept of prognostic distance as an outcome of the acceleration condition applied to the canary device.

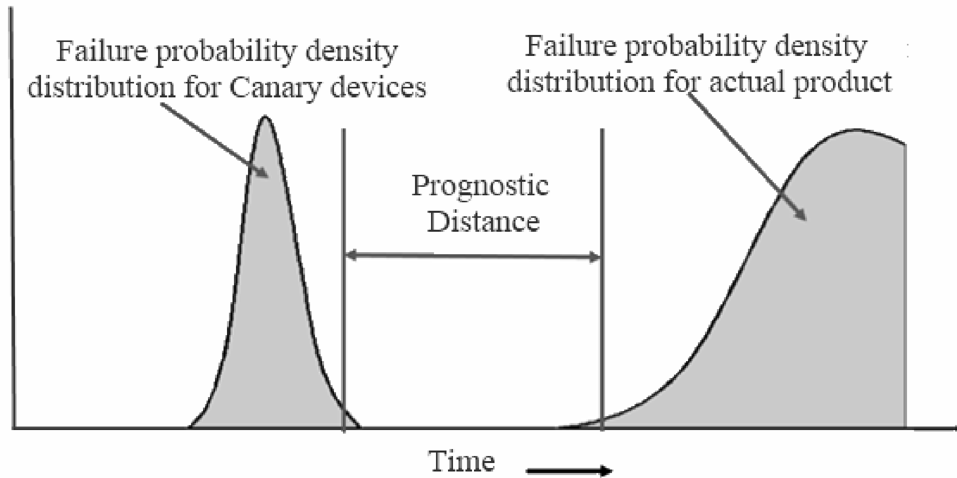

Figure 1: Prognostic distance between canary device and actual product [1]

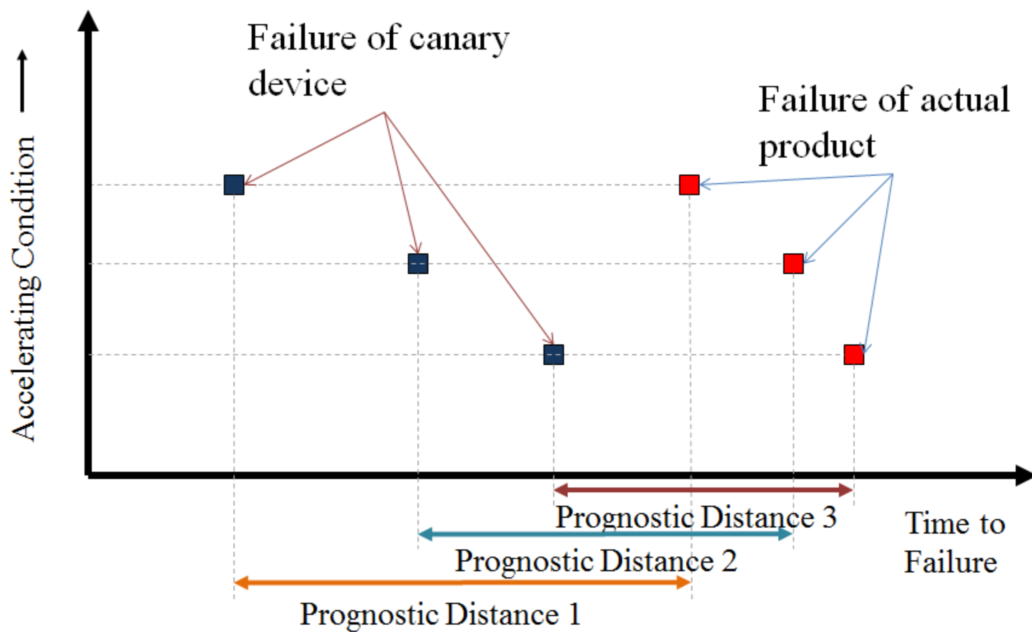

z

Figure 2: Prognostic distance varying with load levels

Canary devices are classified as 1) expendable canaries, 2) sensory canaries, and 3) conjugate-stress canaries [3]. Expendable canary devices are designed such that once a device fails it is no longer operational. Sensory canary devices are designed to

be more sensitive to loading conditions and degrade at a higher rate at lower load levels than the host system. They are able to sense the signs of degradation and impending failure. By collecting and analyzing the sensory input, early warnings of failure can be achieved. These canaries can be used to detect non-traditional signatures of system degradation. Conjugate-stress canaries are based on simultaneous identification of conjugate-stress pairs. Figure 3 shows the classification and sub-classification of canary devices.

Expendable canaries are based on controlled acceleration of failure precursor signatures using error-seeded, sacrificial, nonfunctional elements [3]. Error-seeding techniques may be used individually or synergistically to enhance the degradation rates in canaries. These include geometry error-seeding, material error-seeding, and load error-seeding. Based on their dominant failure mechanisms, expendable canaries can be further categorized into overstress canaries and wear-out canaries. Overstress canaries come into play when the loaded stress exceeds its strength. Wear-out canaries fail due to the accumulation of damage under life cycle operating conditions.

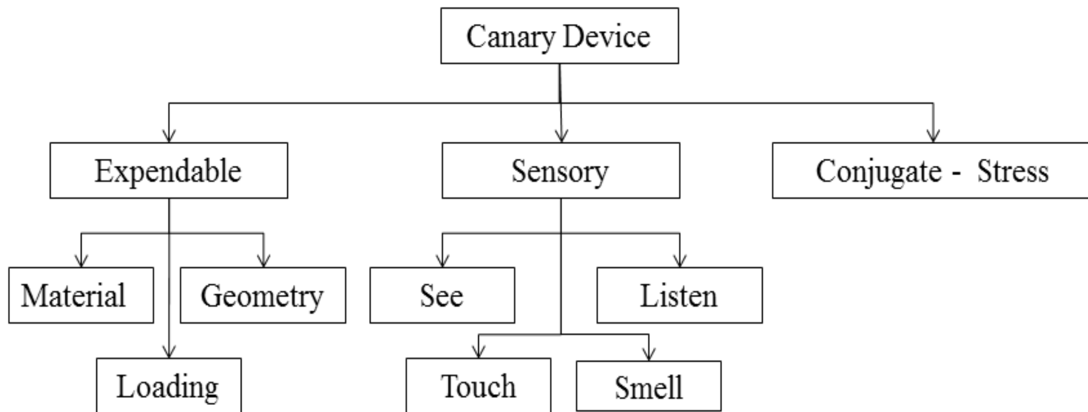

Figure 3: Classification of canary devices [3]

1.3 Solder Interconnect Canary

Solder is used to permanently connect electronic components to the printed circuit board. In operational conditions solder joint fatigue failure is a common failure mechanism for electronic products. The failure mode is an open circuit due to solder cracking resulting in a complete fracture of the joint. In a study conducted to identify the failure site of 170 field returns of various electronic products from over 70 different companies it was seen that 13 percent of the failures occurred in the solder joint interconnects (CALCE internal report).

Chauhan et al., [4] conducted studies on the time to failure of surface mount leadless components with reduced solder attachment areas. Two sets of 2512 type surface mount resistors with the same dimension and rating were tested in that study. The resistors selected had a length of 0.25 inch and width of 0.125 inch and a thickness of 0.022 inch. The terminals of each resistor were reflow soldered onto copper pads that were etched on the printed circuit board (PCB). One set of resistors had regular/ standard solder copper pad dimensions for 2512 resistors (0.125 inch width). The second set of resistors had copper pad width that was reduced to 20 percent of the regular width i.e. 0.025 inch. The solder in both cases wicked all the way up to the top of the resistor. Figure 4 shows the schematic of the surface mount resistors with differing copper pad areas. The test vehicle, an FR4 board with forty 2512 resistors (16 with standard attachment and 24 with reduced attachment), was subjected to temperature cycling condition of -55°C to 125°C with 15 minute dwell at extremes. The ramp rate was approximately 10°C/minute. In this test it was observed that the resistors with reduced copper pad area failed significantly before the resistors

with regular copper pad area. The resistors with reduced pad area can be used as canaries for the resistors with full pad area.

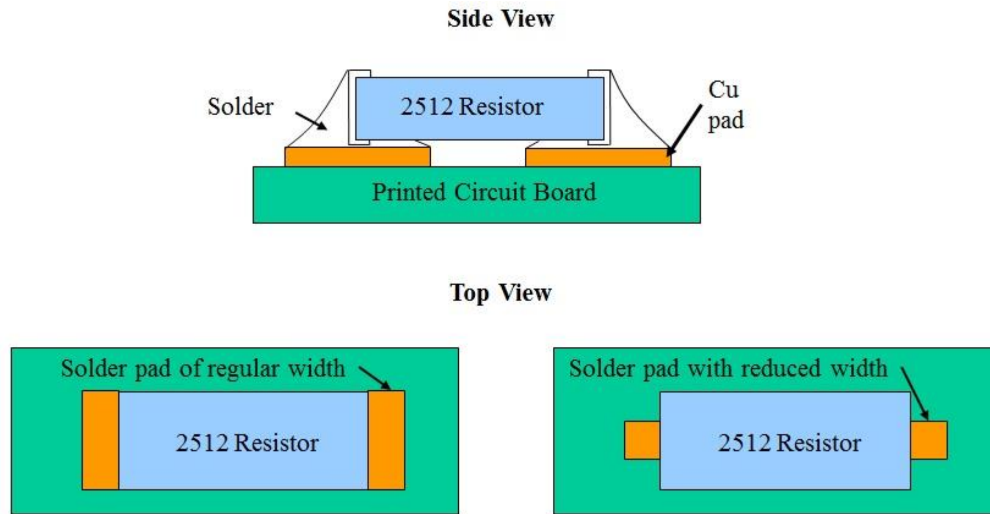

Figure 4: Schematic representation of resistors with varying solder pad area

Chauhan et al., [5] also presented an approach for monitoring ball grid array (BGA) solder interconnects under temperature cycling conditions. In the effort the outer solder ball acts as the canary for the inner solder balls of the BGA. The test sample is a 128 IO BGA subjected to -55°C to 125°C thermal cycling loads. The sizes of the solder balls are same. The prognostic distance is calculated using a PoF model and then validated with testing. Testing showed that the outermost solder interconnect will fail before the inner interconnects. The prognostic distance varies with the distance of the solder ball from neutral position on the BGA. While this approach is feasible in practice it is difficult to implement this solder interconnect canary approach.

An idea proposed in this dissertation is to use a canary device formed by using reduced solder interconnect for SMT resistors to predict the solder joint fatigue failure of ball grid array (BGA) packages. The feasibility of using such a canary for

BGA solder fatigue life prediction is presented in this dissertation. To design the canary with reduced solder attachment area a physics of failure (PoF) model is required so that various combinations of solder pad geometry can be evaluated with respect to the time to failure due to such reduction in solder attachment area.

1.4 Solder Joint Fatigue Failure

Solder joint fatigue is a dominant failure mechanism that plagues electronic systems subjected to thermal cycling loads. The failure mode of solder joint fatigue is an open circuit due to solder cracking, resulting in complete fracture of the joint. Solder joint fatigue failure under thermal cycling conditions can be attributed to the thermo-mechanical stresses in the solder joints caused by differences in the coefficient of thermal expansion (CTE) of the PCB, component, and solder. The cyclic strain induced in the solder due to the CTE mismatch will, over a period of time, cause solder joint fatigue failure. Many researchers have put forth models to predict the cycles to failure under thermal cycling load [6]. The models can be grouped into five major classes based on the fundamental mechanism that induces damage [6]. The five classes are 1) stress-based, 2) plastic strain-based, 3) creep strain-based, 4) energy-based, and 5) damage accumulation-based.

Under thermal cycling loading conditions, the cyclic strains in the solder joint due to CTE mismatch contribute to the degradation of the solder joint. The type of strain induced in the solder can be divided into elastic and plastic strain (time-independent effects) and creep strain (time-dependent effects). The energy-based fatigue models use the total stress-strain hysteresis energy in the solder to estimate the damage. The

damage accumulation-based models use the damage due to crack propagation to estimate the time to failure of the solder. The energy-based and damage accumulation-based models use finite element analysis for model and material parameters.

1.4.1 Engelmaier's Model

A generalized fatigue damage law was first proposed by Morrow on the basis of cumulative visco-plastic strain energy density. Thereafter the Coffin–Manson plastic strain-fatigue life relationship was derived wherein the total number of cycles to failure N_f, is dependent on the plastic strain amplitude $\Delta\varepsilon_f$, the fatigue ductility coefficient, $\acute{\varepsilon}_f$ and the fatigue ductility exponent, *c*. The Coffin-Manson equation [7] is shown in equation 1.

$$\frac{\Delta\varepsilon_f}{2} = \acute{\varepsilon}_f \, (2\,N_f)^c \qquad (1)$$

In the 1980s, Werner Engelmaier developed a model, based upon the Coffin-Manson model, to analytically calculate the fatigue life of a leadless surface mount component subjected to thermal cycling loads. The model developed by Engelmaier addressed such parameters as the temperature cycling frequency, CTEs of the substrate and package, temperatures of the package and substrate, and mean cyclic temperature. The Engelmaier model has been widely adopted in the industry and is still used to conduct a rapid analytical approximation of the time to fatigue failure of components under thermal cycling loads. Engelmaier developed a model for leadless ceramic chips [8]. Equation 1 shows the Engelmaier's equation for leadless components.

$$N_f = \frac{1}{2}\left(\frac{\Delta\gamma}{2\varepsilon_f}\right)^{\left(\frac{1}{c}\right)} \tag{2}$$

Where N_f = mean cycles to failure (N_f (50%)), $\Delta\gamma$ = cyclic plastic shear strain range, ε_f = fatigue ductility coefficient and c = fatigue ductility exponent.

$$c = c_0 + c_1 T_{sj} + c_2 \ln\left(1 + \frac{360}{t_d}\right) \tag{3}$$

Where c_0, c_1 and c_2 are material constants, T_{sj} = mean cyclic temperature and t_d is the dwell time in minutes at the maximum temperature.

$$\Delta\gamma = \frac{Fd(\Delta\alpha\Delta T)*10^{-6}}{2h} \tag{4}$$

Where F is a non-ideal factor ($0.7 < F < 1.2$ for chip components with fillets), d = longest distance between the solder joints and h = solder joint height. Here $\Delta\alpha = (\alpha_s - \alpha_c)$, α_s = CTE of substrate, α_c = CTE of component, $\Delta T = T_{max} - T_{min}$, T_{max} is the maximum temperature and T_{min} is the minimum temperature experienced by the component.

The shortcoming of this model is that it does not consider the solder attachment area for the leadless component. Another issue if that Engelmaier did not specify how the height of the solder was considered. In developing this model Engelmaier considered the solder joint to be cylindrical in shape and only below the component. He did not consider the height of the solder that wicks up the side of the component during the reflow process.

Later Engelmaier developed a model for leaded components [9], wherein he has a term for the area of the solder pad in the equation for the cyclic strain range. Equation 5 shows Engelmaier's cyclic strain range equation for leaded components.

$$\Delta\gamma = \frac{F\,K_d(L_d\Delta\alpha\Delta T)^2 * 10^{-6}}{(200psi)A\,h} \tag{5}$$

Where K_d = diagonal flexural stiffness, and L_d= maximum distance between component center and the most remote component solder joint. Here Engelmaier defined the height of solder (h) as ½ the solder paste stencil height. There is no explanation as to why the ($L_d\Delta\alpha\Delta T$) term is raised to the power 2 and why the 200 psi value was selected.

1.4.2 Preliminary Modification for Engelmaier's Model

Chauhan et al., [4], based on the tests results, suggested a preliminary modifying the Engelmaier's strain metric for leadless packages. It was suggested that the Engelmaier's strain metric be multiplied by the ratio of the regular solder pad area to the reduced solder pad area. Equation 6 shows the modified strain metric.

$$\Delta\gamma = \left(\frac{F\,L_d(\Delta\alpha\Delta T) * 10^{-6}}{h}\right) * \left(\frac{A_f}{A_r}\right) \tag{6}$$

The researchers claim that including A_f / A_r causes the area effect to be the same as the one Engelmaier defined for leaded parts. In the Engelmaier's leaded model though, Engelmaier has the term $(L_d\Delta\alpha\Delta T)^2$ and the Area (A) is in the denominator. For calculation the height of the solder (h) used in the above equation is the diagonal height of solder fillet, whereas Engelmaier used the standoff height since his samples used cylindrical columnar solder geometry for his samples.

Further in the preliminary model the non-deal factor (F) is assumed as 1, whereas Engelmaier advocated the value of F as a range between 0.7 to 1.2. Overall the issue

with the preliminary model is that it is arbitrary and the results of such estimation are too conservative.

1.5 Research Focus

The existing most widely used analytical strain based fatigue model for leadless package (Engelmaier's Model) does not consider the solder pad area. The preliminary modification of the Engelmaier's empirical strain metric proposed by Chauhan et al., is too conservative and arbitrary. The results of the study conducted by Chauhan et al., show that reducing the solder pad area causes the component to fail faster than the components with regular solder pad area. This serves as the motivation for developing a first principles model that takes into consideration the solder pad area to calculate the fatigue failure of solder interconnects of leadless components.

Using a physics of failure (PoF) model that takes into consideration the solder attachment area, various combinations of solder pad geometry can be evaluated with respect to the time to failure due to such reduction in solder attachment area. Such a model will help design an expendable canary device with reduced solder attachment to predict solder joint fatigue failure off Ball Grid Array (BGA) packages.

The research focus of this dissertation is: 1) to develop an analytical model for solder joint fatigue failure in leadless surface mount components, which accounts for solder attachment area, 2) to demonstrate the feasibility of using an external expendable canary device with reduced solder attachment to predict solder joint fatigue failure of Ball Grid Array (BGA) packages.

Chapter 2: First Principles Model for Solder Strain

Consider a leadless surface mount technology (SMT) resistor attached to a printed circuit board (PCB) using solder. For this study the resistor-solder-PCB assembly is subjected to thermal cycling loading only. Starting from room temperature, when the temperature increases, theoretically the resistor material, solder and the PCB expand. As the temperature increases and the material expands t along the X and Y axis and also along the Z axis, Due to the mismatch in the CTE the PCB and solder material expand more than the resistor material. At the bottom interface of the solder and the resistor there is a shear force in the X and Y axis due to the mismatched expansion. There is a shear force between the solder and the end termination of the solder along the Z axis. The solder fillet on the side of the resistor will also expand to the right. The PCB expansion to the right along with the expansion of the solder fillet will cause the resistor to bend in a concave manner. The resistor material will offer a resistance to this bending motion. Figure 5 shows the expansion of the PCB at high temperatures and the effects on the SMT resistor assembly.

At low temperatures the material contracts and since there is a mismatch in the contraction rates of the PCB, solder and resistor material there is a shear force generated in the X and Y axis at the bottom interface between the resistor and solder. The PCB contraction to the left along with the contraction of the solder fillet will cause the resistor to bend in a convex manner. The resistor material will offer a resistance to this bending motion.

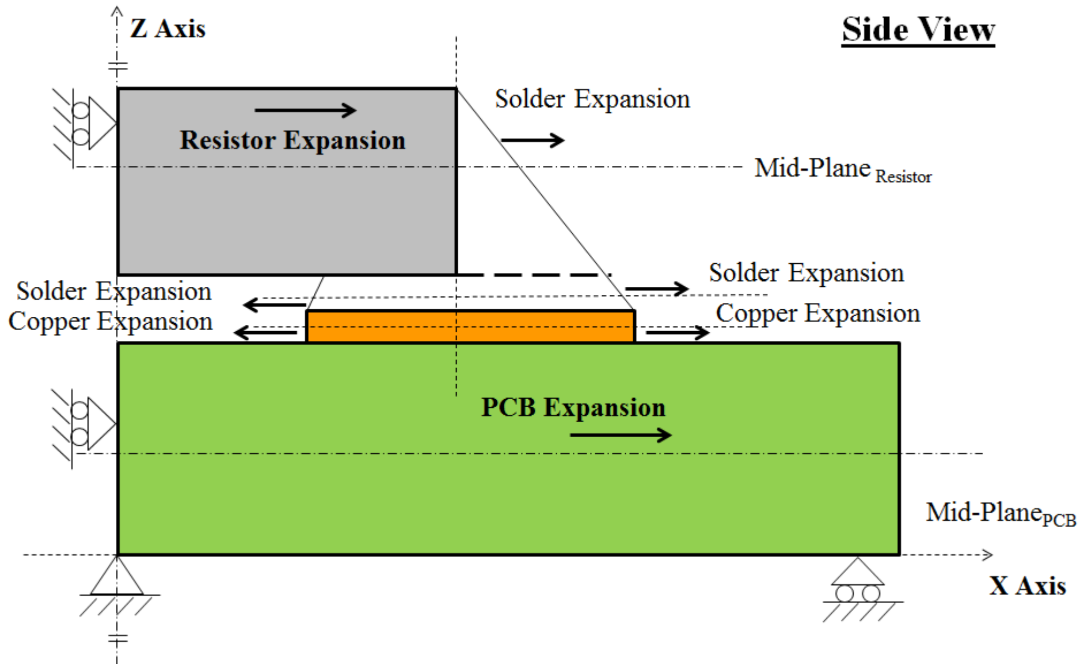

Figure 5: Schematic representation of expansion due to temperature

As the area of contact between the solder and the bottom surface of the resistor decreases the shear stress generated in that interface will increase. Also as the solder fillet thickness reduces, the resistance to expansion of the resistor reduces, thereby increasing the shear stress at the solder-resistor interface. Since the resistor package is subjected to bending moment, the size of the resistor package needs to be considered in fatigue calculations. Besides the CTE mismatch, the copper pad area, the thickness of the solder joint fillet, and the bending resistance of the component (indirectly the size if the package) will also affect the fatigue life of a surface mount leadless package.

2.1 Simplification of solder interconnect geometry

Consider a half cross-section of a SMT resistor with its solder attachment. It is assumed that the solder wicks all the way to the top of the end termination of the

resistor and has a triangular cross-section. For simplification the solder attachment of the resistor is considered to be composed of two separate parts: part 1 – is the solder under the resistor and part 2 – is the solder fillet. Figure 6 shows the simplification of the solder attachment. The solder fillet is simplified as a lead with a rectangular cross-section. The horizontal length of the lead 'l_f' is taken as 1/2 the length of the fillet base 'b'. The vertical length of the fillet 'h_f' is the sum of the solder standoff height 'h_s' and half of the component height 'h_c'. The axial force on the resistor and the PCB is assumed to be the same as with a bimetallic strip [10].

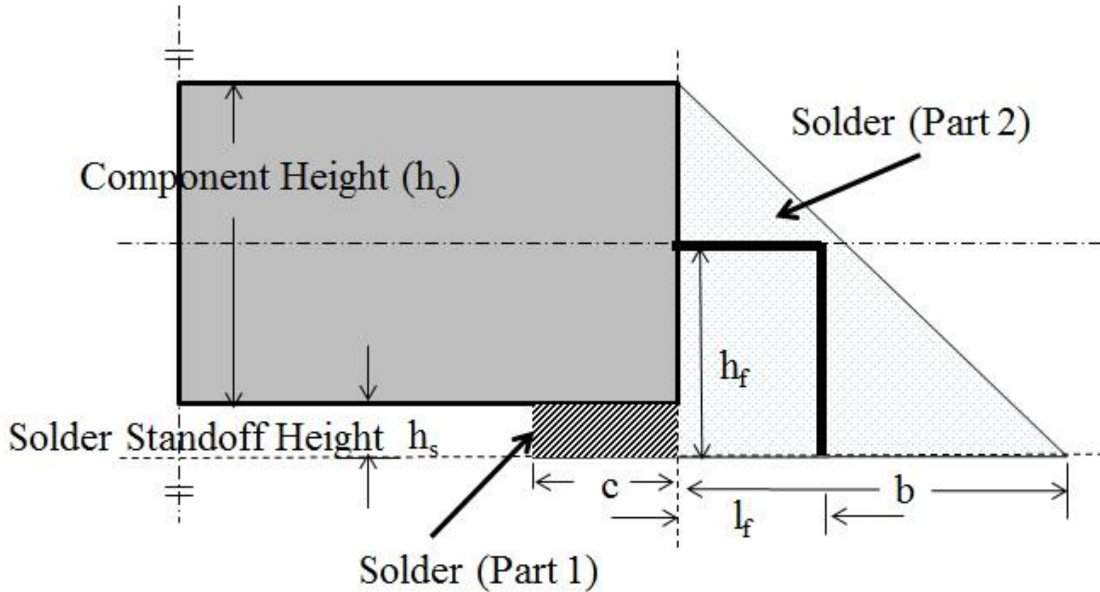

Figure 6: Simplification of solder attachment

Under temperature cycling load the resistor-solder-PCB assembly is subjected to two types of physical changes. The first physical change is the simple expansion/contraction of the material due to high/low temperatures respectively. Figure 7 shows the expansion of a half cross-section of a resistor-solder-PCB assembly under high temperature. Note that the standoff height is deliberately exaggerated to explain displacement. The standoff height between the resistor and

PCB is deliberately exaggerated to explain displacement. The resistor expands horizontally from E-A to E'-A'. The PCB expands from F to F'. The solder part 1 is attached to the resistor and the PCB. The interface between the resistor and solder part 1, moves from B - A to B' - A'. The interface between solder part 1 and PCB moves from C - D to C'- D'. Because of the expansion of the resistor body from E-A to E'- A', the solder part 2 (lead) has a new starting point of H'- G' and expands to the new position H"- G". At equilibrium the sum of the displacements of the component (δ_C), solder part 1 (δ_{S_1}), and solder part 2 (δ_{S_2}) should be equal to the displacement of the PCB (δ_P).

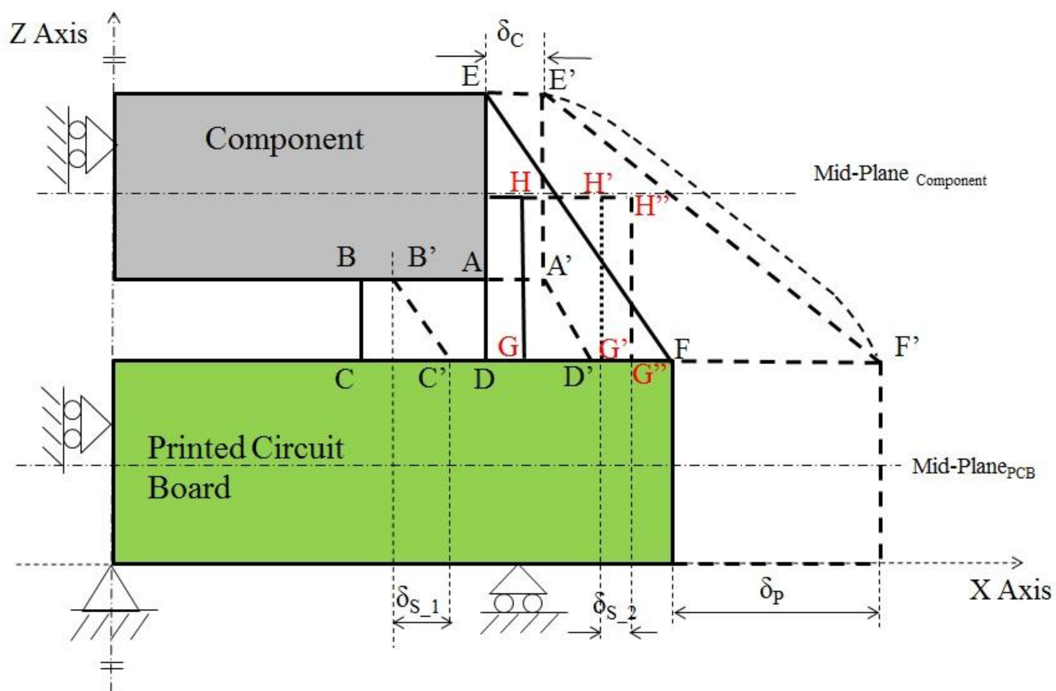

Figure 7: Horizontal displacement

Due to the CTE mismatches the solder, resistor and PCB expand at different rates. The CTE of the PCB is 14 ppm/^{o}C while the CTE of the resistor is 4 – 5 ppm/^{o}C which means that the PCB will expand more than the resistor thereby causing the board to bend. This bending also affects the displacements of the resistor and solder.

Figure 8 shows the effect of the bending on the solder part 2 (lead). Note that the 'Lead' section deliberately exaggerated. Equation 7 shows the displacement of the simplified fillet is a function of the initial expansion (x_0), the angular rotation (θ) and the moment arm (R).

$$\delta_{fillet} = x_0 + R\theta \qquad [11] \qquad (7)$$

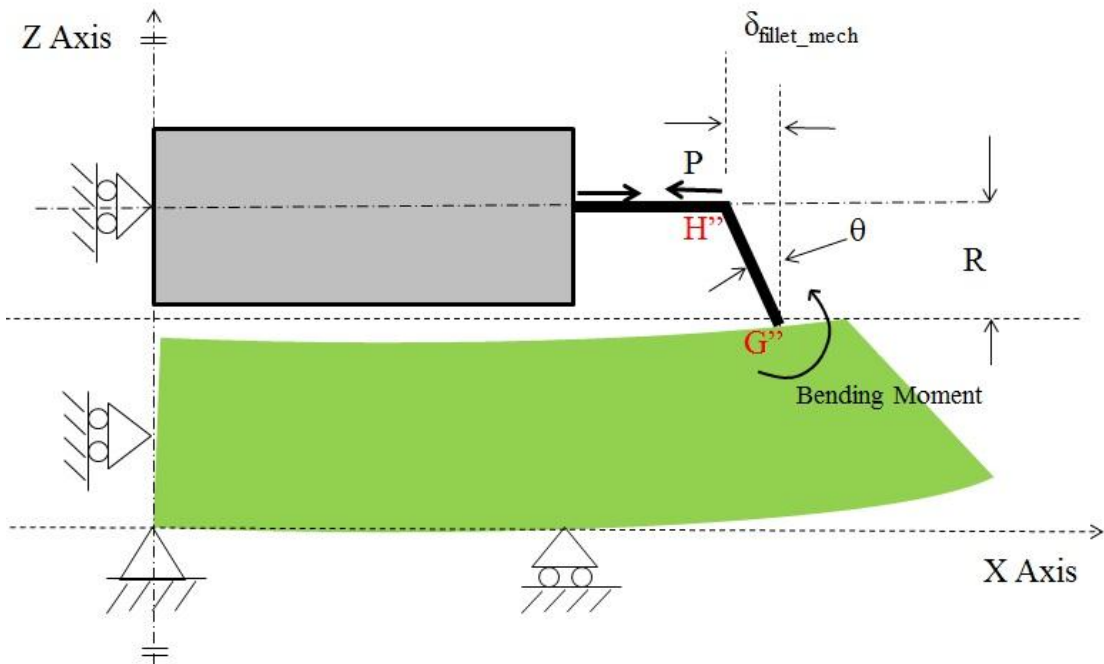

Figure 8: Board bending

2.2 Modeling the assembly as a system of springs

The resistor-solder-PCB assembly is modeled as a spring mass system to calculate the axial force on the resistor- solder part 1 interface. The shear stress and by association the shear strain at this interface is a function of the axial force and the solder area. The shear strain model thus developed is based on basic material properties and geometry. Consider the resistor, solder part 1 and solder part 2

grouping. Figure 9 shows their representation as a spring mass system. Here k_1= stiffness of solder under the resistor, k_2= stiffness of solder fillet, and k_3= stiffness of resistor. P_{RS} = Force on the resistor and solder.

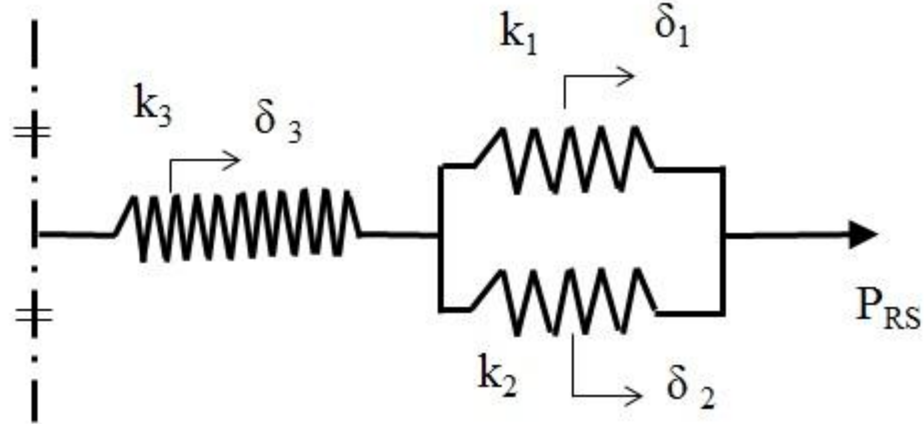

Figure 9: Resistor-solder representation

The total displacement is give as $\delta = \delta_{mechanical} + \delta_{thermal}$.

$$\delta_{RS} = -\frac{P_{RS}}{k_{RS}} + x_R + x_S \tag{8}$$

Where δ_{RS} is the displacement of the resistor - solder group, k_{RS} is the total stiffness of the resistor-solder group, x_R is the thermal expansion of the resistor and x_S is the thermal expansion of the solder part 1and part 2. x_{RS} the total thermal expansion of the resistor solder group = $x_R + x_S$.

$$x_{RS} = \alpha_R l_R \Delta T + \alpha_s l_f \Delta T \tag{9}$$

Where α_R = coefficient of thermal expansion of resistor, α_S = coefficient of thermal expansion of solder, l_R = length of resistor, l_f = length of solder fillet and ΔT = the temperature difference =T_{max} + T_{min}. The effective stiffness of the two solder parts is given by:

$$k_{eff_{solder}} = k_1 + k_2 \quad (10)$$

$$\therefore k_{RS} = \frac{1}{\left(\frac{1}{k_3} + \frac{1}{k_{eff_solder}}\right)} \quad (11)$$

$$\therefore k_{RS} = \frac{k_3(k_1 + k_2)}{k_1 + k_2 + k_3} \quad (12)$$

The stiffness of the solder under the resistor (solder part 1) is given by:

$$k_1 = \frac{A_S G_S}{h_s} \quad (13)$$

Where A_s = area of interface between solder and bottom of component, G_s= Shear modulus of solder and h_s = solder standoff height. The initial displacement of the solder fillet (solder part 2) is given as

$$x_o = \frac{P h_f^3}{E_S I_f}\left(\frac{1}{3} - \frac{h_f}{4h_f + l_f}\right) \quad [11] \quad (14)$$

Where h_f = 'simplified fillet' height, l_f = 'simplified fillet' length, E_s = Elastic modulus of solder, and I_f = Second moment of Inertia of solder fillet. The bending moment at point H" is given by

$$M_{H"} = \frac{2P h_f^2}{4h_f + l_f} \quad (15)$$

$$M_{G"} = P h_f - M_{H"} \quad (16)$$

$$\therefore M_{G'} = P h_f \left(1 - \frac{h_f}{4h_f + l_f}\right) \quad (17)$$

Substituting the values in equation 4 the stiffness of the solder fillet (solder part2) can be calculated.

$$\delta_{fillet_mech} = \frac{Ph_f^3}{E_s I_f}\left(\frac{1}{3} - \frac{h_f}{4h_f + l_f}\right) + \frac{RM_{G''} l_{PCB}}{2E_{PCB} I_{PCB}} \qquad [11] \qquad (18)$$

Where E_{PCB} = Elastic modulus of PCB, I_{PCB} = Second moment of Inertia of PCB and l_{PCB} =length of the PCB.

$$\delta_{fillet_mech} = \frac{P_{RS}}{k_2} \qquad (19)$$

The moment arm R is considered from the mid-plane of the PCB, so $R = h_f + t_{PCB}/2$. t_{PCB} is the thickness of the PCB. By expanding equation 19 the stiffness of the solder fillet (solder part2) can be presented as

$$k_2 = \frac{1}{\left(\frac{h_f^3}{E_s I_f}\left(\frac{1}{3} - \frac{h_f}{4h_f + l_f}\right) + \frac{h_f l_{PCB}\left(1 - \frac{h_f}{4h_f + l_f}\right) * (h_f + t_{PCB}/2)}{2E_{PCB} I_{PCB}}\right)} \qquad (20)$$

The stiffness of the resistor is given by

$$k_3 = \frac{A_R E_R}{l_R} \qquad (21)$$

Where A_R = cross-sectional area of resistor, E_R= Elastic modulus of resistor and l_R = length of resistor.

The whole resistor-solder-PCB assembly can be further represented as a modified spring system shown in Figure 10. Here the resistor-solder group is considered as parallel to the PCB. Here k_4= stiffness of PCB, P = Force on the assembly.

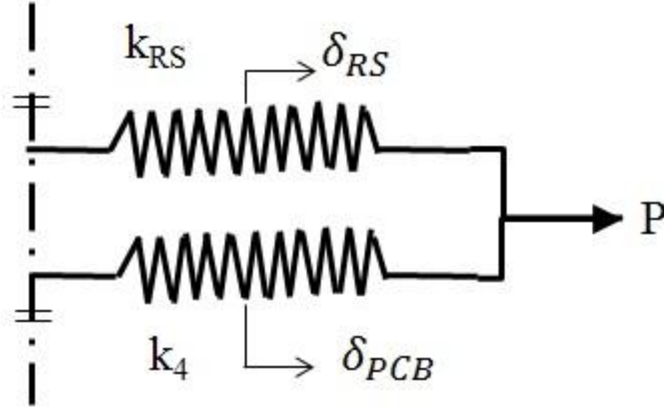

Figure 10: Assembly representation

$$\delta_{PCB} = \frac{P_{PCB}}{k_{PCB}} + x_{PCB} \tag{22}$$

Where δ_{PCB} is the displacement of the resistor-solder group, $k_{PCB} = k_4$ and $x_{PCB} = x_4$. The stiffness of the PCB is given by

$$k_{PCB} = \frac{A_{PCB}E_{PCB}}{l_{PCB}} \tag{23}$$

$$x_{PCB} = \alpha_{PCB} l_{PCB} \Delta T \tag{24}$$

Where x_{PCB} = thermal expansion of PCB, α_{PCB} = coefficient of thermal expansion of PCB, l_{PCB} = length of PCB, and ΔT = the temperature difference.

The expansion of the resistor-solder group should be equal to the expansion of the PCB i.e. $\delta_{RS} = \delta_{PCB}$

$$-\frac{P_{RS}}{K_{RS}} + x_{RS} = \frac{P_{PCB}}{K_{PCB}} + x_{PCB} \tag{25}$$

Since $P_{RS} = P_{PCB} = P$ the above equation can be represented as

$$P = \frac{(x_{PCB} - x_{RS})}{\left(\frac{1}{K_{PCB}} + \frac{1}{K_{RS}}\right)} \tag{26}$$

Substituting the values of x_{PCB}, x_{RS}, k_{PCB} and k_{RS} in equation 26 we get

$$P = \frac{\Delta T[\alpha_p L_p - (\alpha_c L_c + \alpha_s L_f)]}{\left(\frac{k_3(k_1+k_2)+k_4(k_1+k_2+k_3)}{k_3 k_4 (k_1+k_2)}\right)} \quad (27)$$

Knowing the force P, the shear stress (τ) and shear strain range ($\Delta\gamma$) at the interface of the resistor and solder part 1 can be derived as follows:

$$\tau = \frac{P}{A_s} \quad (28)$$

$$\Delta\gamma = \frac{\tau}{G} \quad (29)$$

2.3 Comparison of strain estimates from models

Table 1 shows the comparison of strain range estimates obtained from the Engelmaier strain metric, preliminary modification to Engelmaier's metric proposed by Chauhan et al., and the first principles model developed in this research. The component selected for assessment is a 2512 type resistor, with tin lead solder, subjected to thermal cycling load of -55°C to 125°C with 15 min dwell at extremes.

The Engelmaier's strain metric does not consider pad area for strain calculation. Hence there are no estimates for the resistor with reduced pad widths. The preliminary modification (PM) model shows a very conservative estimate of strain. The strain in the resistor with 20% pad area is 5X times the strain in the resistor with standard pad area. The first principles (FP) model is less conservative than the PM model. The strain difference between resistor with 20% pad area and that with

standard pad area is ≈ 4.5X. The FP model considers the pad area, component size, PCB thickness, thickness of solder fillet and the standoff height.

Table 1: Comparison of strain range estimates

Pad Width	Engelmaier's Strain Metric	Preliminary Modification of Engelmaier' Strain Metric	First Principles model
100 %	0.0179	0.0179	0.0122
60 %	-	0.0298	0.020
50%	-	0.0358	0.0237
40 %	-	0.0448	0.0292
20 %	-	0.0895	0.0547

2.4 Conclusions

The developed first principles based strain metric considers the solder pad area, component size, PCB thickness, thickness of the solder fillet and standoff height. Using this model the solder strains for SMT leadless packages with varying solder attachment geometries can be estimated. This model overcomes the shortcomings of the Engelmaier's strain metric for leadless components, and provides a more accurate strain estimate for components with different solder interconnect geometries. To verify the strain estimates obtained from the analytical model a finite element analysis needs to be conducted. Details of the FEA are presented in the following sub-section.

Chapter 3: FEA and Model Calibration

A finite element analysis was conducted to obtain strain range values in the solder interconnect for leadless SMT resistors. The FEA results would help verify whether the developed first principles model is able to generate the right strain estimates. The first principles model does not account for the inelastic strain and creep strain that affects the fatigue life. An FEA will help identify the difference between the estimate of the FP Model and the FEA. This information is then used to calibrate the FP model so that the calibrated model now accounts for the inelastic and creep strain components in the total solder stain.

3.1 Finite element modelling

To understand the effect of solder pad area, fillet thickness, and component size on the strain in the solder joints, 3-D finite element models of leadless SMT resistors of different sizes and solder pad areas were generated. The geometric features of four resistor packages were created. Table 2 shows the resistor types and their dimensions.

Table 2: Resistor types and dimensions

Resistor Type	Length (in)	Width (in)	Height (in)
2512	0.25	0.12	0.022
1210	0.12	0.10	0.022
1206	0.12	0.06	0.022
0805	0.08	0.05	0.02

For simplicity, the resistor was modeled as a volume of alumina without any tin end termination. The finite element models were generated using ANSYS software.

Models with varying solder pad widths (100%, 60%, 50%, 40%, and 20%) were generated for all the resistor types. Figure 11 shows the half model of a surface mount resistor with a regular solder pad width assembled on a PCB. Figure 12 shows the half model of a surface mount resistor with pad reduced to 20% of the regular pad width, assembled on a PCB.

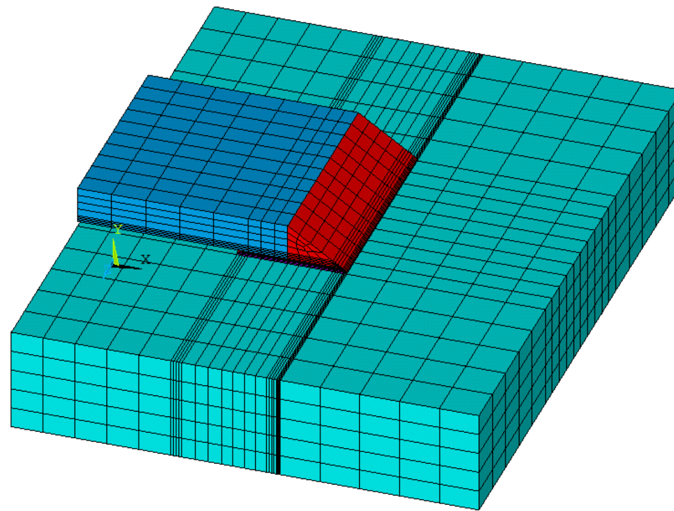

Figure 11: Resistor with regular solder pad width

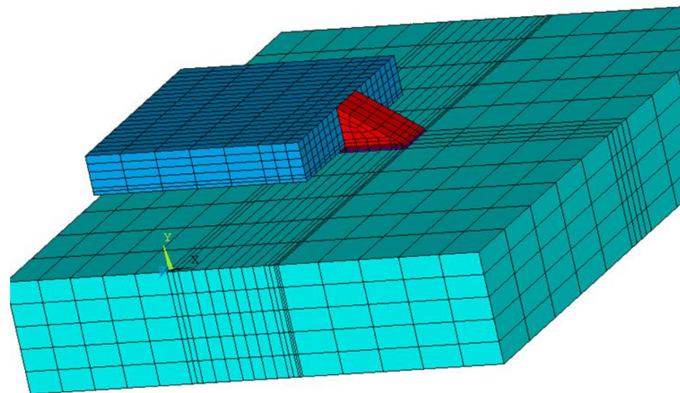

Figure 12: Resistor with reduced solder pad width

The solder material was SnPb and the solder pad on the PCB was plain copper. The solder was modeled as a visco-plastic material with creep (generalized Garofalo model). The PCB thickness was 0.06 in. The CTE values were obtained through testing. The material properties used for modeling are listed in Table 3.

Table 3: Material properties for simulation

Part	Material	Young's Modulus (GPa)	Poisson's Ratio	CTE (ppm/C)
Resistor	Alumina	375	0.22	4.6
Pad	Copper	117	0.35	17
PCB	FR4 Polyclad	23	0.16	14

A simulation matrix was developed to examine the effect of different ΔTs (temperature ranges) and dwell times at the temperature cycling extreme conditions. Table 4 shows the thermal cycling loading matrix. The FE models were subjected to three cycles of each thermal loading profile. For the 1206 and 0805 resistors only the first 3 loading conditions were simulated while the 2512 and 1020 resistor models were subjected to all six loading conditions.

Table 4: Simulation test loads

Test Number	ΔT (^oC)	Temperature Range	Dwell time at extremes (minutes)
1	180	-55°C to 125°C	15
2	140	-15°C to 125°C	60
3	140	-40°C to 100°C	60
4	100	25°C to 125°C	15
5	50	-5°C to -55°C	30
6	50	75°C to 125°C	30

Based on initial simulations it was observed that the solder underneath the resistor body at the interface of the resistor and solder material showed higher strain values than the bulk solder in the fillet portion of the interconnect. Hence, for this study, the total von Mises strain in the solder volume beneath the resistor was considered, as

shown in Figure 13. The thickness of the solder volume selected is half of the standoff height. The strain range is the difference between the average strains in the selected solder volume at the high temperature dwell and the low temperature dwell.

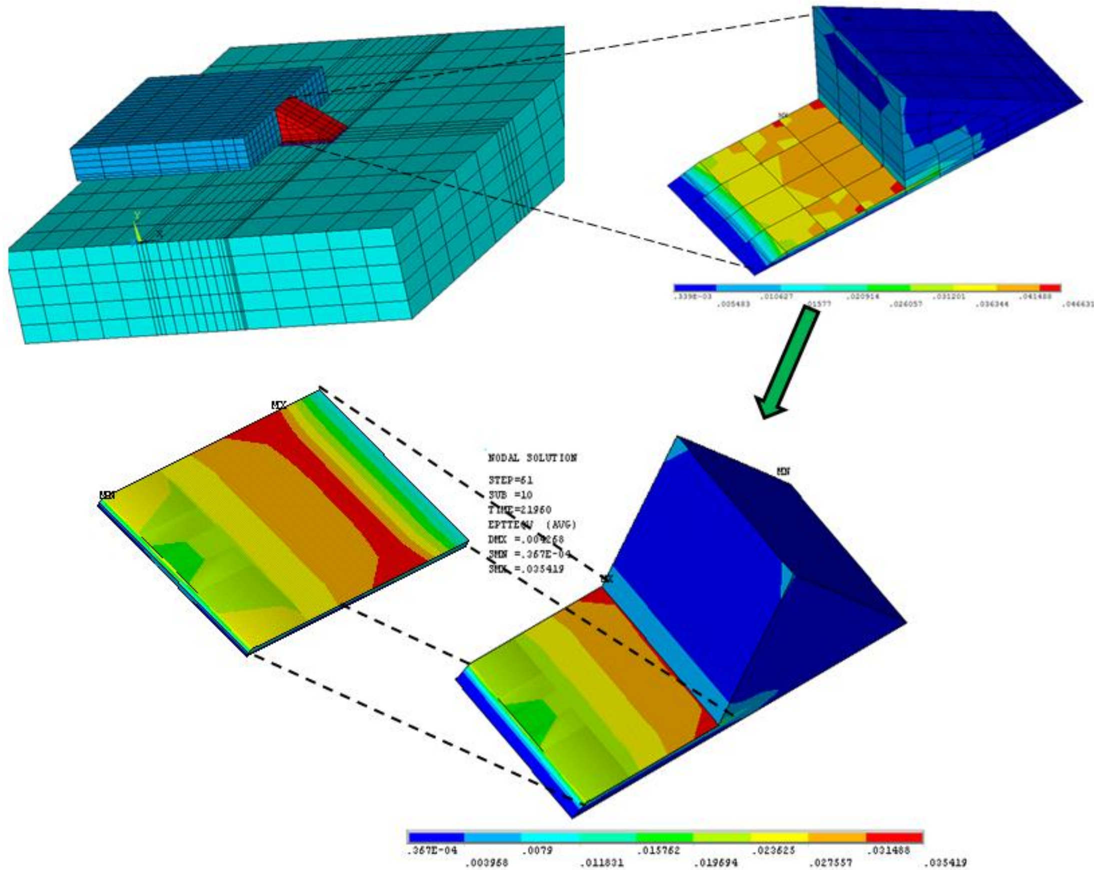

Figure 13: Selected volume for strain range estimation

FE models were also generated to estimate the effect of reduced solder fillet thickness and reduced solder pad length on the strain range. Figure 14 shows a 2-D schematic of the resistor terminal section, solder fillet, copper pad, and PCB. Here, h_{min} is the minimum acceptable solder fillet height per IPC 610 standard [12], $h_{standoff}$ is the standoff height between the resistor and PCB, and $h_{diagonal}$ is the solder fillet thickness. The solder fillet thickness ($h_{diagonal}$) was reduced by reducing the length of the copper pad under the fillet (see Figure 14). The length of the copper pad under the

solder fillet was reduced from 100% to 75%, 50%, and 25%. The copper pad width for these models was 100% (regular pad width). Only models for 2515 and 120 type resistors were generated for this effort. The reduced solder fillet models were subjected to simulated temperature cycling from -55°C to 125°C with 15 min dwell.

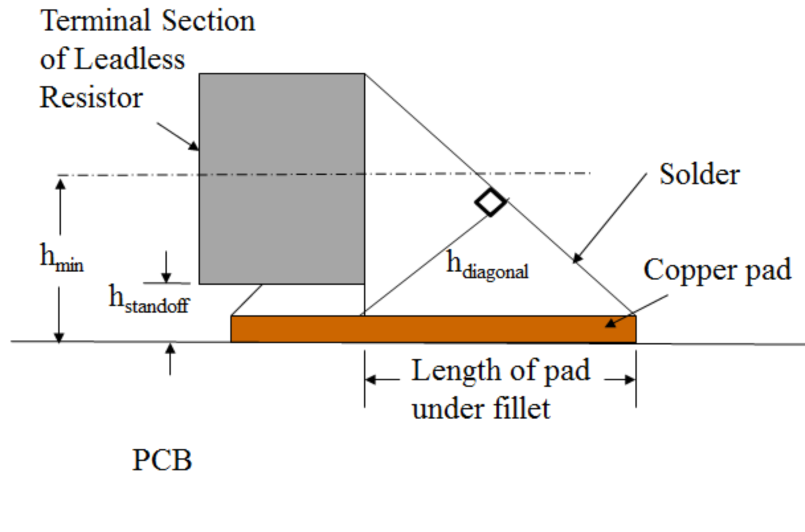

Figure 14: Solder fillet

3.2 Simulation results and analysis

The solder strain range values for the 2512, 1210, 1206 and 0805 resistors with varying solder pad geometries, subjected to the simulated thermal loading conditions, are a compiled in this section. The results are analyzed and conclusions are generated based on these analyses.

3.2.1 Results for varying solder pad area

The simulations showed that the solder interconnect on the resistor with reduced pad area had a higher strain than the solder interconnect on the resistor with regular

pad area. As the solder pad area decreased, the strain in the solder increased. In the case of 2512 resistors subjected to a $\Delta T = 180^{o}C$ ($-55^{o}C$ to $125^{o}C$ temperature loading) on an average there was an increase in total strain range of about 75% between the resistors with 100% pad size and the resistors with 20% pad size. In the case of a 1210 resistor subjected to same loading conditions as the 2512 resistor the average increase in total strain range between the resistors with 100% pad size and the resistors with 20% pad size was 51%. This trend is also seen for the 1206 and 0805 resistors with varying pad areas.

It was also seen that the component size had a significant bearing on the strain in the solder interconnect. The strain decreased as the size of the resistor decreased. Under a $\Delta T = 180^{o}C$ ($-55^{o}C$ to $125^{o}C$ temperature loading), the total strain range in the 1210 resistor with 100% pad size was 30% lower than the total strain range in the 2512 resistor with 100% pad size. A similar difference exists between the 1210 resistor with 20% pad size and the 2512 resistor with 20% pad size. The strains in the solder interconnect of 1206 and 0805 are also lower than the strains in 2512 resistor. This confirms that the size of the leadless SMT resistor is a major factor in the strain induced in the solder joints. Small SMT resistors will have comparatively lower strain in the solder joint than large resistors.

Table 5 shows the percentage increase in total von Mises strain range values in the solder obtained for the FE models of the 2512, 1210, 1206 and 0805 resistors for the two test conditions. Values for the remaining tests also followed the same trend as those shown in Table 5.

Table 5: Percentage increase in strain range values

Pad Width	2512 Resistor		1210 Resistor		1206 Resistor		0805 Resistor	
	Test 1 ΔT= 180°C	Test 3 ΔT= 140°C	Test 1 ΔT= 180°C	Test 3 ΔT= 140°C	Test 1 ΔT= 180°C	Test 3 ΔT= 140°C	Test 1 ΔT= 180°C	Test 3 ΔT= 140°C
100 %	-	-	-	-	-	-	-	-
60 %	30	26	24	21	31	28	42	39
50 %	37	32	25	22	35	33	44	41
40 %	41	37	27	25	42	40	47	46
20 %	75	74	51	51	78	77	69	69

The strain range values obtained from the finite element analysis (FEA) were plotted with respect to the solder pad width. Under all the test conditions, for the 2512 resistor, the strain range is inversely proportional to the solder pad width raised to the power of 0.33. Similarly under all test conditions, for the 1210 resistor, the strain range is inversely proportional to the solder pad width raised to the power of 0.24. The exponent for the 1206 resistors is 0.34 and for 0805 resistor the value is 0.30. For a given SMT leadless component geometry the strain range varies with respect to the solder pad area as a power law with a fixed exponent irrespective of the ΔT. This is an important finding of this study.

Figure 15 shows the plot of solder strain range versus solder pad width for 2512 resistor subjected to Test condition 1 (ΔT= 180°C, temperature range = -55°C to 125°C, dwell time = 15 minutes). Figure 16, Figure 17, and Figure 18, show the same plot under same test condition (Test 1) for 1210, 1206 and 0805 resistors respectively.

Plots for the remaining test conditions, for the four resistor types, is presented in the Appendix A.

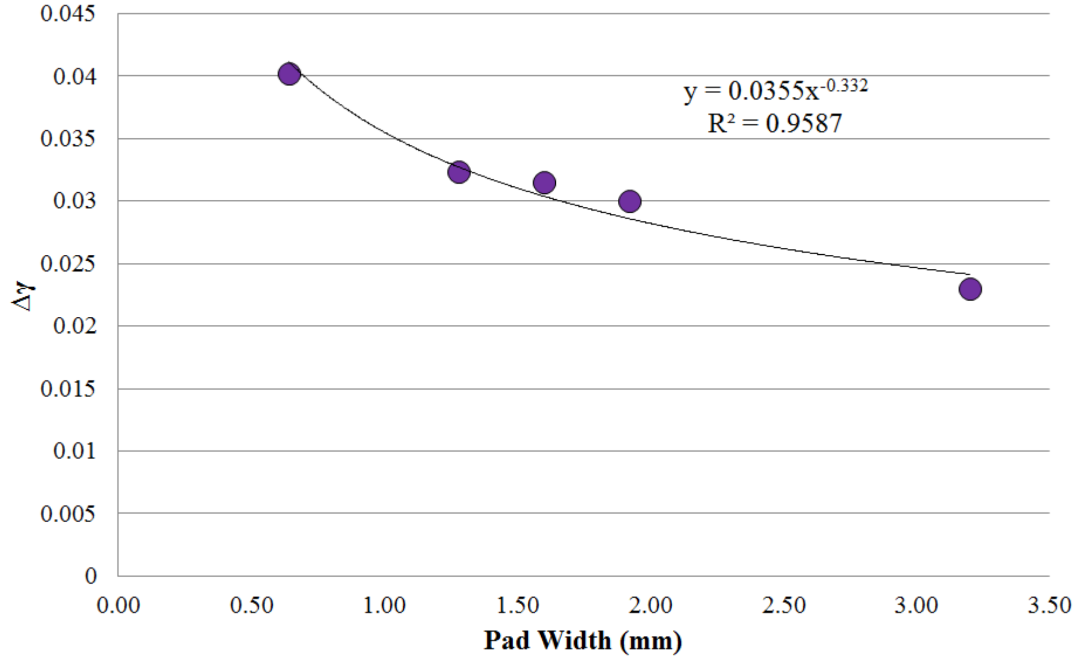

Figure 15: Δγ versus pad width for 2512 resistor (Test 1)

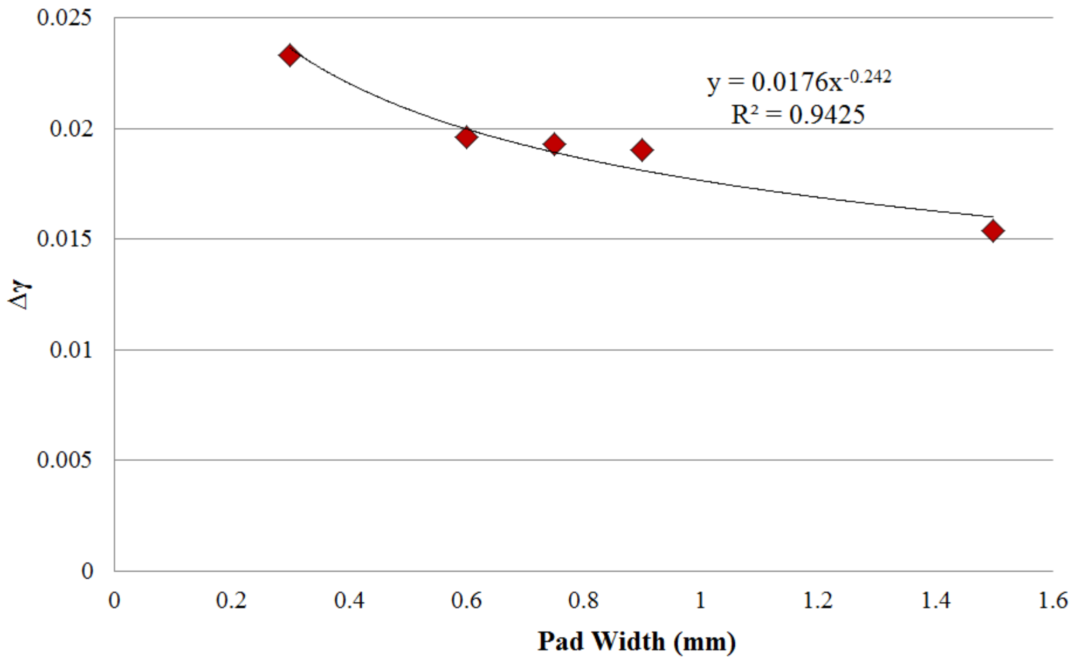

Figure 16: Δγ versus pad width for 1210 resistor (Test 1)

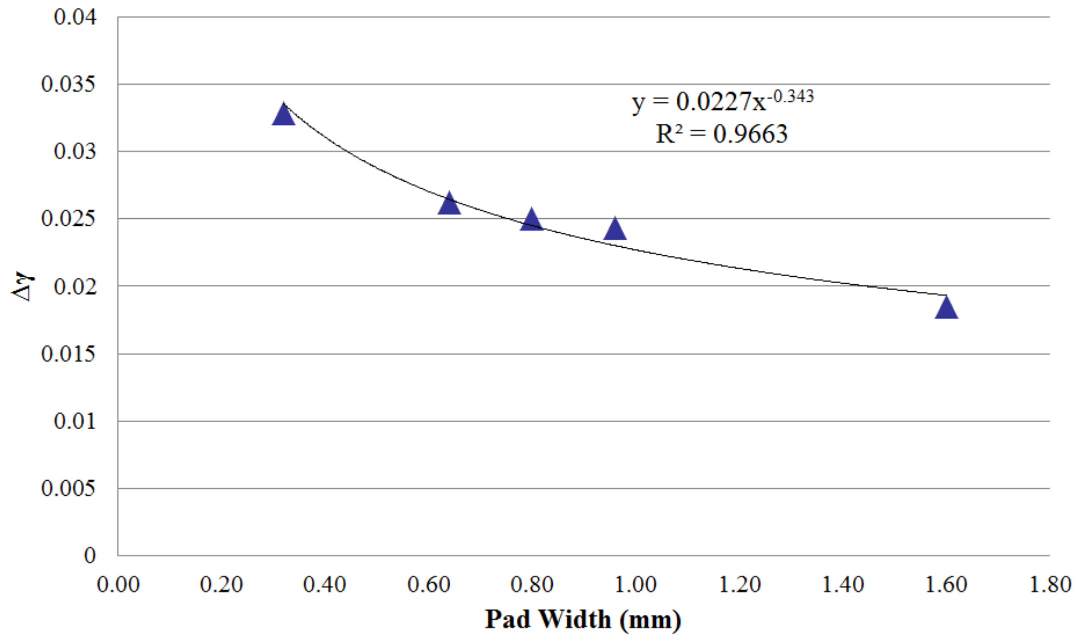

Figure 17: Δγ versus pad width for 1206 resistor (Test 1)

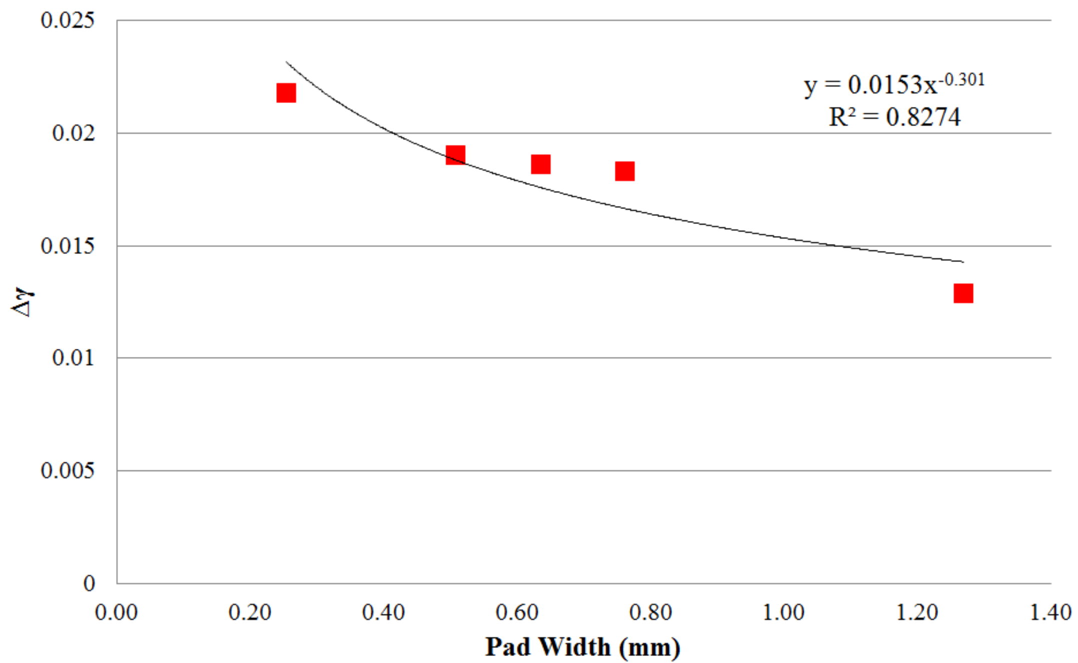

Figure 18: Δγ versus pad width for 0805 resistor (Test 1)

Figure 19 shows a comparison of plots of the strain range versus solder pad width for a 2512 resistor under Test 1 and Test 6. Figure 20 shows a comparison of plots for strain range versus solder pad width for a 1210 resistor for Test 2 and Test 5.

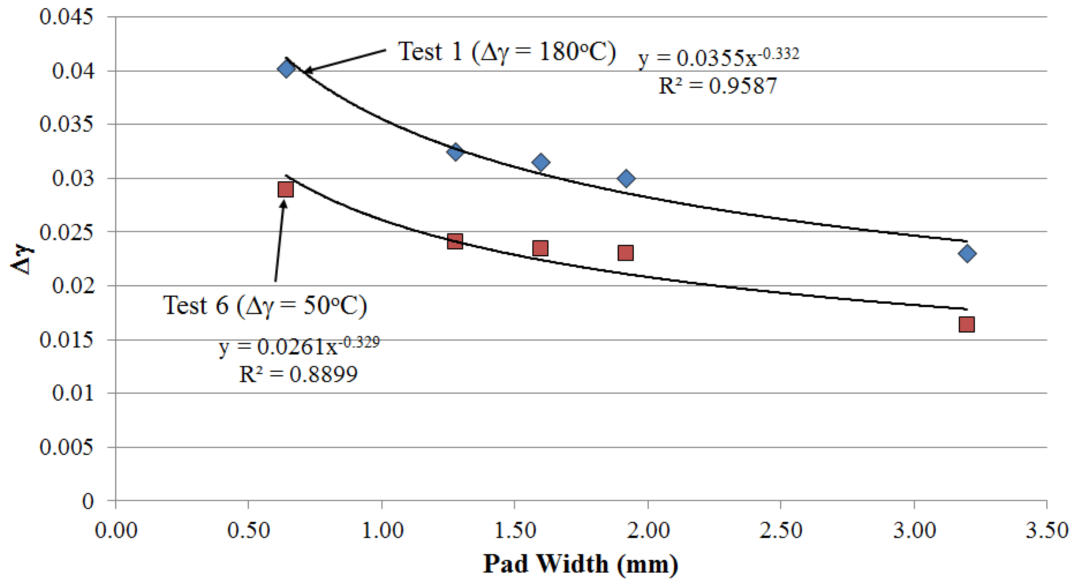

Figure 19: Comparison of Δγ vs pad width for 2512 Resistor

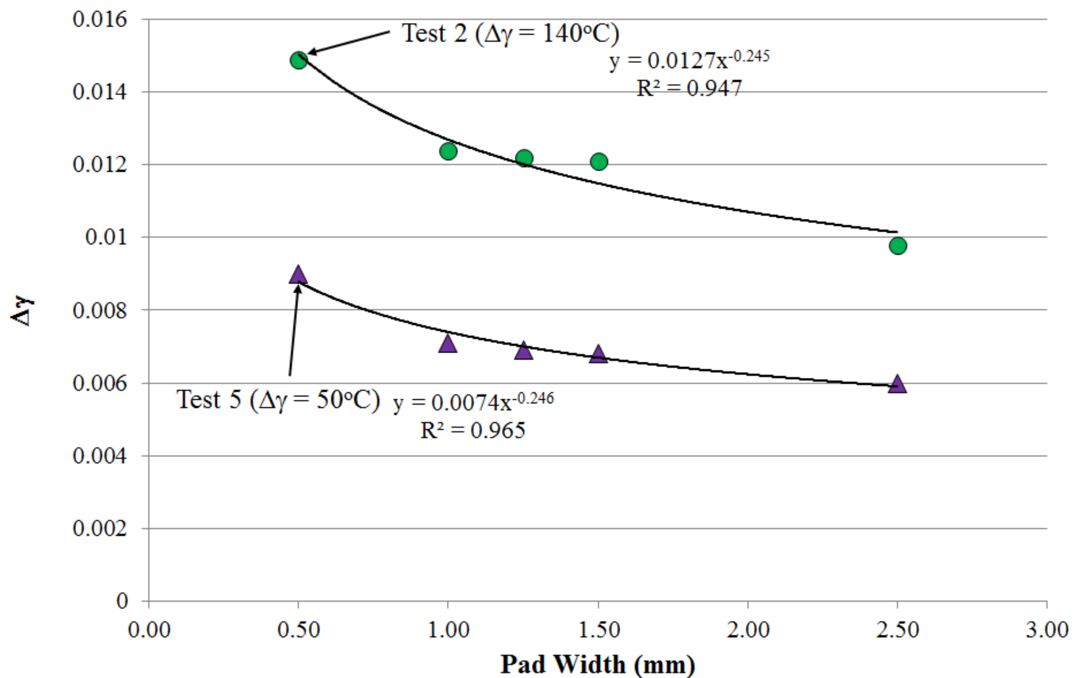

Figure 20: Comparison of Δγ vs pad width for 1210 Resistor

From the simulations it can be seen that the strain range is inversely proportional to the solder pad width. As area reduces the strain range value increases. Solder strain reduces as the size of the component reduces.

3.2.2 Relation between exponent and component geometry

From the FEA strain range data, it was observed that there is a relationship between the exponent and the size of the SMT component. A comparison of the width to length ration of the component and the exponent shows a linear relationship defined by Equation 30. Given this equation the exponent can be calculated for any given two termination leadless SMT component. Table 6 and Figure 21 show the relation between the exponent (factor) and the component geometry.

$$\boldsymbol{Exponent = -0.342 * Width\ to\ Length\ Ratio + 0.51} \qquad (30)$$

Table 6: Relation between component size and exponent

Resistor Type	Length (mm)	Width (mm)	Width to Length Ratio	Exponent
2512	6.3	3.2	0.51	0.33
1210	3.2	2.5	0.78	0.24
1206	3.2	1.6	0.50	0.34
0805	2	1.25	0.63	0.30

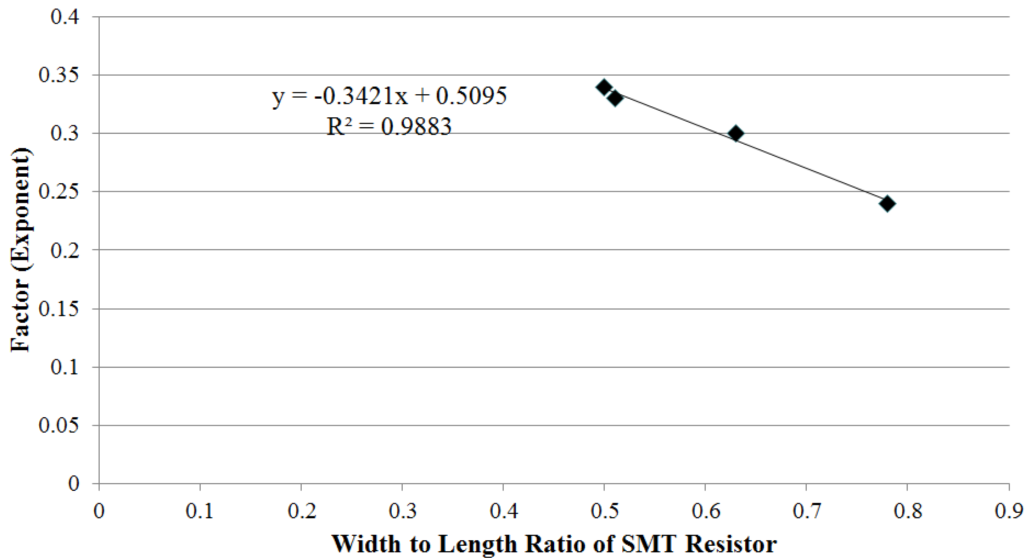

Figure 21: Exponent vs component geometry

3.2.3 Results for varying solder fillet thickness

From the simulations for estimating the effect of the solder fillet thickness it was seen that under -55°C to 125°C thermal loading, for a 2512 resistor with a 75% decrease in solder fillet thickness there was a 69% increase in total strain range in the solder. For the 1210 resistor for the same percentage (75%) of decrease in solder fillet the strain only increased by 53%. As the fillet thickness decreased, the strain range in the solder increased. It can therefore be concluded that the solder fillet thickness affects the strain in the solder joints of a SMT resistor. Unlike with the decrease in solder pad width, the strain range was linearly inversely proportional to the solder thickness.

Table 7 shows the percentage change in total von Mises strain range values versus solder fillet thickness for the 2512 and 1210 resistors under Test 1 (-55°C to 125°C). Figure 22 shows a plot of strain range versus solder fillet thickness for the 2512 resistor, and Figure 23 shows the same for the 1210 resistor.

Table 7: Percentage change in strain range vs pad length and fillet thickness

2512 Resistor			1210 Resistor		
Length of Copper Pad under Solder Fillet (mm)	**Fillet Thickness (mm)**	**Delta Strain %**	**Length of Copper Pad under Solder Fillet (mm)**	**Fillet Thickness (mm)**	**Delta Strain %**
0.89	0.5	-	0.875	0.494	-
0.675	0.45	15	0.65625	0.443	13
0.45	0.36	37	0.4375	0.353	30
0.225	0.21	69	0.21875	0.205	53

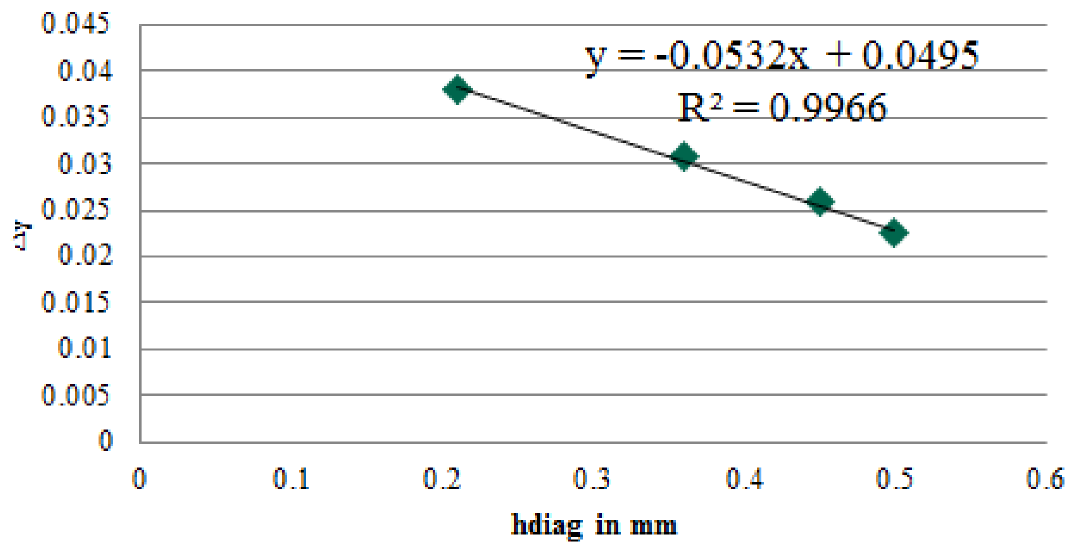

Figure 22: Strain range vs solder thickness for 2512 resistor

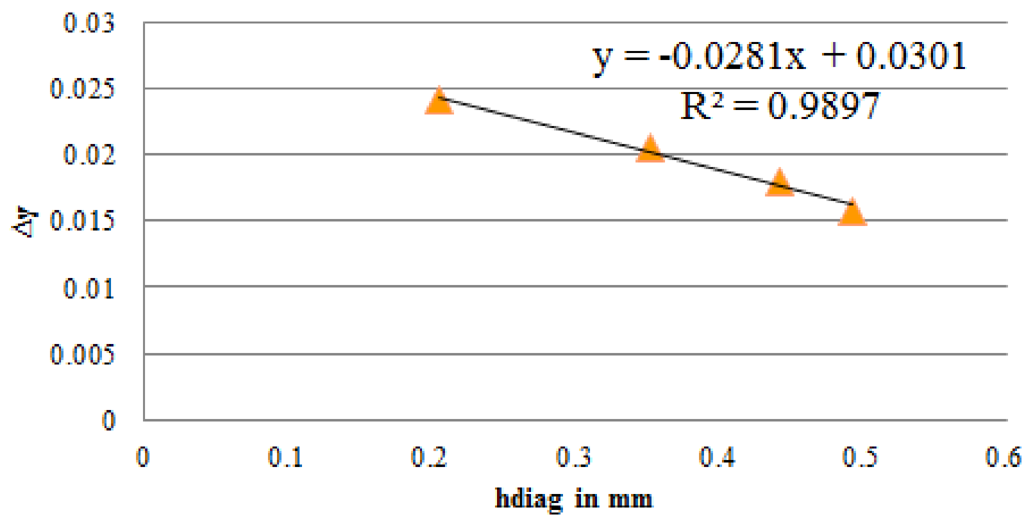

Figure 23: Strain range vs solder thickness for 1210 resistor

The FEA results for resistors with reduced solder fillet thickness makes sense because as the thickness of the fillet reduces, the resistance to thermal expansion of the resistor reduces, thereby increasing the shear stress at the solder - resistor interface. In the first principles model developed in Chapter 2 the fillet thickness is incorporated in the form of length of the simplified solder lead.

3.3 Analytical model calibration

Table 8 shows a comparison of the percentage change in strain range values obtained from FEA, the developed first principles (FP) model and the preliminary modification to Engelmaier's strain metric (PM) proposed by Chauhan et al. The comparison is shown for 2512 and 1210 resistors subjected to a thermal cycling load with a $\Delta T = 180^{o}C$ ($-55^{o}C$ to $125^{\circ}C$ with 15 minute dwell). The FEA results show a lower percentage increase in strain range between the resistors with 100% pad area and the resistors with 20% pad area than those obtained from FP model and the preliminary model.

Table 8: Percentage change in strain range values of FEA and models

Pad Width	2512 Resistor			1210 Resistor		
	FEA	FP	PM	FEA	FP	PM
100 %	0	0	0	0	0	0
60 %	30	64	66	24	60	67
50 %	37	94	100	25	89	100
40 %	41	139	150	27	130	151
20 %	75	348	400	51	310	400

Figure 24 shows a comparison of strain range estimates for 2512 resistor obtained from FEA, first principles model and preliminary modification model. The thermal load condition is $\Delta T = 180^{o}C$ ($-55^{o}C$ to $125^{\circ}C$ with 15 minute dwell).Figure 25 shows a similar comparison for the 1210 resistor. The thermal load condition for 1210 resistor is $\Delta T = 140^{o}C$ ($-15^{o}C$ to $125^{\circ}C$ with 60 minute dwell).

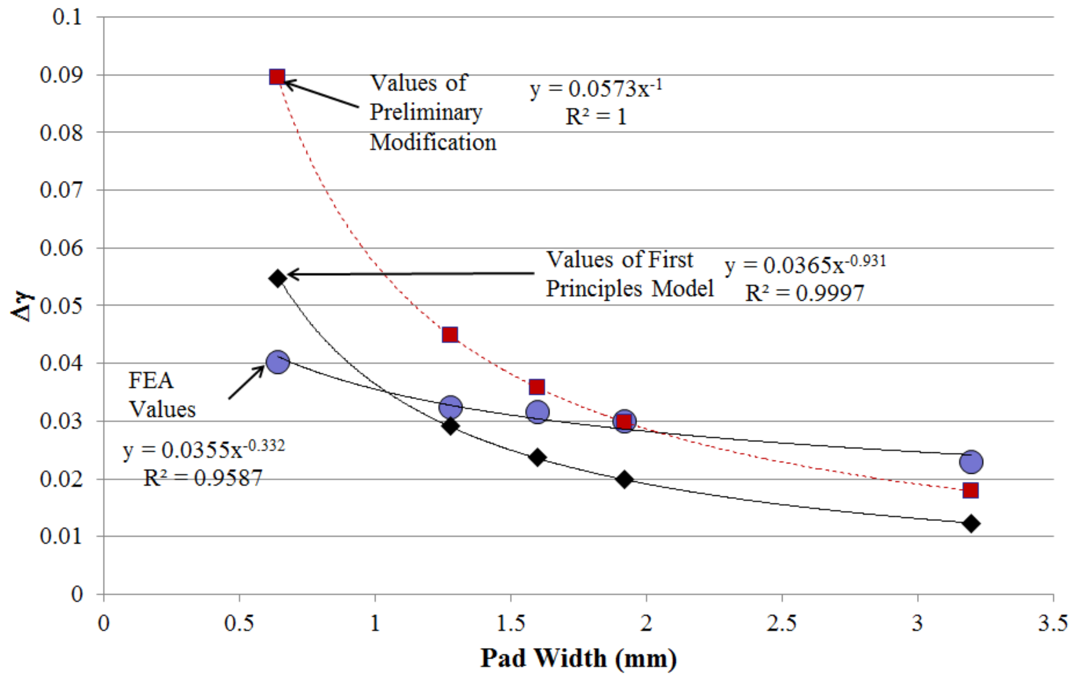

Figure 24: Comparison of strain range estimates for 2512 resistor

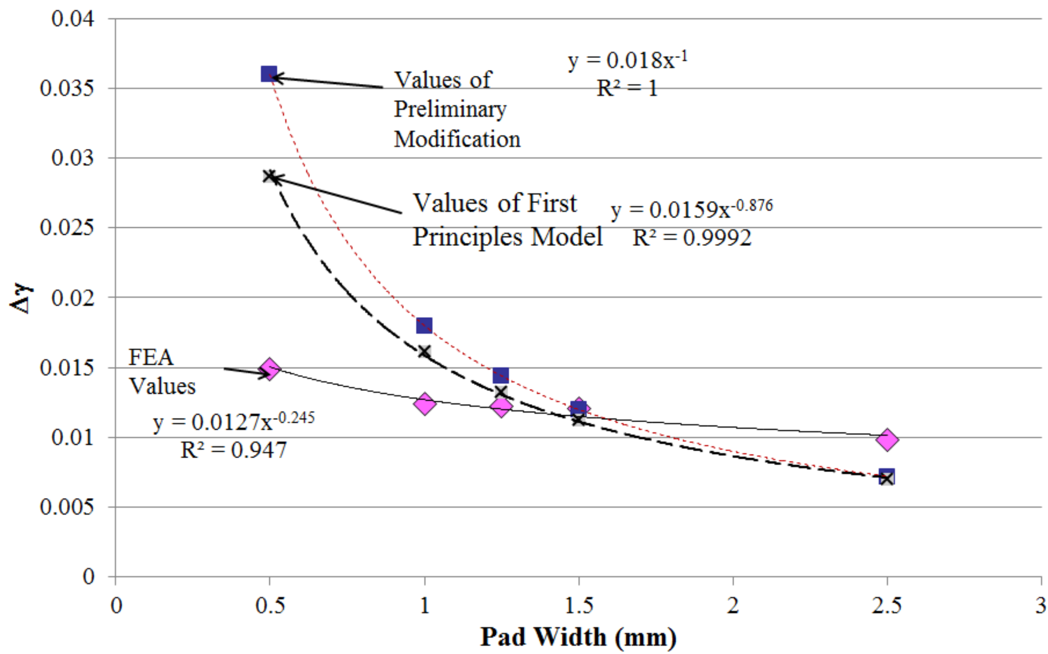

Figure 25: Comparison of strain range estimates for 1210 resistor

From the FEA it was observed that the strain range in the solder was inversely proportional to the solder attachment area. The relation followed a power law. Unlike

the FEA, the first principles model does not account for the inelastic strain and creep strain that affects the fatigue life. Based on the FEA the first principles based strain metric is calibrated to account for the inelastic and creep strain components in the total solder stain estimate. The first principle strain model was modified by adding a power value to the width of the solder pad. The exponent is 0.33 for 2512 resistors, 0.24 for 1210 resistors, 0.34 for 1206 resistors and 0.30 for 0805 resistors. This calibration influences the values of the interface area under the component (A_s), and the effective stiffness of the solder (k_{eff_solder}).

Table 9 compares the solder strain range values in 2512 and 1210 resistors obtained from the FEA model, with the FP model and calibrated FP model. The thermal load condition is $\Delta T = 180^oC$ (-55^oC to $125^\circ C$ with 15 minute dwell).

Table 9: Strain range values for calibrated first principles model

Pad Width	2512 Resistor			1210 Resistor		
	FEA	**CFP**	**FP**	**FEA**	**CFP**	**FP**
100 %	0.023	0.0257	0.0122	0.0154	0.0171	0.0090
60 %	0.03	0.0301	0.02	0.01905	0.0190	0.0144
50 %	0.0315	0.0318	0.0237	0.0193	0.0198	0.0170
40 %	0.0324	0.034	0.0292	0.0196	0.0207	0.0207
20 %	0.0402	0.0419	0.0547	0.0233	0.0239	0.0369

The calibrated first principles (CFP) model estimates of the strain range values are close to those obtained from FEA. For the CFP model the strain difference between 2512 resistor with 20% pad area and that with regular pad area is 1.6 X. The CFP model strain difference for 1210 resistor is 1.4 X.

The strain range values obtained from calibrated FP model does follow the power law relation as seen with FEA results. The strain values follow the trends (increase in strain with decrease in pad area and decrease in strain with decrease in component size) like the FEA estimates. The calibrated FP model follows the FEA estimates with regard to the thickness of the solder fillet.

3.4 Conclusions

From the results if the FEA it can be concluded that the strain range in the solder is inversely proportional to the solder attachment area. More the area lower is the strain. The relation between strain and pad area follows an inverse power law. The size of the component also affects the time to failure. Under the same environmental loading condition, the 2512 resistors failed before the 1210 resistors. The thickness of the solder fillet inversely affected the strain range values. The relation though is a linear function. The length of the copper pad under the solder fillet inversely affected the strain range values.

The finite element analysis confirms that resistors with reduced solder pads sizes have comparatively higher strain range values in the solder and resistor interface than those with standard solder pad size. As the strain range in the solder increases, the fatigue life of the leadless resistor decreases. Leadless SMT resistors with a reduced solder attachment area fail earlier than resistors with regular solder attachment due to strain-induced fatigue when subjected to thermal cycling loads. This result also supports the hypothesis that besides the CTE mismatch, the solder attachment area

also contributes to the fatigue life of the component, and should therefore should be part of any analytical formula to estimate solder strain range.

Based on the results of FEA the first principles (FP) strain metric developed in Chapter 2 is calibrated. This calibration accounts for the inelastic and creep strains in the solder due to thermal cycling. The calibrated FP strain metric shows better fit to the FEA data in comparison to Engelmaier's strain metric and the preliminary modification model.

Chapter 4: Validation Testing

While the calibration of the first principles model presented in Chapter 3 provides estimates closer to FEA it needs to be validated with experimental data. The solder strain range estimates obtained from the calibrated FP model are substituted in the Engelmaier's model for estimating times to failure of components subjected to thermal cycling loading. The time to failure estimates thus obtained need to be compared to experimental data to verify that the time to failure estimates from the model are right. The details of the tests conducted are presented in the following sub-sections.

4.1 Test vehicles and testing

To obtain experimental data on the time to failure of leadless SMT resistors with regular and reduced solder pad areas some test boards were produced. Each test board consisted of 2512 type resistors soldered on to copper pads finished with organic solderability preservative (OSP). The solder material used is tin lead (SnPb) solder. Some of the resistors have the regular size solder pads while the remaining resistors have solder pad with reduced to twenty percent of the regular pad width. Test vehicle 1 has 16 resistors with regular solder pad width and 24 resistors with solder pad widths reduced to 20% of the regular pad width. Test vehicle 2 has 20 resistors each with regular pad width and pad widths reduced to 20% of regular size. Figure 26 shows the validation test vehicle 1 and Figure 27 shows validation test vehicle 2.

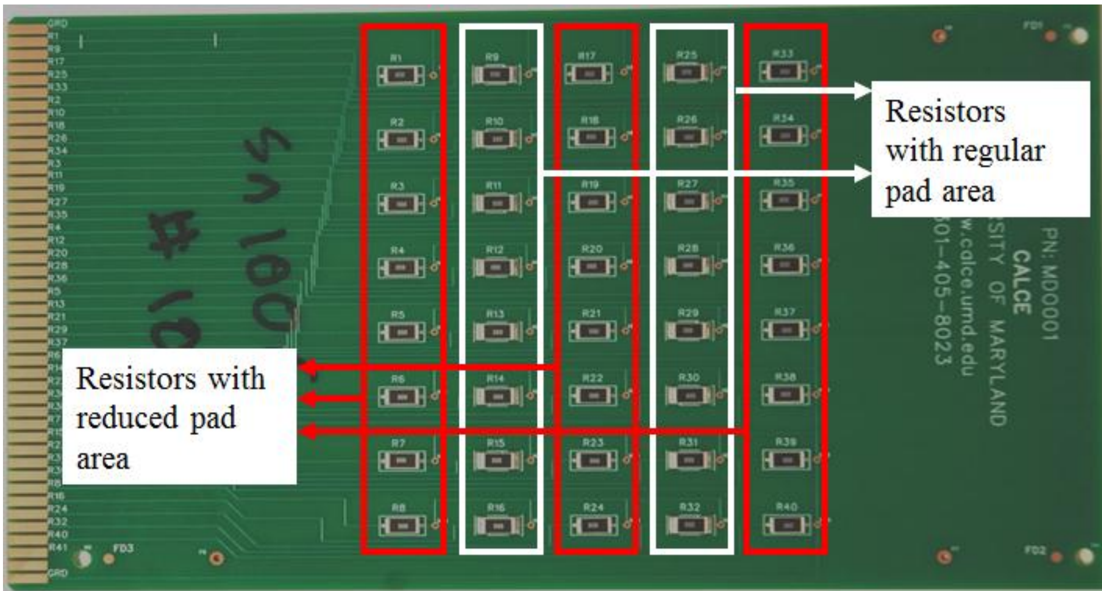

Figure 26: Validation test vehicle 1

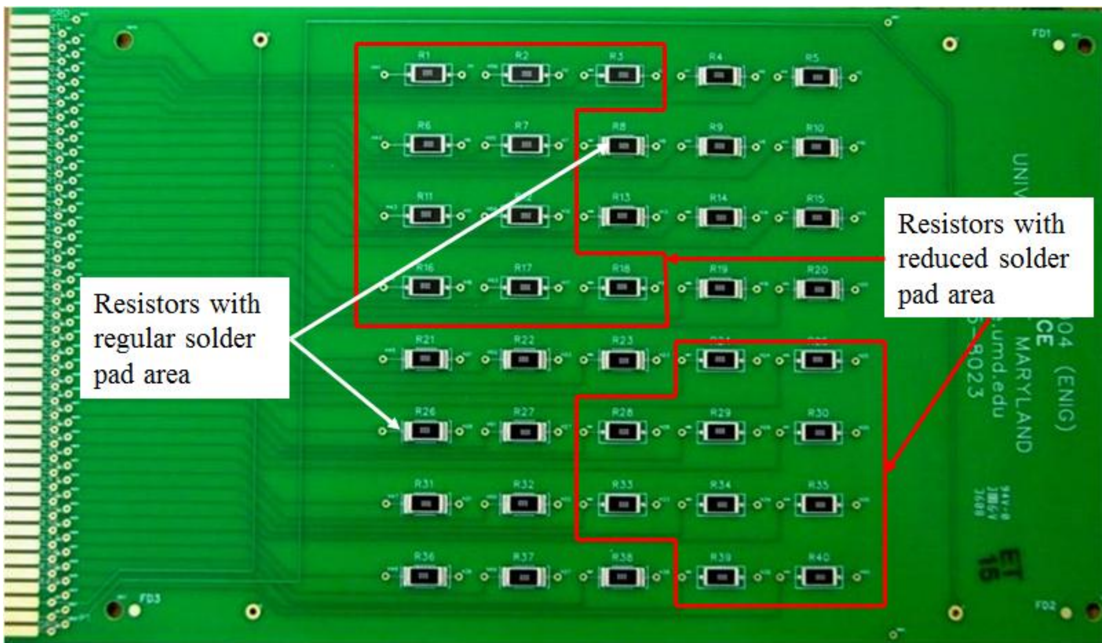

Figure 27: Validation test vehicle 2

Three thermal cycling loading conditions were generated in a laboratory setting. Table 10 shows the validation test matrix. During the testing the resistances of the resistors were monitored in situ so as to note the state of damage of the solder interconnects of the resistors. The failure is defined as the first occurrence of five

consecutive resistance readings that are twenty percent above maximum nominal resistance value (based on the IPC 9701 standard [13]).

Table 10: Validation test matrix

Number of resistors / Test condition	Resistor with 100% pad area	Resistor with 20% pad area
-55°C to 125°C with 15 minute dwell	16	24
0°C to 100°C with 10 minute dwell	20	20
0°C to 100°C with 120 minute dwell	20	20

4.2 Test results and comparison

Testing proved that under same thermal loading conditions the resistors with reduced solder pad areas failed before resistors with regular solder pad areas. Figure 28 shows the Weibull plot of time to failure of the resistors under 0°C to 100°C with 120 minute dwell. Here R100 refers to resistors with regular pad area and R20 refers to resistors with solder pad width reduced to twenty percent of the regular pad width. N50 refers to the time at which fifty percent of the resistors of that particular category have failed. Figure 29 shows the plot for test data under 0°C to 100°C with 10 minute dwell, and Figure 30 shows the Weibull plot for test data under -55°C to 125°C with 15 minute dwell.

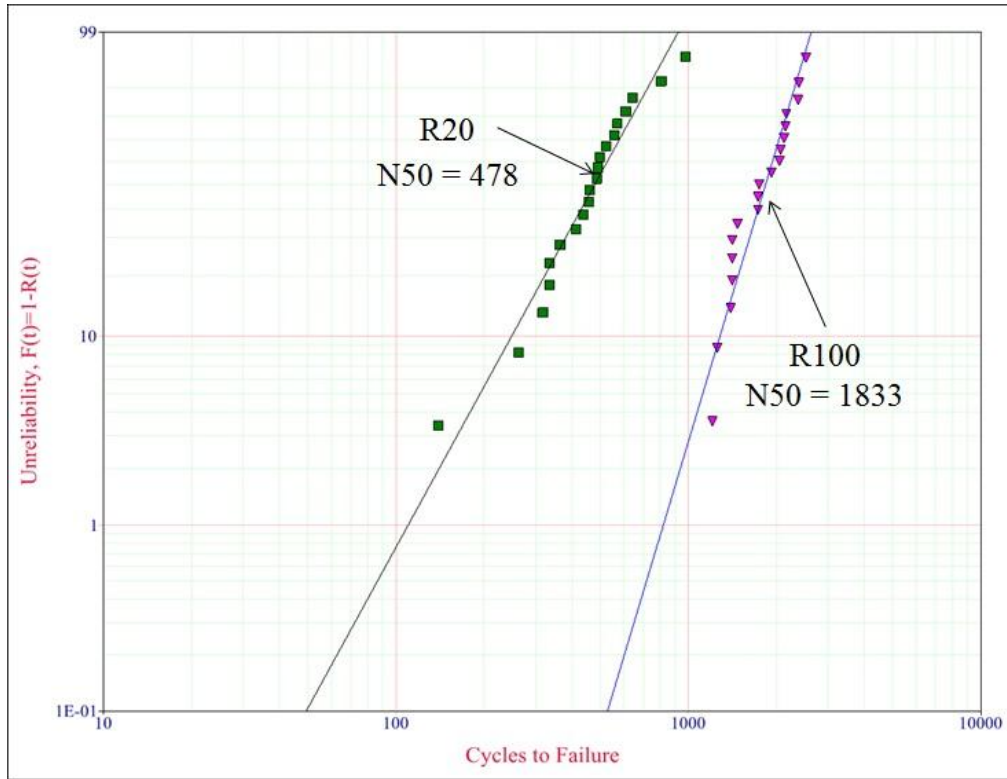

Figure 28: Validation test data (0°C to 100°C with 120 minute dwell)

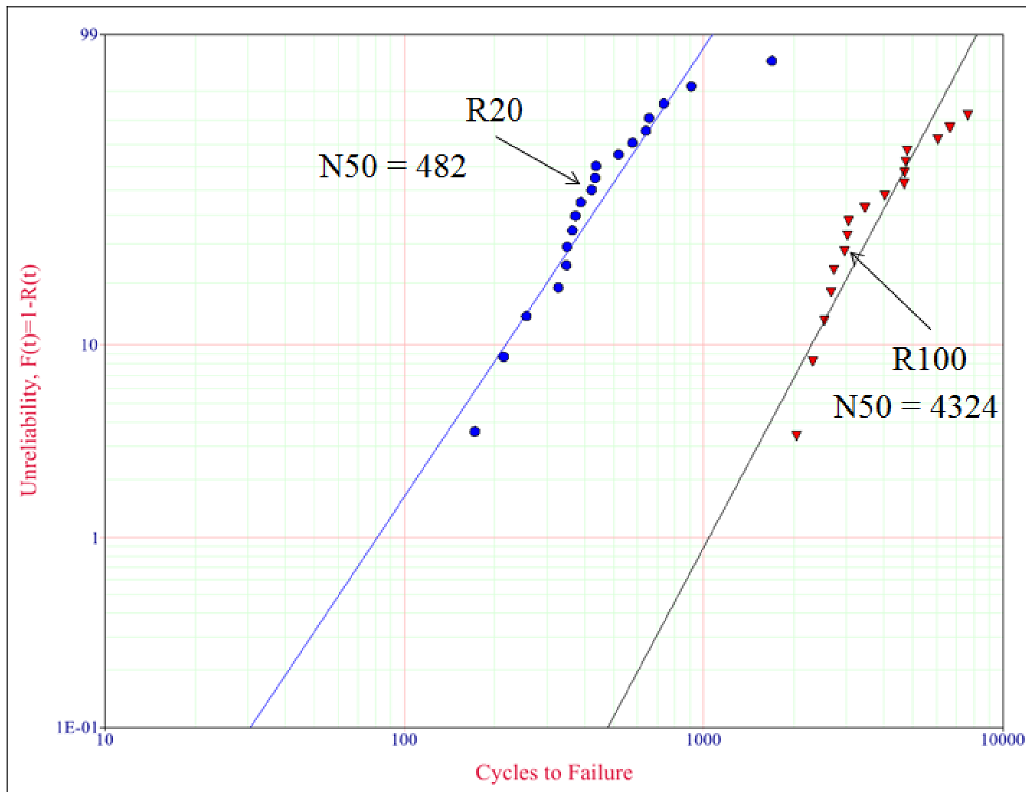

Figure 29: Validation test data (0°C to 100°C with 10 minute dwell)

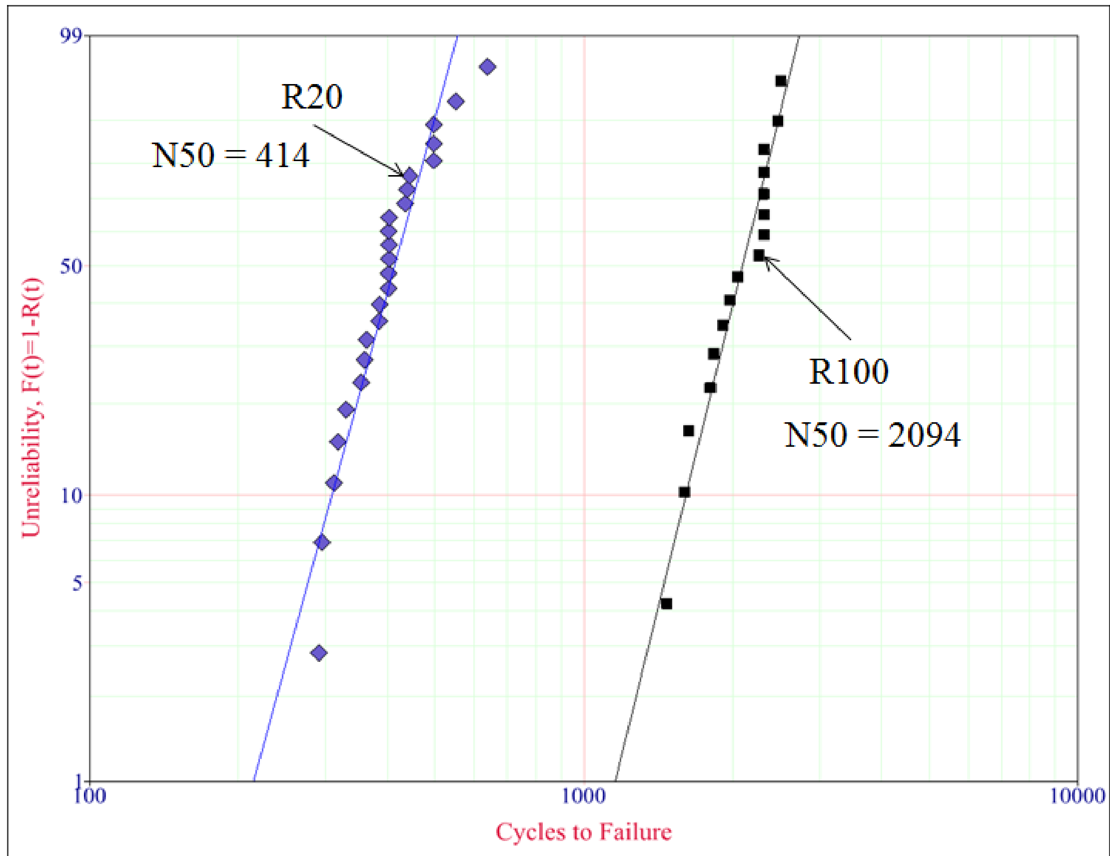

Figure 30: Validation test data (-55°C to 125°C with 15 minute dwell)

Table 11 shows the test data for the three different loading conditions. The test data is compared to the estimate obtained from the Engelmaier's model wherein the solder strain rage is calculated using the calibrated first principles model. It can be seen that the test data mostly matches with the physics of failure model estimates. This validates the calibrated first principles strain metric developed in this study.

Table 11: Cycles to failure comparison

Test Condition	Pad Area	Test Results (N50)	Results of PoF model with Calibrated First Principles Strain Metric (N50)
-55°C to 125°C with 15 minute dwell	100 %	2101	1834
	20 %	414	417
0°C to 100°C with 10 minute dwell	100 %	4324	4434
	20 %	482	1159
0°C to 100°C with 120 minute dwell	100 %	1833	1861
	20 %	478	553

4.3 Conclusions

The calibrated first principles model for calculating the strain range in the solder interconnects of leadless SMT package has been validated. The comparison of the test results with estimates from the PoF model using the calibrated FP strain metric show that the PoF estimates are close to the experimental data.

Chapter 5: Feasibility of Canary Design

As described in Section 1.3 of Chapter 1, an idea proposed to use an expendable canary device formed by using reduced solder interconnect for SMT resistors to predict the solder joint fatigue failure of ball grid array (BGA) packages. The solder interconnect canary is selected because even though the shape of the solder interconnect is different the hypothesis is that since the failure mechanism, mode and site is the same, the resistor with reduced solder attachment will fail before the BGA package and can be hence used to predict the failure of the BGA.

To accurately predict the BGA failure it is vital to know the prognostic distance between the BGA and the canary device. Since the feasibility of such a match up has not been ascertained, the first step involves a rapid assessment of time to failure of the canary (resistor with reduced solder attachment area) and the target system (BGA) using PoF models. Based on the information from the PoF models the canary devices a can be designed. Finally to evaluate this concept the canary and target system have to be tested under specified loading conditions. If the canary devices fail before the target system then the concept is validated. The following subsections describe the process of estimating the feasibility of using a canary approach to predict the life of commercial electronic products.

5.1 PoF model estimates

The Engelmaier's PoF model with the Engelmaier's strain range metric for leadless packages and fatigue ductility exponent is used to calculate the time to failure for the BGA. The BGA considers for such an assessment was a 192 IO chip

array ball grid arrays (CABGA). The Engelmaier's model with the calibrated first principles strain range model is used to estimate the time to failure for the resistor with reduced solder attachment area. Two type of SMT resistors were considered for this assessment: 2512 type and 1210 type. Different solder pad areas (100%, 60%, 50%, 40%, and 20%) were considered for both the 2512 and 1210 resistors.

The feasibility of using the canary approach was determined for two different thermal cycling loading conditions. Table 12 shows the calculated cycles to failure values for BGA from the PoF Model and Table 13 shows the calculated cycles to failure values for the resistors with reduced solder attachment. Here the resistors with 20% solder pad width are designated as R20; resistors with 50% solder pad width are designated as R50, and so on till resistors with regular solder pad width: R100. N_{50} is the cycles to failure of 50% of the component.

Table 12: PoF model estimates of cycles to failure for BGA

Thermal cycling condition \ Component	Cycles to Failure of BGA N_{50}
-55°C to 125°C with 15 min dwell	1539
-15°C to 125°C with 60 min dwell	800

Table 13: PoF model estimates for cycles to failure for canaries

Resistor Type	Thermal cycling condition	R100 N_{50}	R60 N_{50}	R50 N_{50}	R40 N_{50}	R20 N_{50}
2512	-55°C to 125°C with 15 min dwell	2378	1815	1652	1479	1045
	-15°C to 125°C with 60 min dwell	2080	1638	1503	1351	988
1210	-55°C to 125°C with 15 min dwell	1834	1236	820	696	417
	-15°C to 125°C with 60 min dwell	1659	1155	793	677	424

Based on the estimates from the PoF models it can be seen that some leadless SMT resistors with a reduced solder attachment area will fail earlier than the BGAs due to strain-induced fatigue when subjected to thermal cycling loads. Both 1210 and 2512 resistors with 20% pad size may be used as canaries for the BGA under the two thermal cycling loads mentioned above. The difference between the time to failure (TTF) of the canary and the TTF of the BGA is the prognostic distance. For example, for a BGA operating in -15°C to 125°C with 60 min dwell conditions, if a 2512 resistor with 20% pad area is used as the canary, the PD = 376 cycles.

Based on feasibility estimates from the PoF models prototypes were designed and assembled. These prototypes were tested to validate the theory of using canaries to predict BGA failure. The following sections describe the prototypes, the tests and the results of testing

5.2 Prototype testing

Two types of test vehicles were designed and assembled for the feasibility study. Test vehicle 1 consisted of a Polyclad HR 370 printed circuit board (PCB) with one BGA package and four resistors. The BGA was a chip array ball grid array (CABGA) and had 192 interconnect solder balls. The resistors were 1210 resistors with a length of 0.125 in and a width of 0.10 in. Of the 4 resistors, one had the standard solder attachment width (0.1 in), and the other three had solder attachment widths reduced to 60%, 40% and 20% of the standard, respectively. The solder used was SnPb. The type of pad finish that was used for test vehicle 1 was organic solderability preservative (OSP). Figure 31 shows feasibility test vehicle 1.

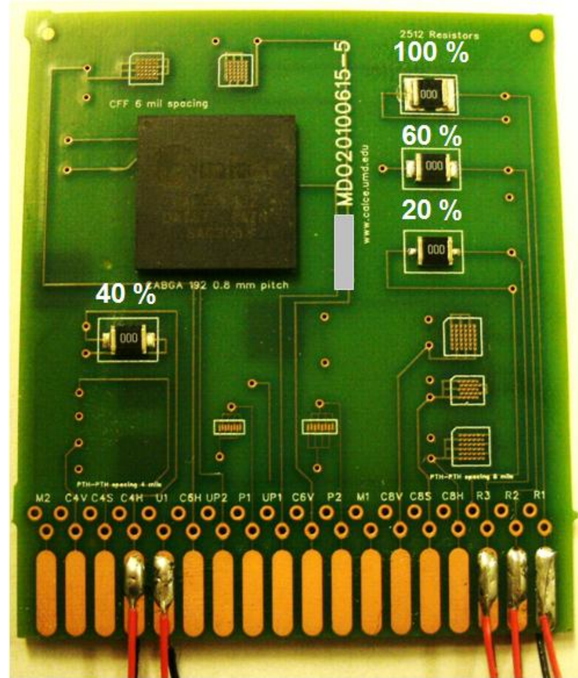

Figure 31: Feasibility test vehicle 1

Test vehicle 2 consisted of a Polyclad HR 370 PCB with four BGA packages and six resistors. The BGAs were chip array ball grid arrays (CABGAs) and each had 192 interconnect solder balls. The resistors were 2512 resistors, each with a length of 0.25 in and a width of 0.125 in. Two of the resistors had standard solder attachment width (0.25 in): two of the remaining four resistors had a reduced attachment width of 50% of the standard area, and the last two resistors had a reduced solder attachment width that was 20% of the standard area. The solder used was SnPb. The type of pad finish used for test vehicle 2 was electroless nickel electroless palladium immersion gold (ENEPIG). Figure 32 shows feasibility test vehicle 2.

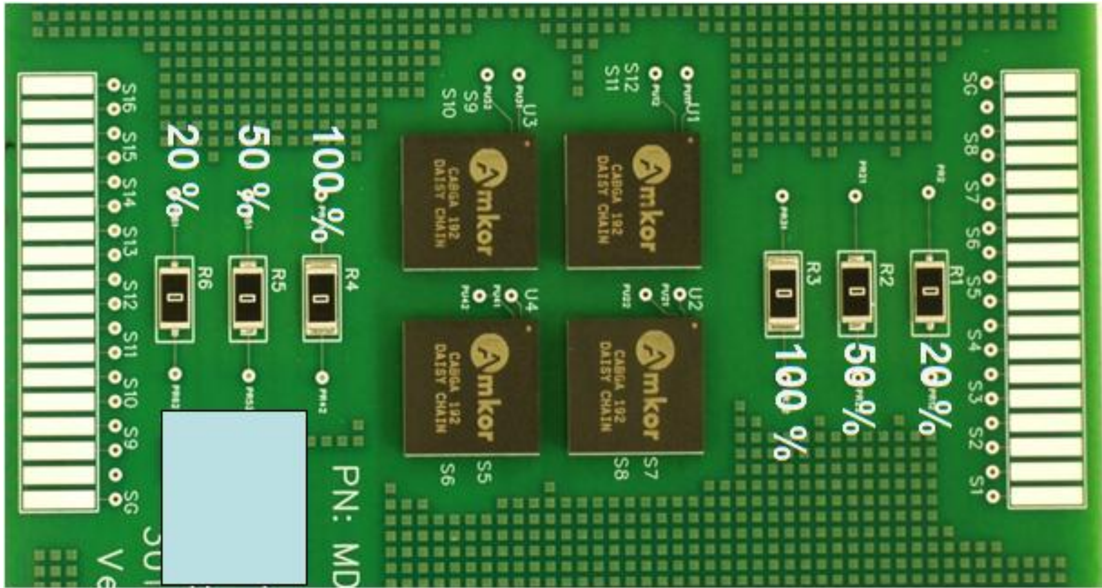

Figure 32: Feasibility test vehicle 2

Test vehicle 1 was subjected to two temperature cycling conditions, while test vehicle 2 was subjected to only one temperature cycling condition. Table 14 shows the overall test matrix for this study. The resistance of the resistors and the daisy-chained BGAs are continuously monitored. Failure is defined as the first occurrence of five consecutive resistance readings that are 20% above maximum nominal resistance (based on IPC 9701 [13]). This criterion is applicable for both the resistors and the BGA package.

Table 14: Feasibility test matrix

Test Vehicle Type / Test condition	Test Vehicle 1 (# of samples)	Test Vehicle 2 (# of samples)
-55°C to 125°C with 15 min dwell	13	6
-15°C to 125°C with 60 min dwell	13	-

5.3 Results and comparison

From the test results it was observed that in under both loading conditions for test vehicle 1, the 1210 type resistors with reduced solder attachment failed prior to the BGA. All the resistors with 20% solder attachment area failed before the BGAs failed. The resistors with 40%, 60%, and 100% solder attachment areas had very few failures. For test vehicle 2, it was also observed that the 2512 type resistors with reduced solder attachment failed before the BGA packages. The resistors with 20% and 50% solder pad areas failed before the BGAs. Table 15 shows the test results for test vehicle 1 and Table 16 shows the test results for test vehicle 2. The tables also include the actual prognostic distance and the prediction from the POF model. Here the resistors with 20% solder pad width are designated as R20 and resistors with 50% solder pad width are designated as R50. N_{50} is the cycles to failure of 50% of the component.

Table 15: Cycles to failure for feasibility test vehicle 1

Component / Test condition	BGA N_{50}	R20 N_{50}	Actual PD	Predicted PD
-55°C to 125°C with 15 min dwell	2270	1902	368	494
-15°C to 125°C with 60 min dwell	2085	1456	629	-

Table 16: Cycles to failure for feasibility test vehicle 2

Component	Cycles to Failure N_{50}	R20 Vs BGA		R50 Vs BGA	
		Actual PD	Predicted PD	Actual PD	Predicted PD
R20	654	885	1122	112	843
R50	1491				
BGA	1603				

Figure 33 shows the Weibull plot of the cycles to failure of R20 vs. BGA for test vehicle 1 under loading conditions of -15°C to 125°C with 60 min dwell.

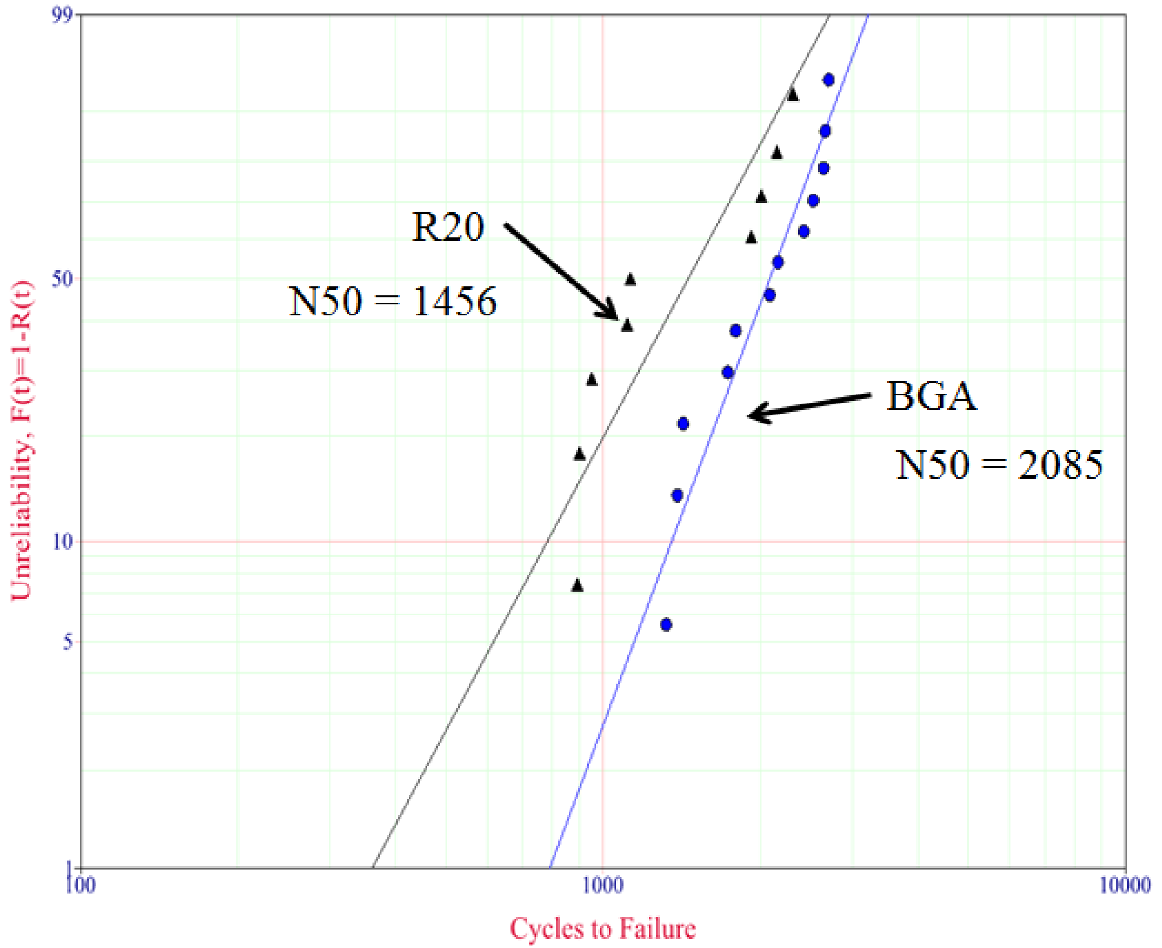

Figure 33: Results for feasibility test vehicle 1

Figure 34 shows the Weibull plot of the cycles to failure of R20 vs. R50 vs. BGA for test vehicle 2 under loading conditions of -55°C to 125°C with 15 min dwell.

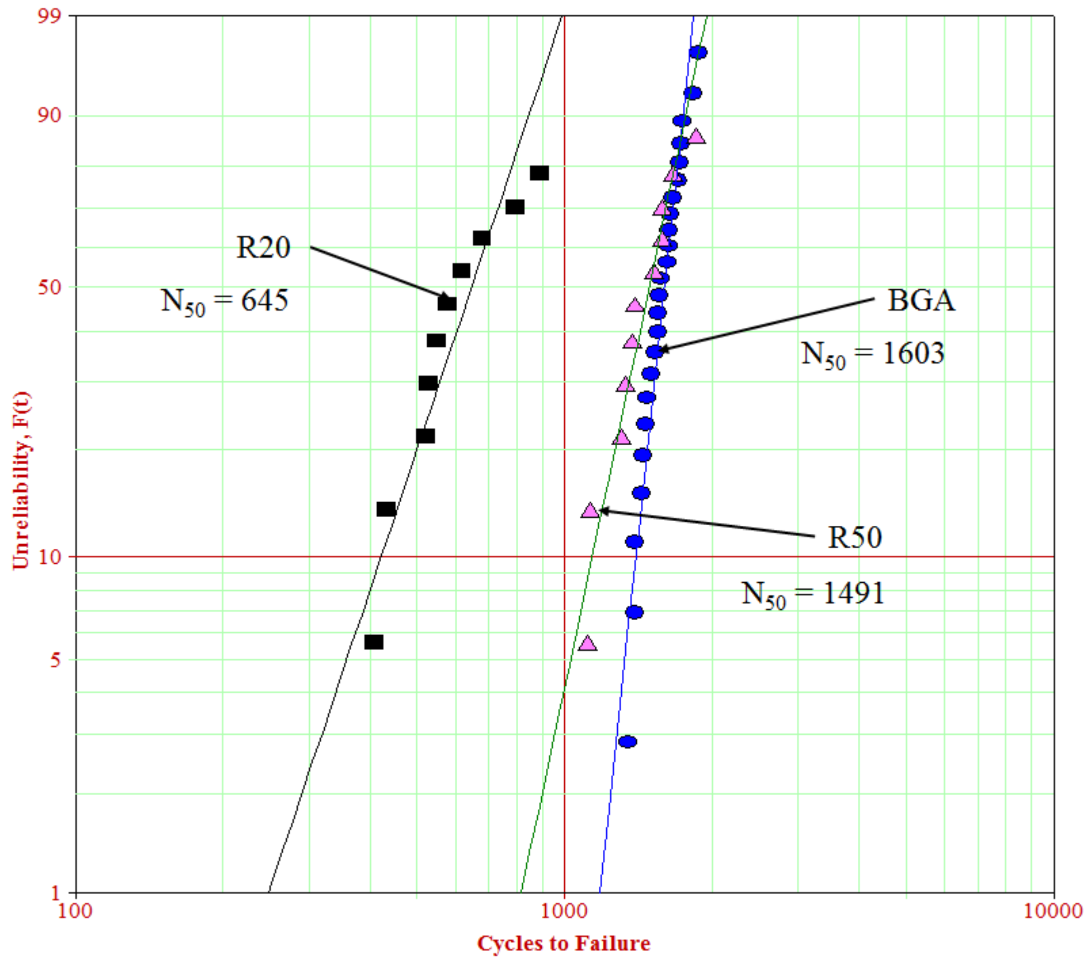

Figure 34: Results for feasibility test vehicle 2

From the experimental data it can be seen that the canary device (resistor with 20% pad width) will fail before the 192 IO BGA.

5.4 Conclusions

The feasibility of using a leadless chip resistor with reduced solder attachment area as a canary device to predict the failure of ball grid array (BGA) component has been proved through testing and validation. Based on experimental data, it is concluded that under the same temperature cycling load conditions, 50% of the resistors with reduced solder attachment failed before 50% of the BGAs. Resistors

with 20% solder pad area can be used as canaries for predicting the solder fatigue failure of the 192 I/O CABGAs. In this case, the prognostic distance is the difference between the N_{50} of the resistor canary device and the N_{50} of the BGA package.

The 2512 resistor with 20% pad area provides a longer prognostic distance than the 1210 resistor with 20% pad area. The PoF model with calibrated first principles equation can be used to generate an initial design of canary device. The PoF model using strain range from calibrated FP equation gives a conservative estimate of cycles to failure for the canary device. Overall, it can be concluded from the feasibility study that a geometry error-seeded expendable canary can be used to predict the failure of commercially mass produced electronic packages.

Chapter 6: Methodology Development

Many studies have been conducted on a variety of systems using the PoF and data-driven approaches to prognostics. However, one prognostic method that has not gained mainstream implementation is the use of canary devices to predict the failure of a system. In this chapter the available literature on the use of canary devices is reviewed and a methodology presented to develop and implement a canary device to predict failure in electronic products.

6.1 Literature review on canary devices

A literature search has yielded only a small number of publications with regard to using canary devices to predict the degradation and failure of systems. Even so, the applications of using canary devices include determining the corrosion in mechanical structures, predicting certain failures in electronic circuits, applications in biomedical field, and a defense application. This section presents a summary of the published literature on canary devices.

Rosunally et al. [14] proposed using “canary structures” to estimate the corrosion of iron structures in a ship that is undergoing conservation. These canary structures were smaller versions of the actual iron structures and were treated with chlorine concentration solution and placed in relatively harsher environments to accelerate corrosion. Trials conducted on another ship would be used to calibrate the canary structures so as to estimate the degradation in the actual structures of the ship under conservation. The process of developing the canary device, the physics-of-failure (PoF) model to estimate the corrosion degradation in the canary, and the number of

such canary devices needed for accurate prognosis have not been discussed in the paper. No results have been published as of yet with respect to this study.

Han et al. [15] presented the concept of a "canary-containing" packet that can be attached to the casings of weapons systems. The idea was that the canary devices would undergo environmental loading identical to the external casing of the weapons system. The challenge in implementing such a canary packet lies in developing and identifying materials that mimic the behavior of the energetic materials in the weapon system and encasing that material to equate the stress conditions in the weapon and the canary packet. A method for developing such a canary and implementing it was not discussed in the paper.

Shea et al. [16] presented a canary structure to detect the anodic oxidation of poly-silicon electrodes in MEMS (micro-electro-mechanical system). The canary structure consisted of poly-Si wires with reduced width placed near the functional poly-Si wires in the MEMS. The indicator of anodic oxidation is an increase in resistance of the canary wires. It was shown that at higher relative humidity, the canary oxidizes faster and becomes an open circuit. However, a physics-based model for correlating the corrosion of the wire to the geometry of the wire was not presented. Also missing from the study was a method for extrapolating the time to failure of the canary wire to the time to failure of the functional poly-Si wires.

Otsuka et al. [17] proposed and demonstrated a canary flip-flop structure to reduce the overestimated voltage in a multi-core processor system on chip. This canary flip-flop system has two flip-flops (FF). The main FF is augmented by a delay buffer and a redundant FF. The redundant FF acts as the canary to catch timing errors.

This is predicted by comparing the main FF value and the redundant FF value. When the timing error is detected, an alarm signal triggers the dynamic voltage scaling system, which then increases the system voltage. It was demonstrated experimentally that the canary FF helped to achieve energy saving of up to 26% over traditional structures. In this study the term canary is used to refer to a component that acts as a negative state reference. The physics behind the delay in switching is not presented. The number of canary FFs needed to maintain the field reliability of the processor is not discussed.

Calhoun et al. [18] present a study using canary flip-flops in dual-test chips, which enabled field reliability and power savings of over 40 times the prevailing power usage. The canary flip-flops consistently failed at higher supply voltages than the core flip-flops. Experiments showed that the canary flip-flops correctly alerted a controller when the supply voltage became high enough to trigger failure. In this study, the term “canary” is used to refer to a component that acts as a state reference for any given voltage. However, the number of canary FFs required and a practical implementation of the proposed canary FF has not been demonstrated.

Wang et al. [19] demonstrated a 90nm 128Kb SRAM test chip in which the canary cells track changes in temperature and data retention voltage. These canary cells protect the core cells in a closed loop positive supply voltage scaling system. Several banks of canary cells were designed to fail across a range of voltages above the DRV of the SRAM cells. However, the number of canary devices needed and a practical implementation method for canaries are missing.

Ridgetop Group [20] has developed canary devices called "sentinels" for advance warning of device failures. The canary devices focus on chip level failure mechanisms, including time-dependent dielectric breakdown (TDDB), hot carrier injection (HCI), and failure due to negative bias temperature instability and radiation exposure. In general, a canary is a pad-limited CMOS device that is tailored for a specific failure mechanism. The prognostic distance is adjusted by scaling the area of the cell. Ridgetop has nominally set this at 80% of the statistical end-of-life point. However, the models for the extrapolation of the time to failure of actual components have not been discussed. The number of canaries required for accurate prediction has also not been discussed.

Goodman et al. [21] developed a prognostic chip to monitor the TDDB of metal–oxide–semiconductor field-effect transistors (MOSFETs). The prognostic cell contains a number of prognostic devices with different oxide thicknesses to which a sufficiently large voltage is applied to precipitate gate oxide failure. Knowing the time to failure of the canary devices and the amount of over voltage applied, the fraction of useful life consumed is calculated using empirical models. The constants required for the model are dependent on the oxide thickness. The canaries are designed such that 99% of them fail before 1% of MOSFETs fail. However, the study does not discuss the determination of prognostic distance and the number of canaries required for accurate prediction.

Keese and Giaever [22] presented a biosensor canary that was used to monitor the general state of a cultured animal cell tissue. This canary method is called electric cell-substrate impedance sensing (ECIS). The idea is to sense the impedance of small

gold electrodes attached to the bottom of the tissue culture vessel. If healthy, the cultured cells will attach and spread on the electrode, thus changing the impedance of the electrodes. Cancerous cells will not attach as they can grow when suspended in a solution. The impedance values have to be recalculated depending on the cell type, temperature, pH value of solution, and many different factors with regard to cell culture. However, a model for impedance correlation to different types of tissues and the volume of tissues grown was not discussed. A practical implementation of the concept has also not been demonstrated in literature.

Petrovick et al. [23] developed a biosensor called CANARYTM (cellular analysis and notification of antigen risks and yields) that is able to identify pathogens in a very rapid, sensitive, and specific manner. The sensor uses genetically engineered white blood cells that emit light within seconds after being exposed to particular pathogens of interest. Biosensors have been developed to identify a variety of bacteria and viruses, including anthrax, smallpox, plague, E. coli, and foot-and-mouth virus. This canary is sensitive to particular contaminants and can be used to detect pathogens faster than other biological systems.

Chauhan et al. [5] presented an approach for monitoring BGA interconnects under temperature cycling conditions. The outer solder ball acts as the canary for the inner solder balls of the BGA. The prognostic distance is calculated using a PoF model and then validated with testing. The prognostic distance varies with the distance of the solder ball from neutral position on the BGA. A methodology for implementation of the canary approach is missing. The number of canary solder balls needed to estimate the field reliability of BGA not discussed.

Lall et. al., [24] to [33], has used microstructural changes in the solder interconnects as leading indicators of fatigue failure in components subjected to thermo-mechanical stresses. In these studies samples subjected to various levels of thermal cycling have been cross-sectioned and observed under the microscope and the grain sizes have been characterized. Based on the correlation between the grain growth and stress levels mathematical relations have been developed to estimate the time to failure of the component. The phase growth varies with the thermal loading. It has been shown that the phase growth increases proportionately to the number of loading cycles. While a specific work flow applicable to using the phase growth to indicate the time to failure has been presented, a general methodology applicable to any type of canary device is missing. Also the number of canaries required for prediction has not been presented in these studies.

The challenge for anyone interested in applying the canary approach for prognostics is that there is no formal process to follow. The literature reviewed here does not present a widely applicable methodology for development and implementation of canary devices for prognostics. Issues including how to develop a prediction scheme for the target system in field conditions, and how many canaries may be needed for prediction, are not addressed by the above mentioned literature. A comprehensive widely applicable methodology is presented in the following sub-section.

6.2 Methodology for canary based prognostics

A general methodology for development and implementation of canary devices is presented. Figure 35 presents the general methodology that can be applied across many different fields and products.

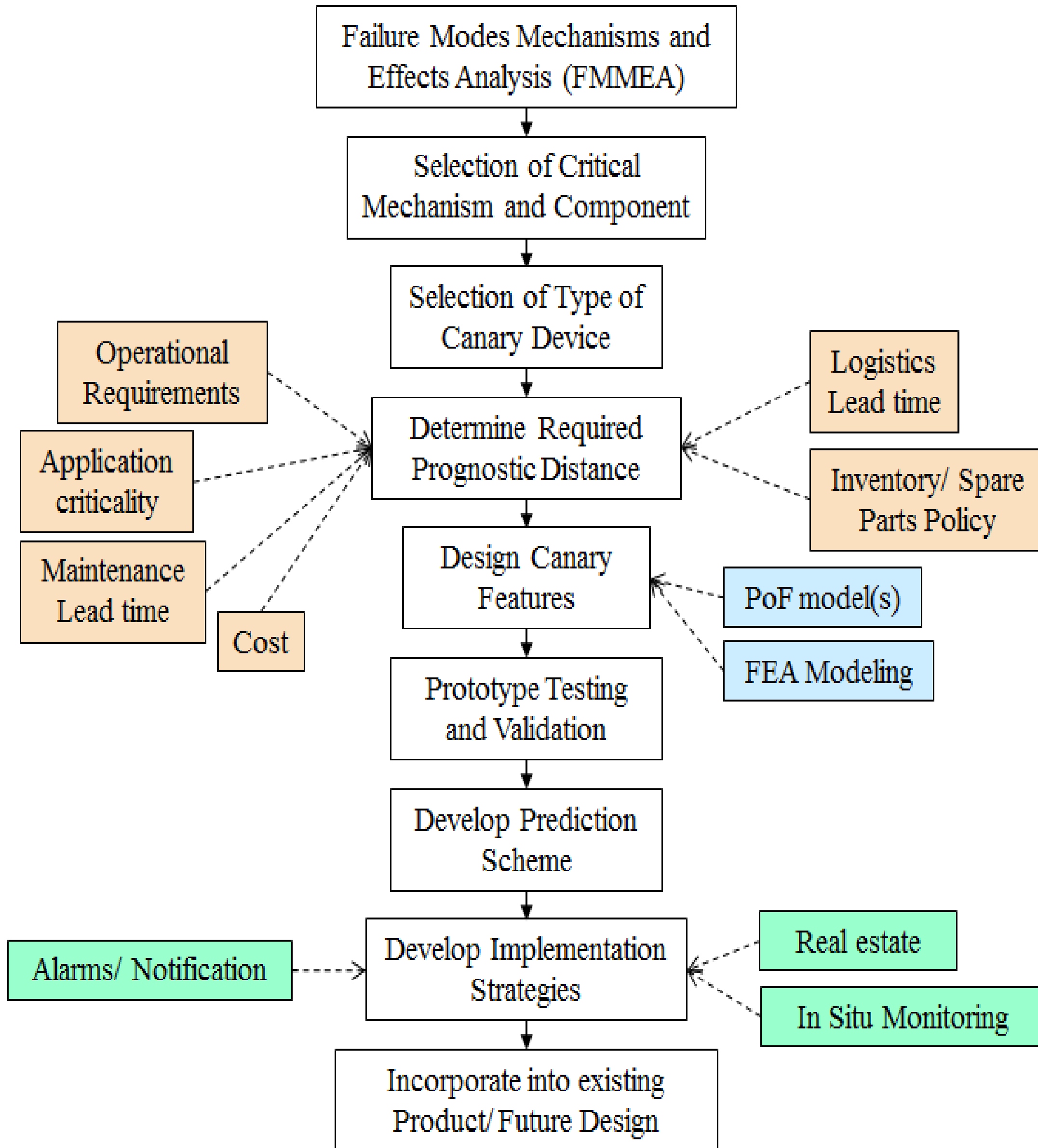

Figure 35: Methodology for canary-based prognostics

The first step in the process is to conduct a failure modes, mechanisms, and effects analysis (FMMEA) [34] of the target system. This step will help in identifying all the possible ways in which the target system can fail under its life cycle environmental loading conditions. The study by Mathew et.al, [35] details the step by step process of performing a FMMEA.

The next step is the selection of the critical failure mechanism and critical failure site. There may be multiple failure mechanisms that affect the target system depending on the application and life cycle loading. It is necessary to select the most critical mechanism(s) under the operational loading conditions, since that is how the target system is most likely to fail. Further, it is necessary to identify which component in the target system is the most susceptible to failure. The canary device should be designed to mimic the failure of the component most likely to fail in the target system.

The next stage is to select the type of canary device to be used to monitor the target system. As explained in section 3, the designer can choose according to the need, whether the canary device should be an expendable canary, sensory canary, or a conjugate-stress canary. The next step is to determine the prognostic distance required so that once the canary fails, the users have sufficient time to carry out the necessary maintenance actions. Many different factors have to be considered when determining the required prognostic distance, such as the criticality of the target system to overall mission success, the operational requirements of the target system, maintenance lead time, the logistics lead time, the inventory and spare parts policy, and the costs associated with implementing the canary approach. The associated costs are a

function of many parameters, including the cost of incorporating the canary into the product, the cost of monitoring the canary device, the cost of false positives, and the cost of missed failures.

The next step is to design the canary device. If the selected canary is an expendable canary, then that canary device should be designed such that it fails by the same failure mechanism as the target component. If it is a sensory canary, then the canary must be designed to be more sensitive than the target component to rising loading conditions that would cause the target component to fail and then provide sufficient warning of such a rise in loads. Therefore, it is important that the canary be designed on the basis of a physics of failure model that accounts for the factors that influence the failure mechanism of the product. The designer may modify the parameters of the model so that the designed expendable canary fails before the target component and fails within a certain time period such that the desired prognostic distance is achieved. It may be necessary to conduct finite element analysis to develop and update the model parameters.

Once the canary device has been designed, it is necessary to conduct prototype testing and validation of the concept. After this step, it is necessary to develop a prediction scheme including estimating the number of canaries required to accurately predict the failure of the target system, and developing what if scenarios to account for variation in field operational and loading conditions. Too few canaries could lead to missed failures, while too many canaries could cost more but have a minimal impact on the prediction accuracy. It is, therefore, necessary to identify the right sample size for the canary devices. It is necessary to develop strategies to utilize the

information obtained from implementing canary devices under varying field loading conditions.

The next step in the process is to develop an implementation strategy for the canary, including how it will be monitored, identifying the real estate within the target system in which to incorporate the canary devices, the method of notification of impending product failure, and future maintenance actions. The final step is to incorporate the canary device into the target system and to continuously monitor the device. The canary design can also be incorporated into future design revisions of the target system.

Each of the steps presented in Figure 35 can be further expanded to take into consideration factors that affect that particular step. This general methodology provides a guideline for developing and implementing the canary-based prognostics approach.

6.3 Conclusions

A review of the available literature on the use of canaries to predict failure has been presented here. Although some researchers have made progress in the use of canary devices, there is limited existing literature on this subject matter. A comprehensive methodology to develop and implement canary-based prognostics for in-situ failure prediction has been presented. Issues associated with the approach including identification of critical failure mechanisms, canary design, testing and validation and practical implementation have been covered.

Chapter 7: Implementation of Canary Based Prognostics

In the Chapter 6 a methodology for canary based prognostics was presented. In Chapter 5 the feasibility of using an external expendable canary device (resistor with reduced solder attachment area) for predicting the failure of the target system (BGA) has been proved. The issues facing the implementation of canary based prognostics include determining how many canary devices are needed to predict the failure of the target system with some confidence, and how to predict the target system failure when the operational conditions are different from those that were used to design the canary device.

The possibility of getting a false alarm with just 1 canary device for predicting the failure of a product may be high. It is not feasible to have too many canaries to monitor only one target component. Based on experimental data from the prototype testing and validation phase, Monte Carlo simulations can be conducted to estimate the effect of the number of canaries on the prediction accuracy. Using Monte Carlo analysis, the times to failure for different sample sizes of canary devices can be generated. The number of canaries needed can be a function of the probability of missing the failure and the total associated cost. The following sub-sections tackle the two issues faced during the implementation phase.

7.1 Failure prediction scheme

The prognostic distance (PD) is the difference between the time to failure (TTF) of the target system and the TTF of the canary. Figure 36 shows a schematic representation of the probability distribution of time to failure for a canary device and

the associated target system. N1 = Time to failure of 1 % of population, N50 = Time to failure of 50 % of population, and N99 = Time to failure of 99 % of population. For a given distribution of TTF of target system and canary the PD can vary depending on the PD scheme selected. PD1 is the difference between the N1 of the target system and N99 of the canary. PD2 is the difference between N1 of target and N50 of canary. PD 3 is the difference between N50 of target system and N99 of canary. PD 4 is the difference between N50 of target system and N50 of canary.

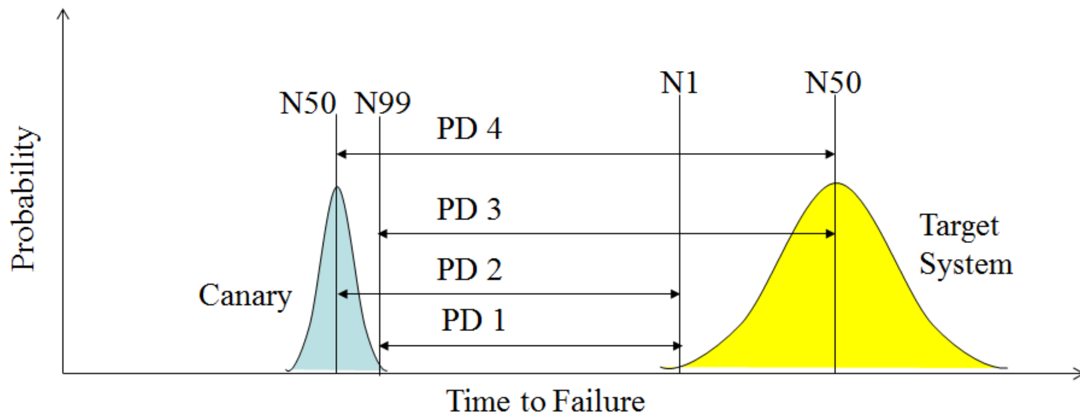

Figure 36: Multiple prognostic distances

For a given distribution of TTF of target system and canary the PD can vary depending on the PD scheme selected. The issue facing the implementation of canary based prognostics is to determine when the target system will fail under operational conditions. Here a new term is introduced in the form of the '*Product to Canary Ratio'*. The product to canary ratio (PCR) is the ratio of time to failure of product to time to failure of the canary. The PCR values are estimated at the design phase based on the estimates of the PoF models. The PoF models used to design the canary will present a TTF estimated depending on the input parameters to the model. Likewise

the PoF model applicable to the target system will generate a TTF for the target system. Equations 31 through 35 show the different PCR values based on times to failure.

$$PCR = \frac{TTF_{Product}}{TTF_{Canary}} \quad (31)$$

$$PCR_{N50:50} = \frac{N50_{Product}}{N50_{Canary}} \quad (32)$$

$$PCR_{N50:99} = \frac{N50_{Product}}{N99_{Canary}} \quad (33)$$

$$PCR_{N1:50} = \frac{N1_{Product}}{N50_{Canary}} \quad (34)$$

$$PCR_{N1:99} = \frac{N1_{Product}}{N99_{Canary}} \quad (35)$$

There are two possible scenarios that can occur in operational conditions: Case 1) the target system and canary are operated under a fixed loading condition and fixed loading range. (Example: temperature cycling condition -55°C to 125°C with 15 min dwell), and Case 2) the loading condition for the target system and canary are known but the loading range varies. (Example: System subjected to temperature cycling loading, but temperature range is not known due to lack of ability to monitor environmental loads).

Consider Case 1: The type of loading and the load range are known. The target system and canary are operated in the fixed loading condition and loading range. In this study the target system (BGA) and the canary device (resistor with reduced solder attachment area) are subjected to temperature cycling condition -55°C to 125°C

with 15 min dwell. In this case the TTF of the target system can be estimated by multiplying the relevant field TTF statistic for the canaries with the corresponding PCR value. For example if during the development process, PD4 is selected as the required prediction estimate, then the TTF of the target system can be estimated by multiplying the relevant field TTF statistic for the canary device with the corresponding PCR value (see Equation 36). Since the loading condition and range are fixed, the failure of the canary device will also serve as a validation of the PoF estimate.

$$TTF(N50)_{Target\ System} = N50_{canary} * PCR_{N50:50} \quad (36)$$

Consider Case 2: The type of loading is known but there is no information about the loading range. Assume the target system (BGA) and the canary device (resistor with reduced solder attachment area) are subjected to temperature cycling conditions but the loading range and dwell time is not known. In such a scenario the PCR statistic cannot be employed since the PCR values will be different for different loading ranges for the same loading condition. For this specific loading condition (temperature cycling) there are two different approaches to estimate the TTF of the target system.

Approach 1, assumes that the dwell time, and mean cyclic temperature in operational conditions is the same as the dwell time, and mean cyclic temperature used during the design phase to design the canary. Let ΔT_D = design condition temperature difference, and ΔT_A = actual field temperature difference. The time to failure $N_f(\Delta T_D)$ for the canary device can be estimated using the Engelmaier's model

with calibrated FP Strain equation. The $N_f(\Delta T_A)$ for the canary is obtained from the field data. As per the assumption the dwell times and mean temperature don't change, hence the effective ΔT_A can be back calculated from the probabilistic Engelmaier's equation [36] with the calibrated First Principles strain formula. Given the TTF values for the canary device, Equation 37 (probabilistic Engelmaier's model) can be used to back calculate the temperature difference.

$$Nf(x\%) = \frac{1}{2}\left(\frac{\Delta\gamma_{Calibrated\ FP\ Model}}{2\varepsilon_f}\right)^{\left(\frac{1}{c}\right)}\left(\frac{ln(1-0.01x)}{ln0.5}\right)^{\left(\frac{1}{\beta}\right)} \tag{37}$$

Where x = desired failure probability value, β = shape factor of 2-parameter weibull distribution, $\Delta\gamma$ is the cyclic plastic shear strain range, ε_f is the fatigue ductility coefficient, and c is the fatigue ductility exponent. The effective ΔT_A can be then used in the PoF model for the target system to predict its life under actual field conditions The effective acceleration factor (AF) for the canary device can be estimated as shown in equation 38.

$$AF = \frac{N_f(\Delta T_D)}{N_f(\Delta T_A)} \tag{38}$$

In *Approach 2*, no assumptions are made about the dwell time and mean cyclic temperatures. Since there are three unknown values: temperature difference (ΔT), mean cyclic temperature (T_{sj}), and dwell time (t_d) at extremes, data needs to be collected to solve for these three values. Three canary devices each with varying solder pad area, but different form each other should be designed and incorporated along with the target system in the field. The three canaries are designed to fail at different times but all fail before the target system. Under operational conditions

when all three canaries fail, the TTF information for each canary can be used to generate three equations with three unknowns. The TTF information can be substituted in the equation 39 below.

$$Nf_{Canary\,(i)} = \frac{1}{2}\left(\frac{\Delta\gamma_{Calibrated\,FP\,Model(i)}}{2\varepsilon_f}\right)^{\left(\frac{1}{c}\right)} \tag{39}$$

Solving the three equations with three unknowns, the values of the ΔT, T_{sj}, and t_d can be calculated. Using the calculated ΔT, T_{sj}, t_d values in the PoF model for the target system, its life under actual field conditions can be predicted.

7.2 Confidence in number of canary devices selected

Confidence in the prediction of life of Target will depend on η (characteristic life) and β (shape parameter) of the two distributions (TTF of canary and TTF of target) in time and the selected PD scheme. Let, β_T = Shape parameter for Target, η_T = characteristic life (scale parameter) for Target, β_C = Shape parameter for Canary and η_C = characteristic life (scale parameter) for Canary.

If the η of the distributions are close then there is a possibility that the distributions intersect, i.e. for a fixed β_C, as the η_C increases the probability that the canary will fail after the Target System increases. Figure 37 illustrates the case of increasing η. Also, if the β (shape parameter) of the distributions are small then the TTF data is spread over a larger time period and there is a possibility that the distributions will intersect, i.e. for a given η_C, as the β_C decreases the probability that the canary will fail after the Target System increases. Figure 38 illustrates the case of

decreasing β. If the two distributions intersect then there is a probability that the canary may fail after the target system. It is therefore important to find out the probability of the canary failing after the target system fails.

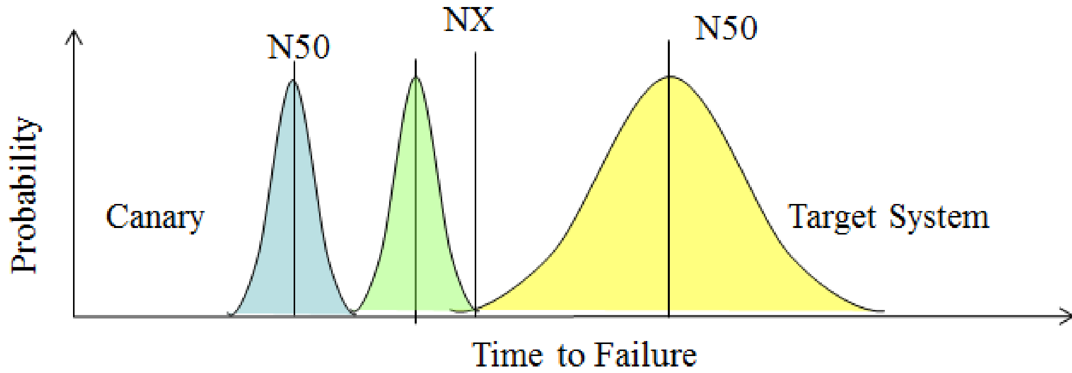

Figure 37: Effect of changing η_C

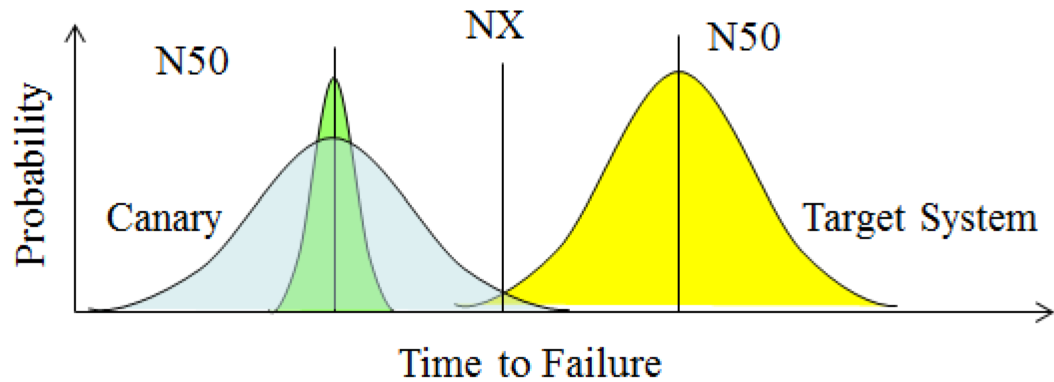

Figure 38: Effect of changing β_C

7.2.1 Procedure

To have confidence in the target system failure prediction using a given number of canaries, it is necessary to identify the probability of missing the target system failure. It is proposed that to estimate the number of canaries required for generating a prediction of TTF of the target system, an analysis of the probability of missing the failure of the target system be conducted prior to implementation of the canary

approach. The following is a procedure to generate the confidence in the number of canaries:

1. Select an acceptable threshold value for the probability of missing target system failure. *Ex. For a particular application the acceptable probability of missing target system failure is = 1 %.*

2. From the prototype validation and testing stage of the Methodology for Canary Prognostics, determine the β and η of Target System and the Canary Device.

3. Using the β and η statistic for the Canary device conduct a Monte Carlo simulation to generate multiple sets of time to failure (TTF) data for varying number of canary devices. *Ex. 20 sets of TTF data for 3, 5, 7…etc. canary devices.*

4. Calculate the probability of missing the target system failure for each set of canary TTF data for each selected number of canary devices. *Ex. Calculate probability of missing Target System failure for 1st set of TTF data for 3 canaries, 2nd set of TTF data for 3 canaries, and so on till the probability has been calculated for all data sets for each selected number of canary device.*

5. Plot the distribution of probability of miss for each selected number of canary devices. *Ex. Plot the pdf of all probability of miss for 5 canary devices.*

6. Next plot the reliability (probability) of achieving the "probability of miss" for each number of canary devices. *Ex. Generate a plot of probability on the y axis and probability of miss on the x axis for 7 canary devices.*

7. Estimate the probability that a given number of canary devices will have a probability of miss equal to the set threshold. *Ex. The probability that a 1 % target system failure will be missed if 3 canary devices are used is 10%.*
8. Plot the probability of the "Probability of Miss" versus the number of canary devices.
9. This plot will help determine the confidence in the number canary devices that is chosen to be incorporated in the target system.

7.2.2 Calculating the probability of missing target system failure

Consider two extreme cases for a given β_T and η_T: 1). if the β_C is high and η_C is much lower than $\eta_{T,}$ then the probability of miss is very low. In such a case the difference in the Probabilities from step 8 will be small for different number of canaries. In such an event implementing the least number of canaries makes sense. 2). if the β_C is low i.e. the TTF data has a wide spread and η_C is much closer to $\eta_{T,}$ then the probability of miss is very high. Here the difference in the probabilities from step 8 will be large for different number of canaries. Here more number of canaries may have to be implemented or the canary design has to be changed to reduce the probability of miss.

Consider the case of using a resistor with reduced solder attachment area as a canary for predicting the failure of a BGA (target system). Let P_M = probability of that TTF of Canary exceeds TTF of Target, P_S = probability of that TTF of Target exceeds TTF of Canary, and R_{canary} = reliability of canary device.

$$f_{Canary}(C) = pdf\ of\ TTF\ of\ Canary\ (Resistor) \quad (40)$$

$$f_{Target}(T) = pdf\ of\ TTF\ of\ Target\ (BGA) \quad (41)$$

The probability that the canary will fail before the target is estimated by solving the equation 42 shown below.

$$P_M = P\left[TTF\ of\ Canary\ \geq TTF\ of\ Target\right] =$$

$$\int_0^\infty f_{Target}(x).R_{Canary}(x)dx \quad (42)$$

$$R(t) = \int_t^\infty f(C)dC \quad (43)$$

$$\therefore P_M = \int_0^\infty f_{Target}(T).[\int_T^\infty f_{Canary}(C)dC]dT \quad (44)$$

$$P_M = 1 - P_S \quad (45)$$

$$P_S = P\left[TTF\ of\ Target \geq TTF\ of\ Canary\right] =$$

$$\int_0^\infty f_{Canary}(C).[\int_C^\infty f_{Target}(T)dT]dC \quad (46)$$

7.2.3 Example case

An example of conducting an analysis to estimate the number of canaries is presented here. The target system is a BGA with tin-lead solder interconnects. The target system is a BGA is a chip array ball grid array (CABGA) with 192 IO. The canary device is a 2512 resistor with solder pad width reduced to 20% of regular width and with tin-lead solder. Experimental data is available for the time to failure of the BGAs and resistors under temperature cycling loads of -55°C to 125°C with 15 min dwell. The threshold for the probability of missing target system failure is set at 5%. Table 17 shows the test data statistics for the BGA and resistor.

Table 17: Prior experimental data

Component	Characteristic life η (Cycles)	Shaper parameter β
Resistor (Canary)	718	3.92
192 IO BGA (Target System 1)	1606	3.875

For this analysis data was generated using the Monte Carlo data generation function in Weibull++ software. Equation 47 shows the formula to generate the data points.

$$N_{(Instance\ of\ TTF)} = \eta * \left(LN \left(\frac{1}{1-RAND()} \right) \right)^{\left(\frac{1}{\beta}\right)} \tag{47}$$

Where β = shape parameter (or slope), η = scale parameter (or characteristic life), *LN* = natural logarithm, *N* = an instance of time to failure and *RAND ()* is a random number generator function. For this analysis the inputs to the equation are the η and β values from experimental data of resistors and BGAs as shown in Table 17.

For the canary device twenty sets of 20, 15, 10, 5 and 3 data points were generated, while for the Target system only one set each of 20 data points were generated. For the canary device for each data set the N50 and N99 at 95% confidence level was calculated while for the target system, the N1 and N50 at 95% confidence level was calculated. The probability that the canary will fail before the target is estimated by solving the equation 42. Table 18 shows the probability of missing the target system failure if 20, 15, 10, 5 or 3 canaries are used to monitor the

target system. It can be see that the probability of missing the BGA failure is low irrespective of the number of canaries used (as long as canaries fail with a fixed β). The reason for that there is sufficient difference between the characteristic life (η) of the canary device and the target systems.

Table 18: Probability of missing target system failure

Data Generation Run	20 Canaries	15 Canaries	10 Canaries	5 Canaries	3 Canaries
Run 1	5.91	3.75	2.78	2.77	7.8
Run 2	7.52	6.81	4.7	4.47	4.6
Run 3	8.93	5.63	3.27	6.26	2.91
Run 4	7.79	6.54	6.19	4.35	3.6
Run 5	3.44	6.25	5.11	4.04	3.19
Run 6	4.3	4.32	3.61	5.61	4.31
Run 7	10.06	2.52	5.76	6	4.52
Run 8	7.98	3.7	4.45	3.55	5.32
Run 9	9.8	7.95	2.89	2.94	1.4
Run 10	9	5.36	7.11	7.64	2.5
Run 11	8.22	6.33	4.56	3.95	2.78
Run 12	7.16	7.29	5.38	4.22	3.9
Run 13	4.52	5.86	5.16	3.78	2.87
Run 14	4.41	4.05	6.24	6.11	4.12
Run 15	4.15	7.51	3.88	7.05	5.16
Run 16	7.22	6.24	6.11	4.68	2.99
Run 17	6.15	5.99	5.23	5.17	3.67
Run 18	4.95	5.37	5.49	3.88	4.05
Run 19	2.11	3.38	2.96	2.87	5.56
Run 20	3.45	5.11	5.76	2.66	5.28

Figure 39 shows an example of a plot of the interference of the distributions of the 20 canaries and the target system. Figure 40 shows the same plot with 5 canaries and the target system. Figure 41shows the reliability (probability) versus probability of missing target system failure, for the selected number of canaries. The probability of probability of miss ≤ set threshold (5%) versus the number of canaries selected, is plotted in this figure. Figure 42 gives the confidence in implementing the specific number canaries. It can be seen that as the number of canaries increases the probability of getting the probability of missing target system failure increases.

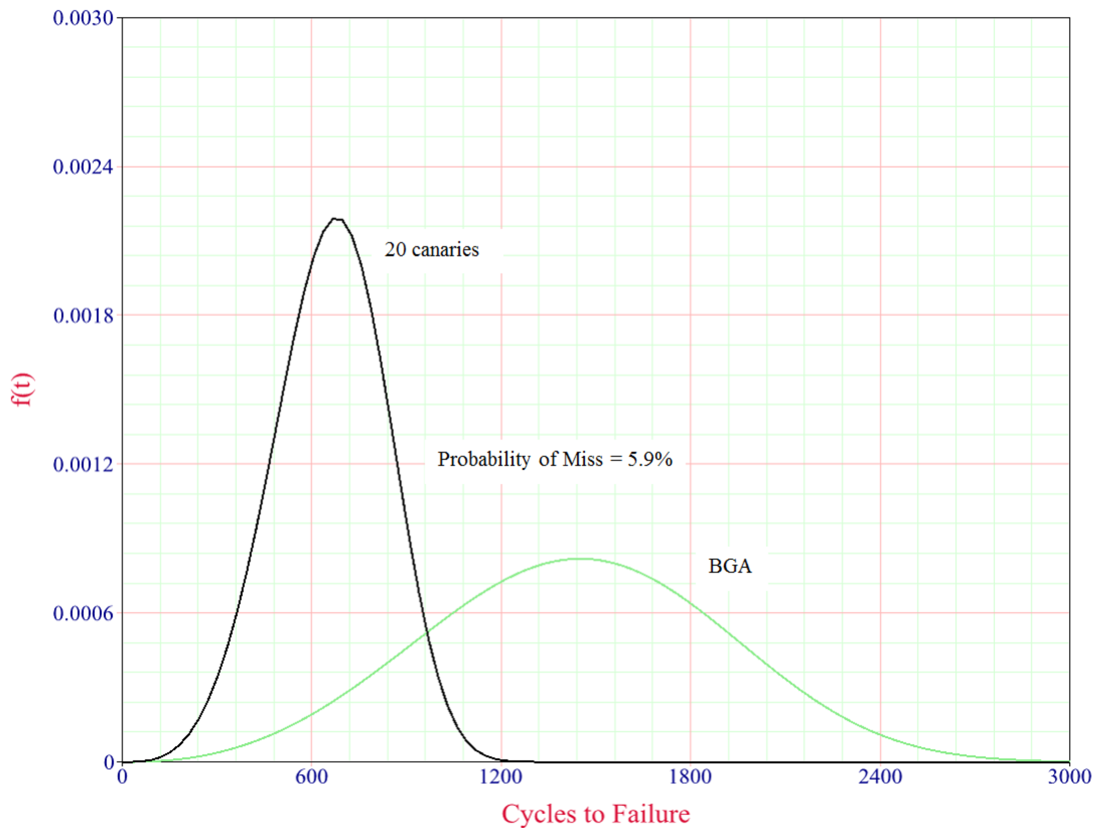

Figure 39: Twenty Canaries vs target system (Run 1)

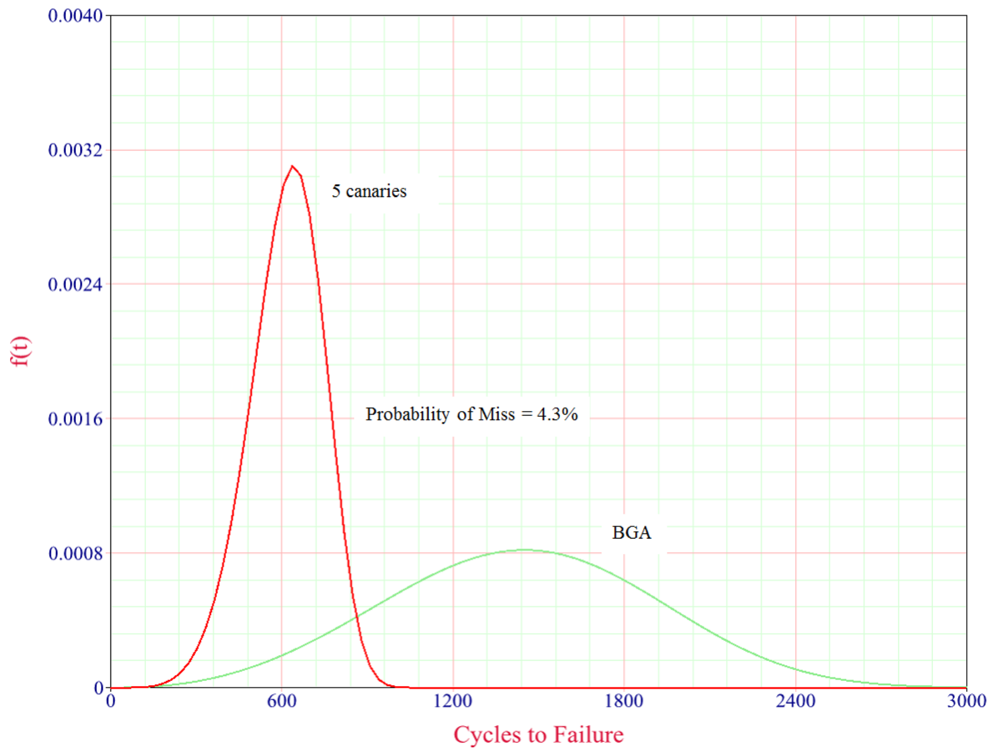

Figure 40: Five Canaries vs target system (Run 4)

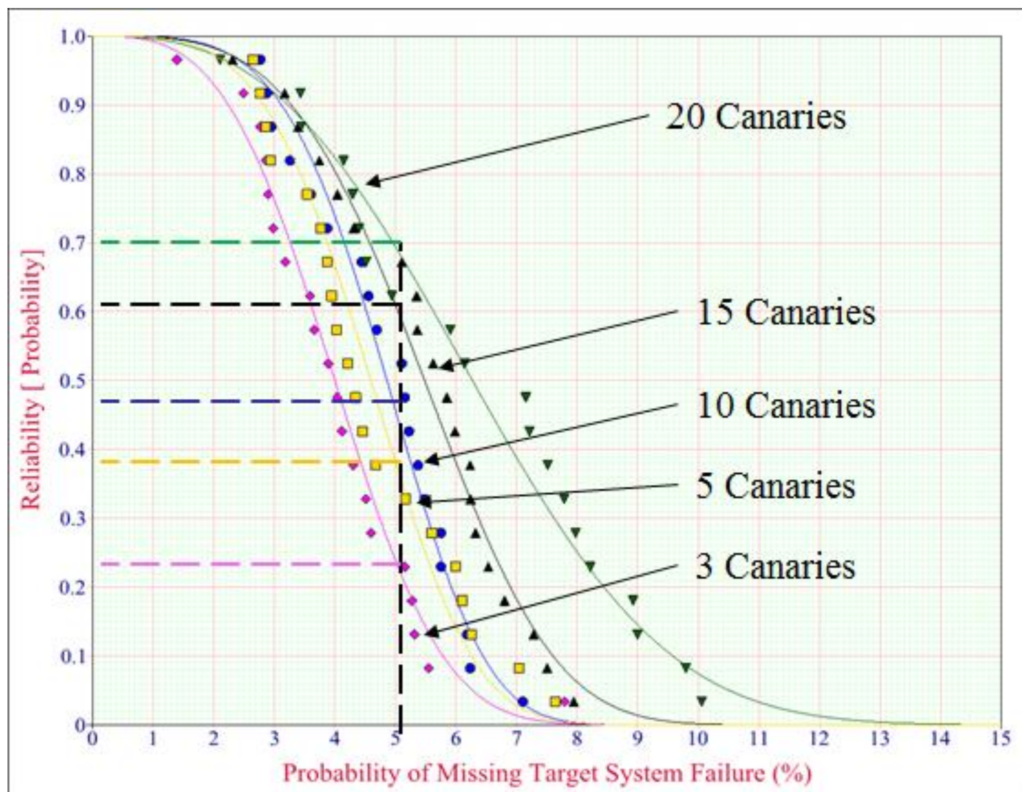

Figure 41: Probability of Probability of Miss

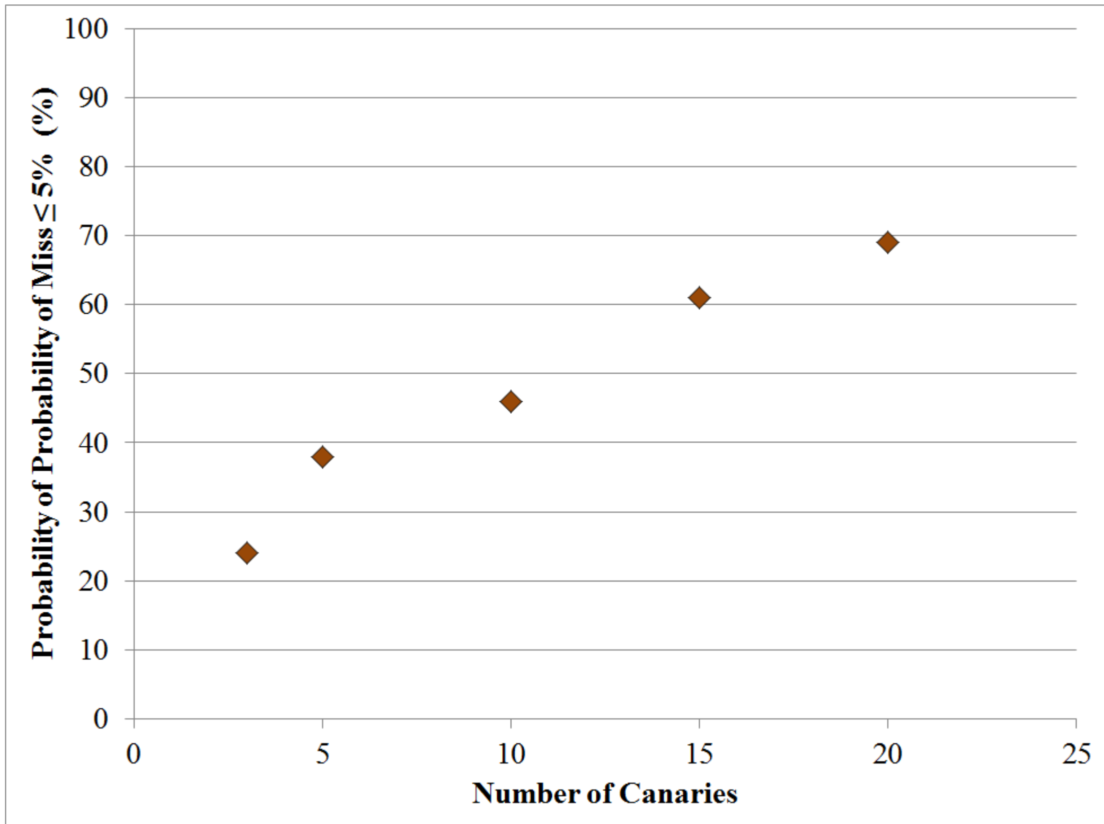

Figure 42: Number of Canaries Vs Probability of Miss

7.3 Conclusions

For a given distribution of TTF of target system and canary the prognostic distance can vary depending on the PD scheme selected. The product to canary ratio (PCR) values are estimated at the design phase based on the estimates of the PoF models. The field TTF for the target system can be estimated by multiplying the relevant field TTF statistic for the canaries with the corresponding PCR value. Approaches to predict field failure of the target system when the field conditions are not known have been explored herein

If there is only one canary device the confidence in the prognostic distance is low since the failure could be on any side of the Canary TTF distribution. As the number

of canaries increase the confidence in the prediction will increase because the TTF information is in the form of a distribution. Practically it is not feasible to have too many canaries to monitor just 1 target.

In case the distributions of the canary and the target are close, there is a probability that the TTF of the canary may exceed the TTF of the target. Monte Carlo simulations can help estimate the effect of number of canaries on the probability of missing the target failure. The number of canaries deployed will depend on the acceptable probability of missing the target failure, the required accuracy of prediction and cost of canaries.

Chapter 8: Dissertation Contributions

1. Developed, calibrated, and validated a first principles based analytical model for solder joint fatigue failure in leadless surface mount components, which accounts for solder attachment area.

2. Developed a simplified model to represent an assembly of leadless surface mount component, solder interconnect and printed circuit board as system of springs.

3. Demonstrated that for a given two termination SMT component geometry and for different thermal profiles the strain range varies with respect to the solder pad width as a power law with a fixed exponent.

4. Developed an equation to estimate area factor for leadless SMT components based on their geometric features.

5. Demonstrated the feasibility of using an external expendable device with reduced solder attachment to predict solder joint fatigue failure of Ball Grid Array (BGA) packages.

6. Developed a methodology for design, development and implementation of canary devices for prognostics.

7. Demonstrated an approach for estimating number of canary devices, and the confidence therein, to be implemented to predict failure of target system.

8. Demonstrated potential approaches to predict target system failure for varying loading ranges.

Chapter 9: Future Work

The data in this dissertation, to develop the calibrated first principles model to estimate strain range in the solder joints of a leadless SMT component, has been obtained by testing tin lead (SnPb) solder. It will be useful to generate the data for lead free solder and validate the generality of the developed model. The tasks outlined below may be conducted as part of a Master of Science thesis.

1. Conduct FEA analyses for 2515, 1210, 1206 and 0805 resistors with different pad sizes, assembled on PCB with lead free solder, and subjected to multiple temperature conditions to get the area exponents for lead free solder.
2. Substitute new exponent values in the developed Calibrated First Principles Model to estimate the strain range for the resistor assemblies with lead free solder.
3. Calculate the expected life (N50) of the resistor assemblies for different loading conditions.
4. Test resistor on PCB assemblies with lead free solder to generate test data for 2515, 1210, 106 and 0805 resistors with varying pad size.
5. Compare and validate the applicability of the developed Calibrated First Principles Model for assemblies with lead free solder.
6. Update Calibrated First Principles Model if needed to provide accurate estimates for both tin lead and lead free solder.

Appendix A: FEA – Graphs and Tables

In this appendix the graphs and tables associated with the data obtained from FEA are presented.

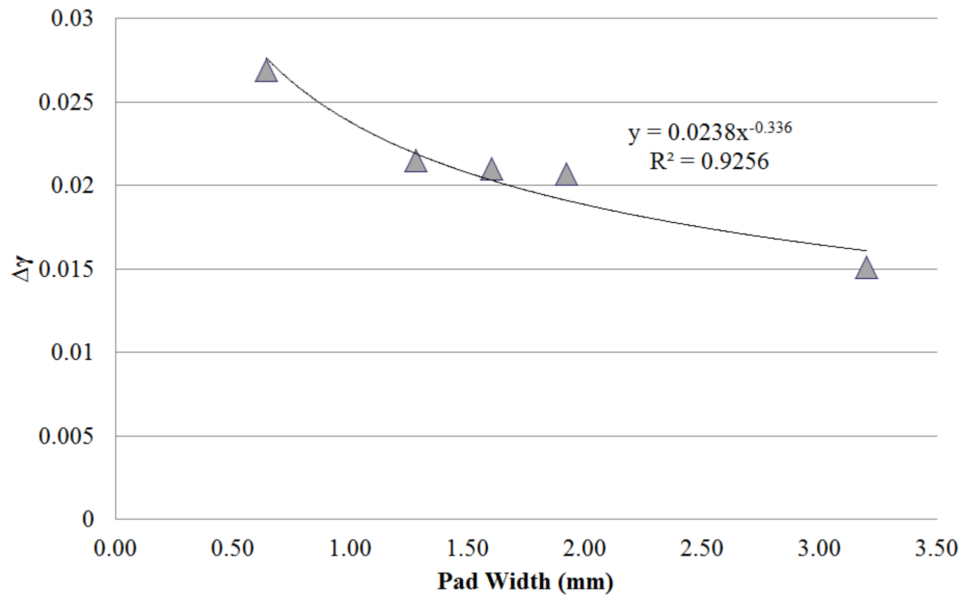

Figure 43: Δγ versus pad width for 2512 resistor (Test 2)

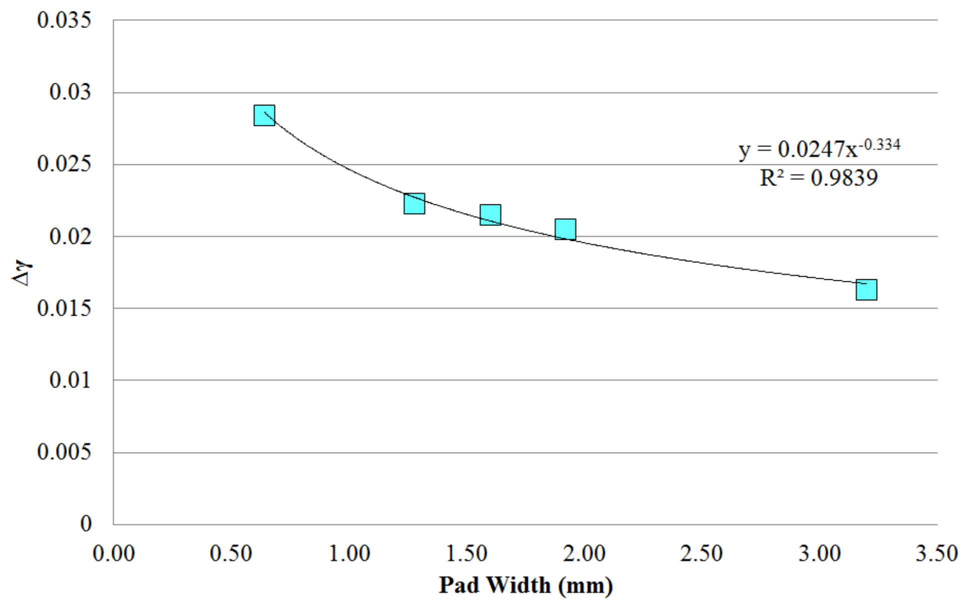

Figure 44: Δγ versus pad width for 2512 resistor (Test 3)

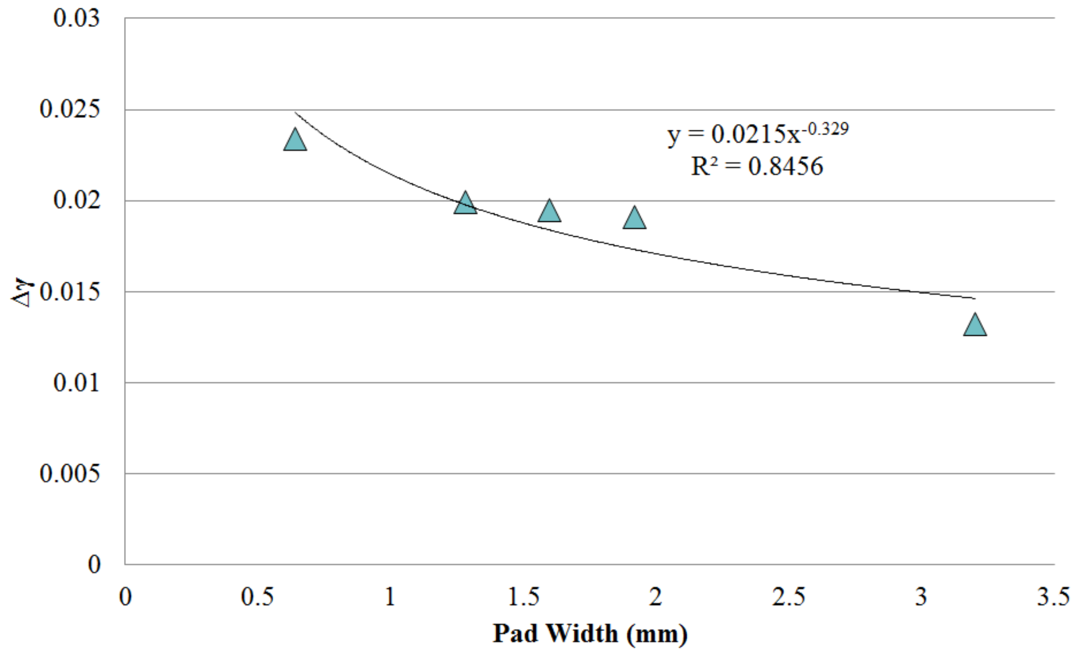

Figure 45: Δγ versus pad width for 2512 resistor (Test 4)

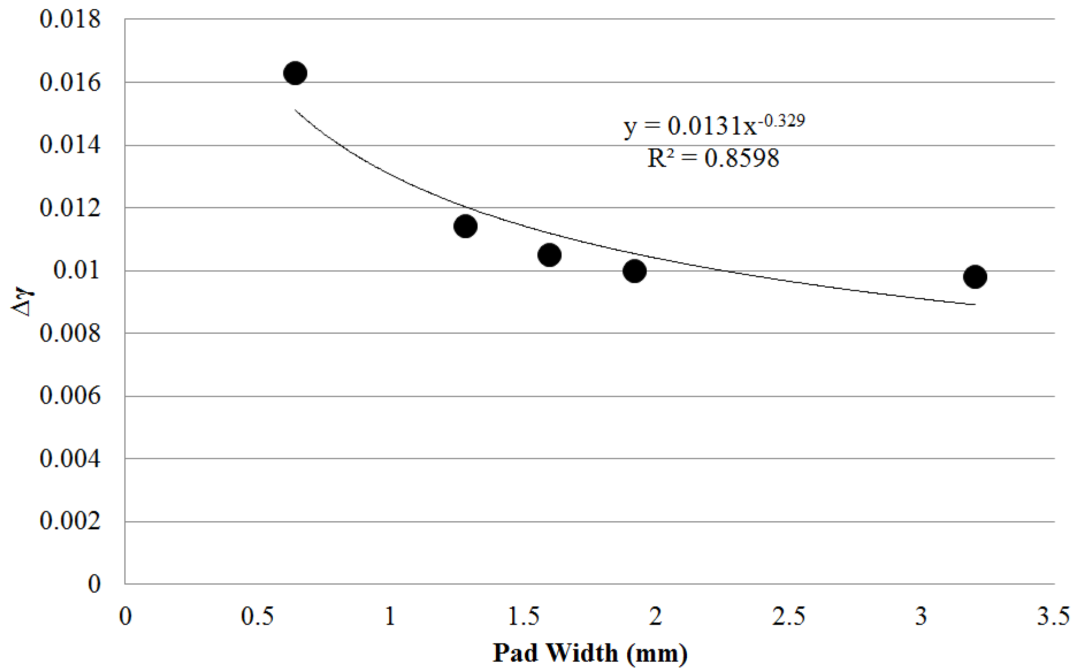

Figure 46: Δγ versus pad width for 2512 resistor (Test 5)

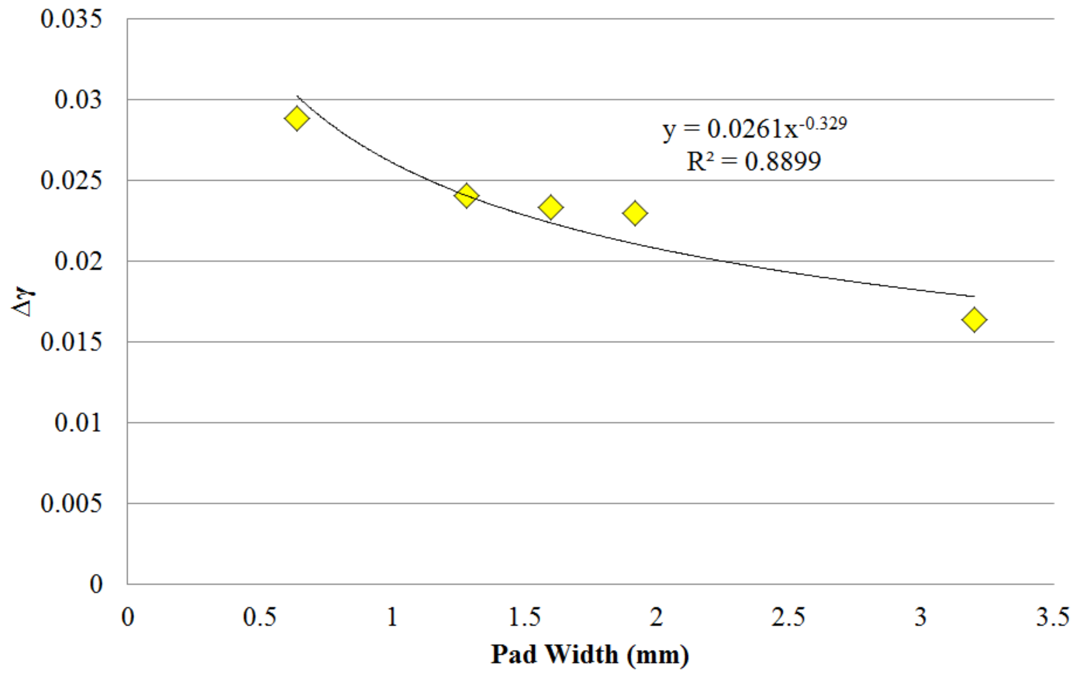

Figure 47: Δγ versus pad width for 2512 resistor (Test 6)

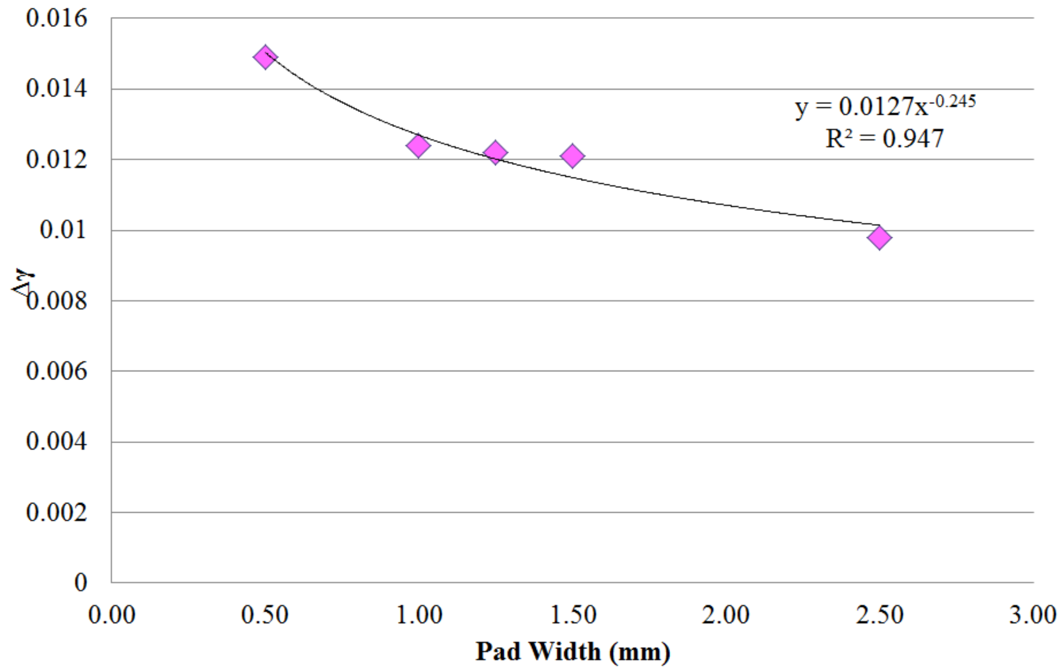

Figure 48: Δγ versus pad width for 1210 resistor (Test 2)

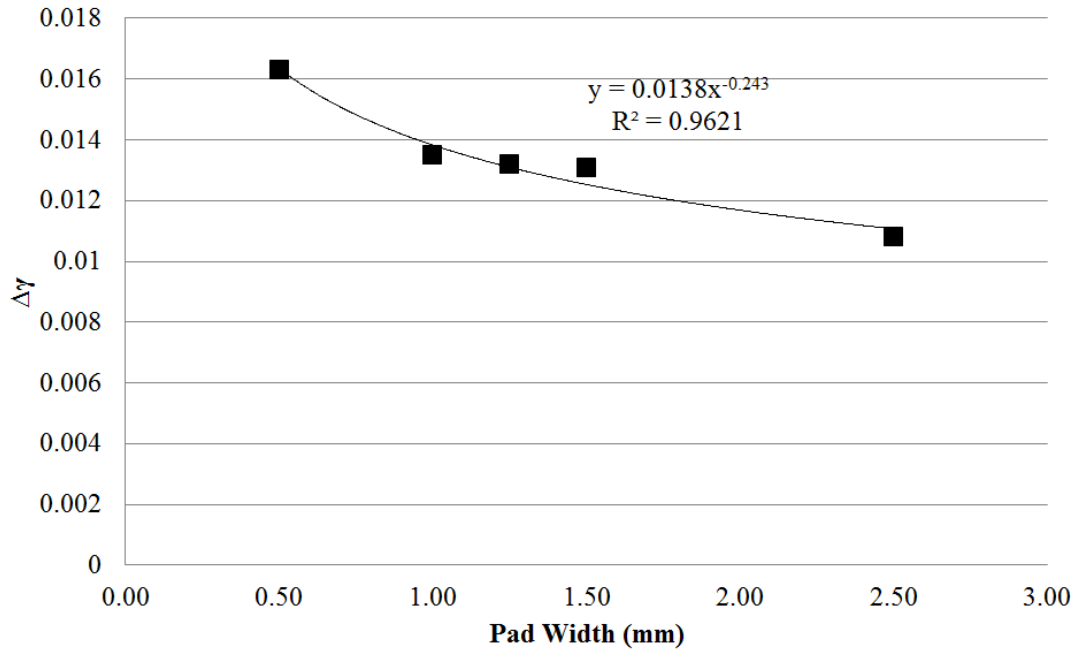

Figure 49: Δγ versus pad width for 1210 resistor (Test 3)

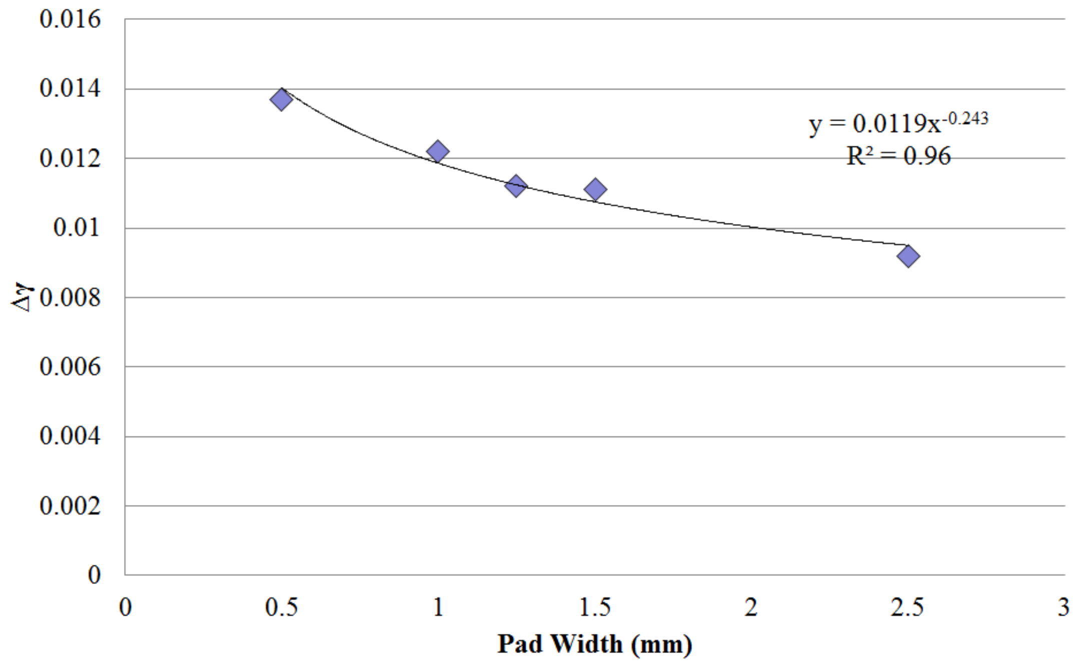

Figure 50: Δγ versus pad width for 1210 resistor (Test 5)

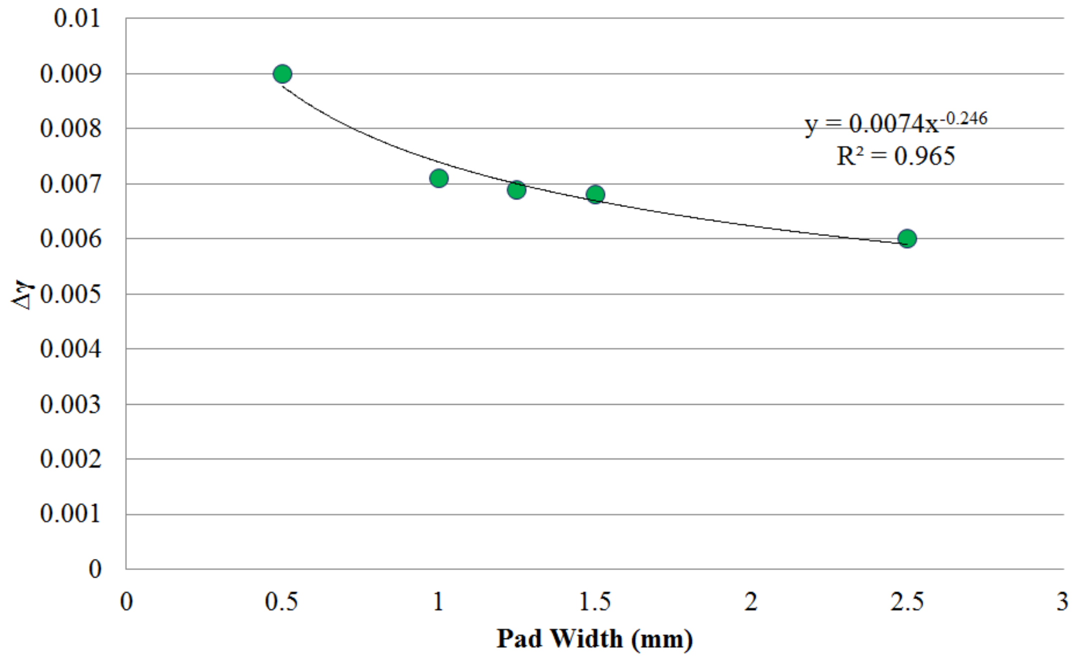

Figure 51: Δγ versus pad width for 1210 resistor (Test 4)

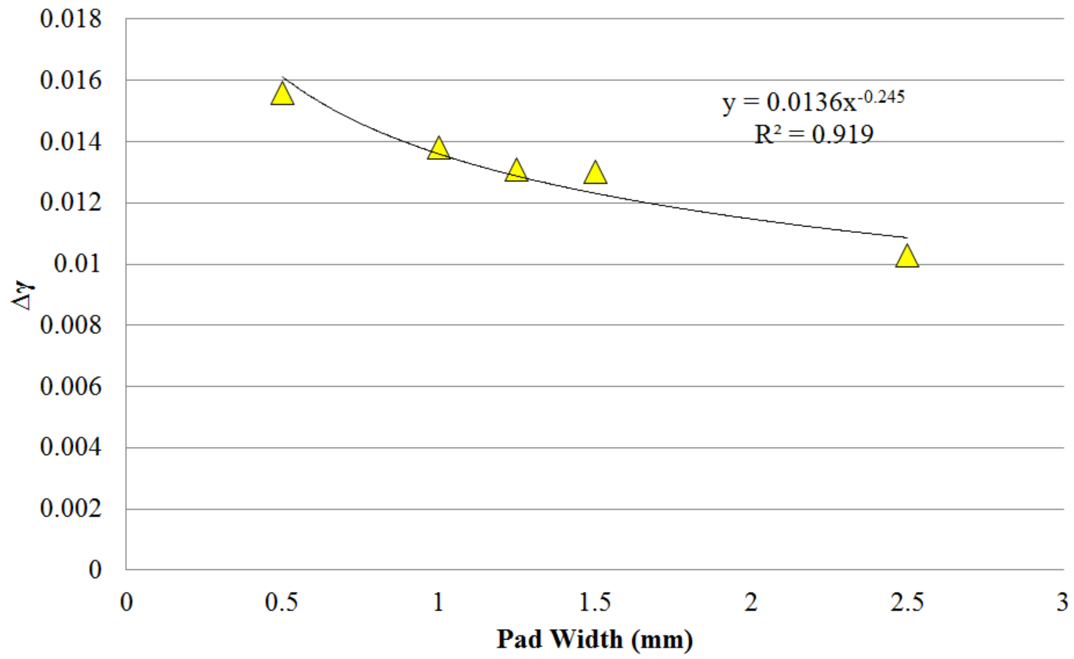

Figure 52: Δγ versus pad width for 1210 resistor (Test 6)

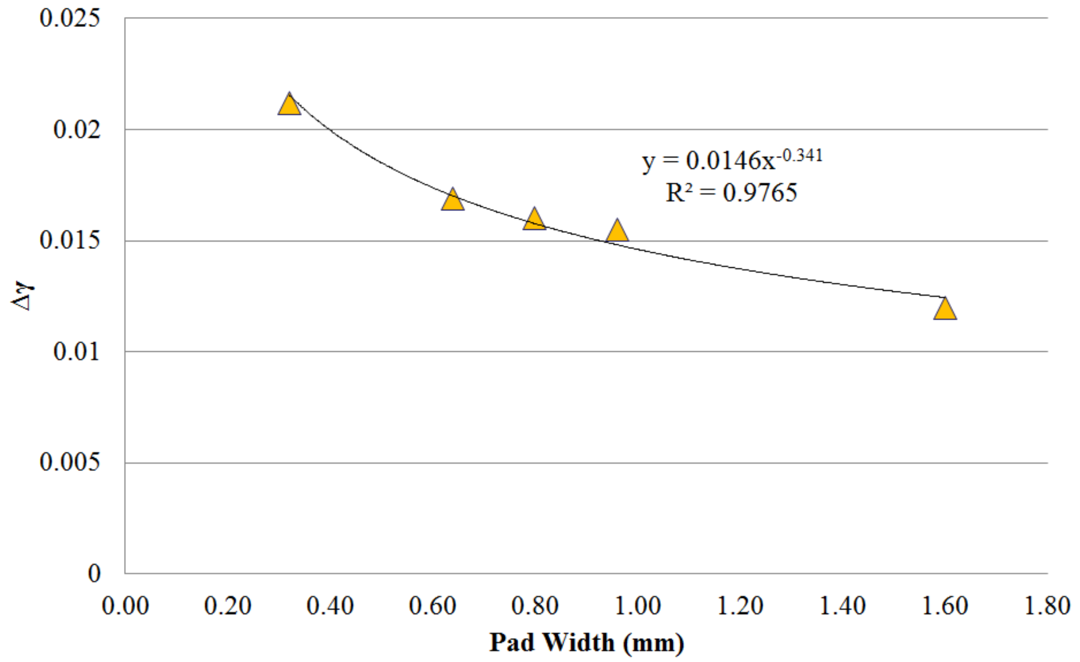

Figure 53: Δγ versus pad width for 1206 resistor (Test 2)

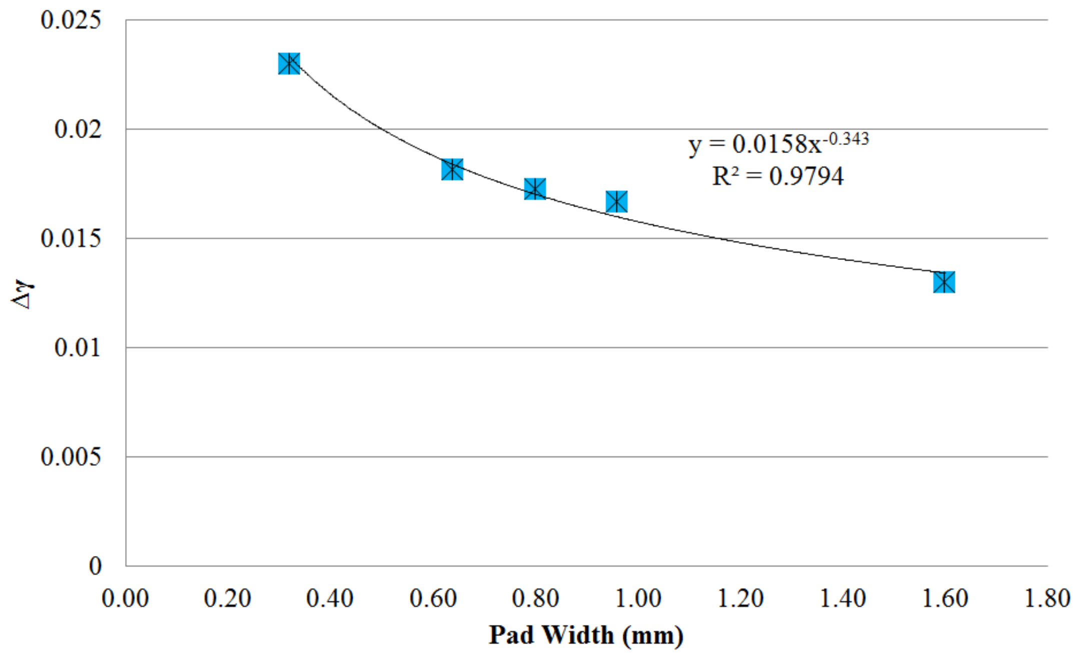

Figure 54: Δγ versus pad width for 1206 resistor (Test 3)

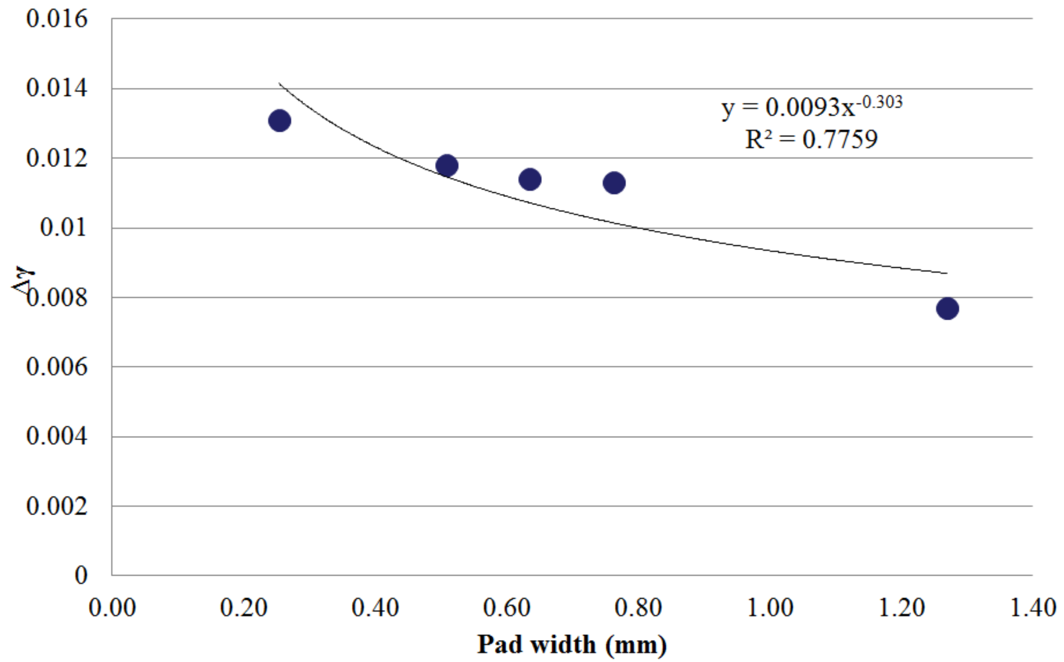

Figure 55: Δγ versus pad width for 0805 resistor (Test 2)

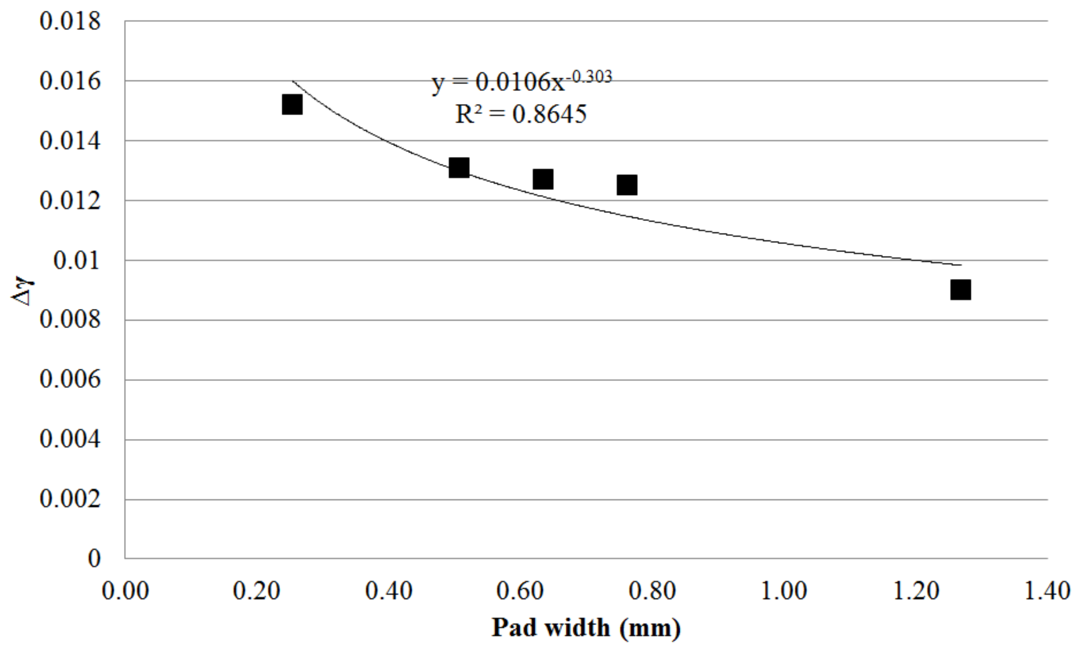

Figure 56: Δγ versus pad width for 0805 resistor (Test 3)

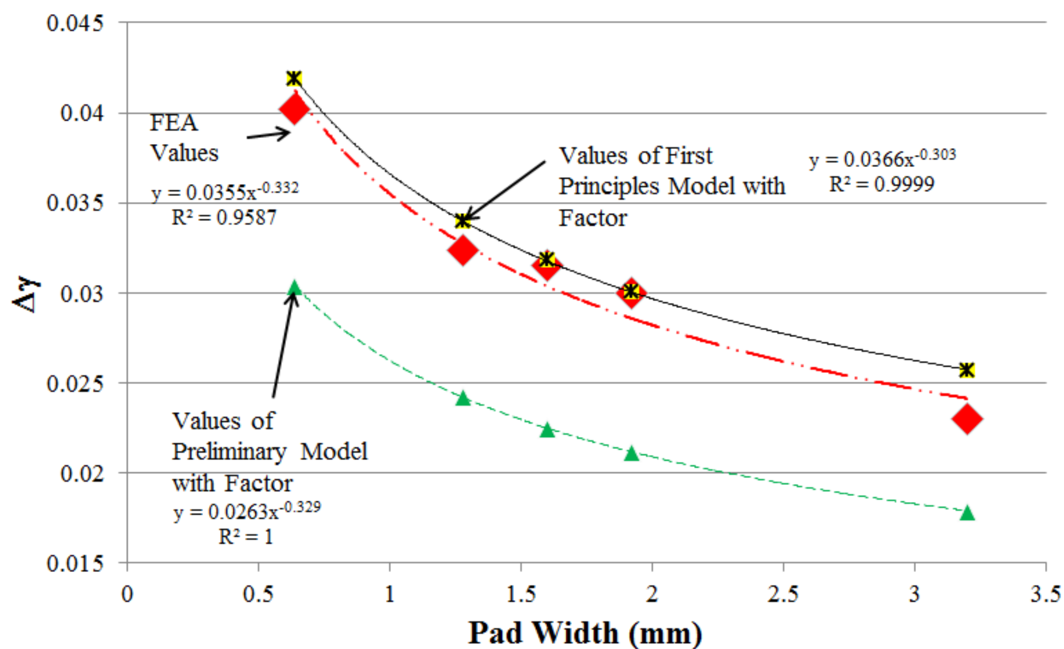

Figure 57: Comparison of strain range with calibrated models for 2512 resistor

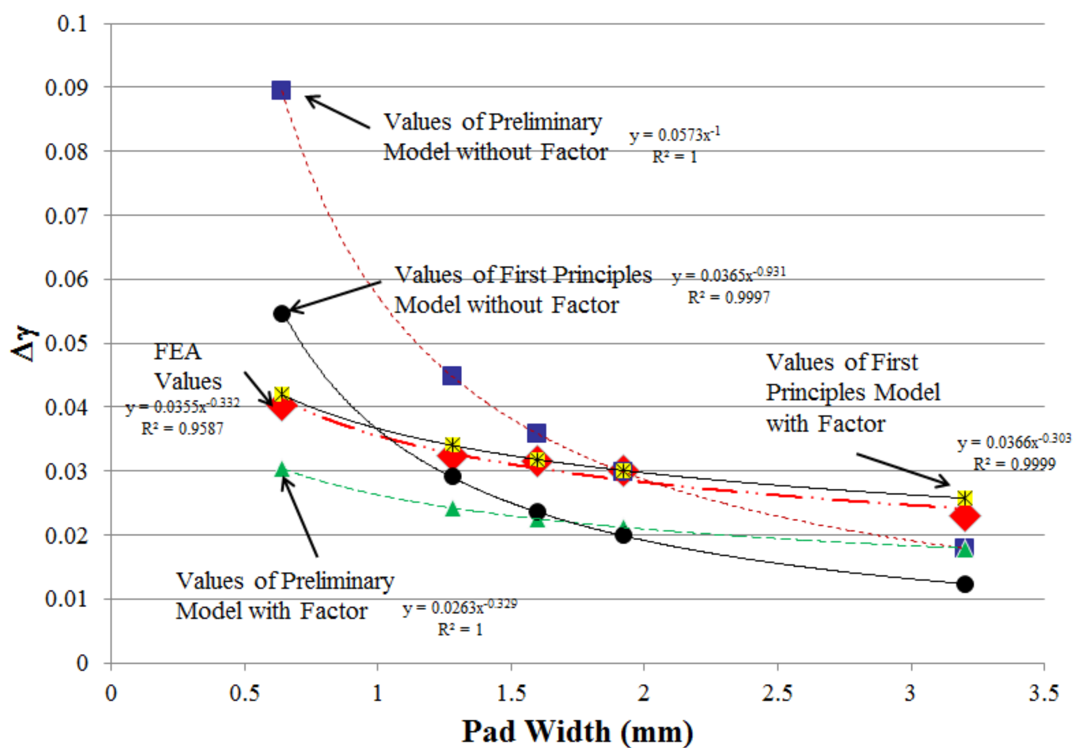

Figure 58: Strain comparisons for 2512 resistor

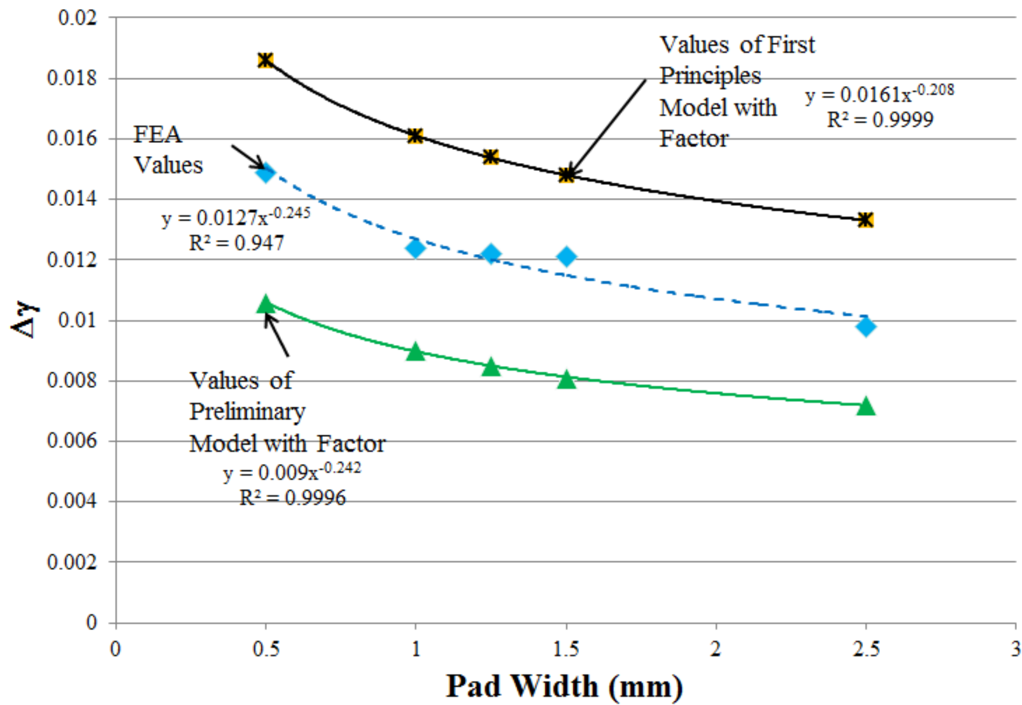

Figure 59: Comparison of strain range with calibrated models for 1206 resistor

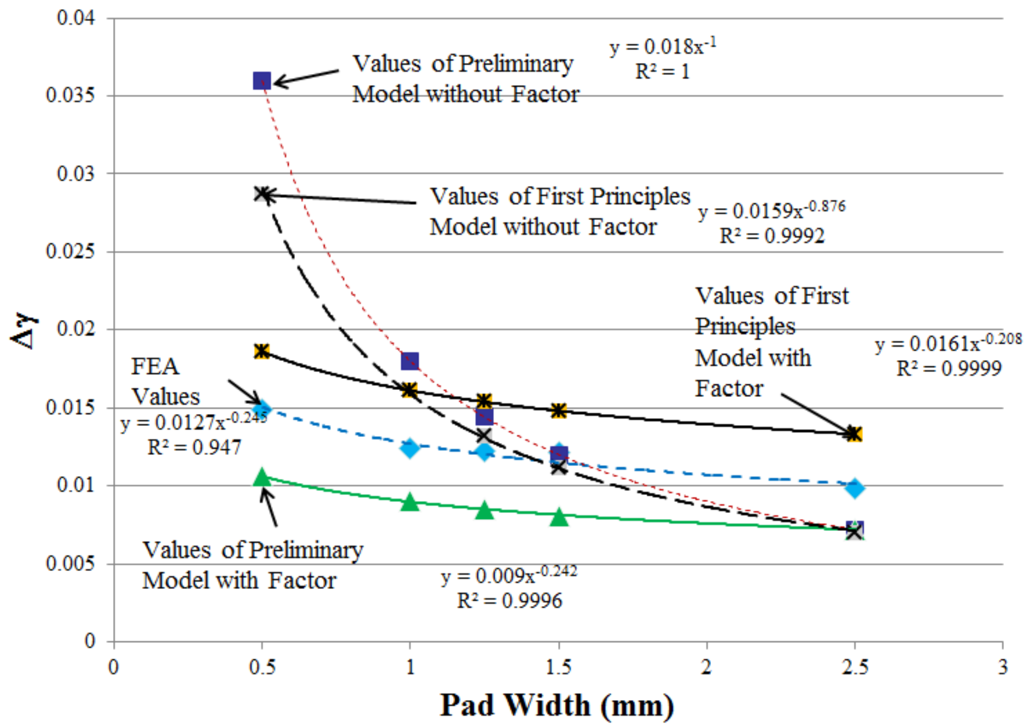

Figure 60: Strain comparisons for 1210 resistor

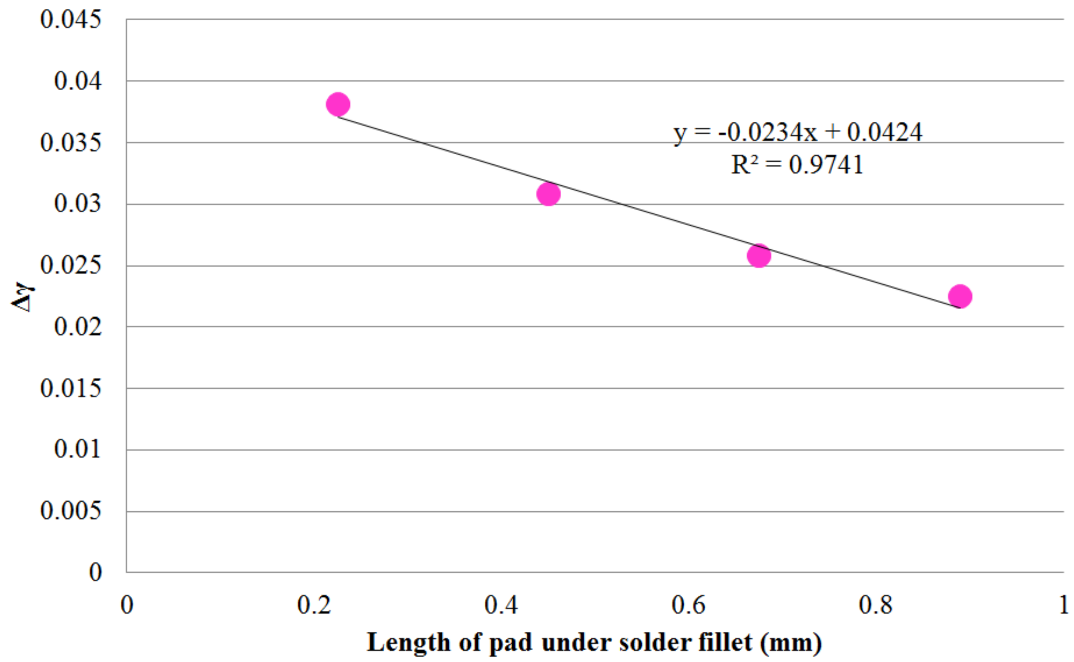

Figure 61: Strain range vs pad length under fillet for 2512 resistor

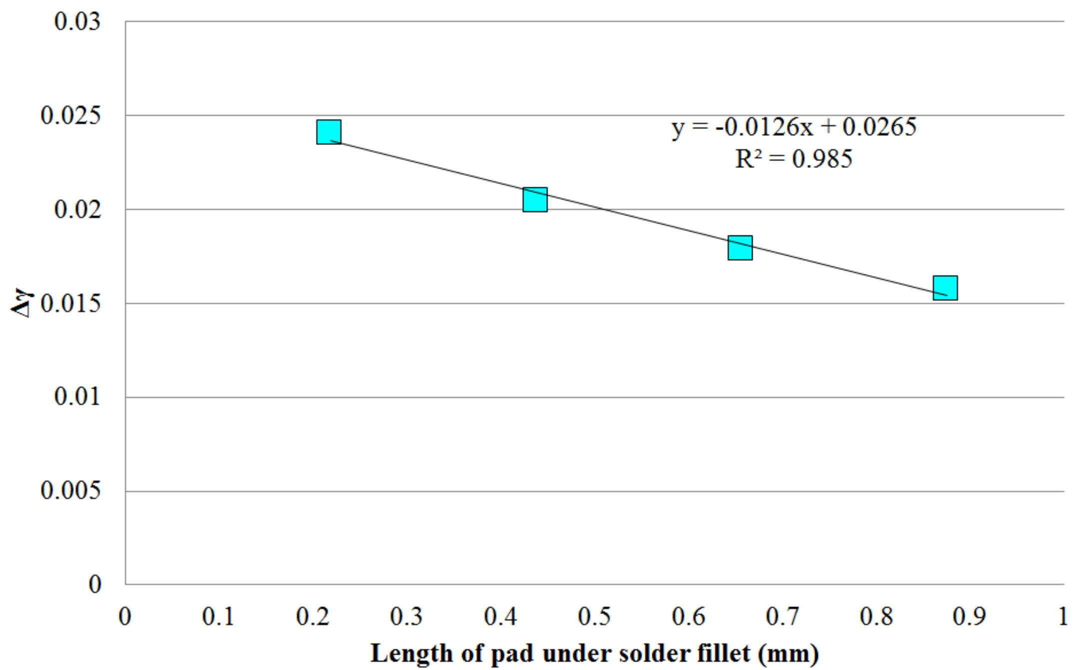

Figure 62: Strain range vs pad length under fillet for 1210 resistor

Table 19: FEA strain data for 2512 resistor

Pad Width	-55°C to 125°C (15 min dwell)	-15°C to 125°C (60 min dwell)	-40°C to 100°C (60 min dwell)	25°C to 125°C (15 min dwell)	75°C to 125°C (30 min dwell)	-5°C to -55°C (30 min dwell)
	ΔT = 180°C	ΔT = 140°C	ΔT = 140°C	ΔT = 100°C	ΔT = 50°C	ΔT = 50°C
100 %	0.023	0.0151	0.0163	0.0132	0.0164	0.0098
60 %	0.03	0.0207	0.0205	0.0191	0.023	0.01
50%	0.0315	0.021	0.0215	0.0195	0.0234	0.0105
40 %	0.0324	0.0215	0.0223	0.0199	0.0241	0.0114
20 %	0.0402	0.0269	0.0284	0.0234	0.0289	0.0163

Table 20: FEA strain data for 1210 resistor

Pad Width	-55°C to 125°C (15 min dwell)	-15°C to 125°C (60 min dwell)	-40°C to 100°C (60 min dwell)	25°C to 125°C (15 min dwell)	75°C to 125°C (30 min dwell)	-5°C to -55°C (30 min dwell)
	ΔT = 180°C	ΔT = 140°C	ΔT = 140°C	ΔT = 100°C	ΔT = 50°C	ΔT = 50°C
100 %	0.0154	0.0098	0.0108	0.0092	0.0103	0.006
60 %	0.01905	0.0121	0.0131	0.0111	0.013	0.0068
50%	0.0193	0.0122	0.0132	0.0112	0.0131	0.0069

Pad Width	-55°C to 125°C (15 min dwell)	-15°C to 125°C (60 min dwell)	-40°C to 100°C (60 min dwell)	25°C to 125°C (15 min dwell)	75°C to 125°C (30 min dwell)	-5°C to -55°C (30 min dwell)
	ΔT = 180°C	ΔT = 140°C	ΔT = 140°C	ΔT = 100°C	ΔT = 50°C	ΔT = 50°C
40 %	0.0196	0.0124	0.0135	0.0122	0.0138	0.0071
20 %	0.0233	0.0149	0.0163	0.0137	0.0156	0.009

Table 21: FEA strain data for 1206 resistor

Pad Width	-55°C to 125°C (15 min dwell)	-15°C to 125°C (60 min dwell)	-40°C to 100°C (60 min dwell)
	ΔT = 180°C	ΔT = 140°C	ΔT = 140°C
100 %	0.0185	0.012	0.013
60 %	0.0243	0.0155	0.0167
50%	0.025	0.016	0.0173
40 %	0.0262	0.0169	0.0182
20 %	0.0329	0.0212	0.023

Table 22: FEA strain data for 0805 resistor

Pad Area	-55°C to 125°C (15 min dwell)	-15°C to 125°C (60 min dwell)	-40°C to 100°C (60 min dwell)
	ΔT = 180°C	ΔT = 140°C	ΔT = 140°C
100 %	0.0129	0.0077	0.009
60 %	0.0183	0.0113	0.0125
50%	0.0186	0.0114	0.0127
40 %	0.019	0.0118	0.0131
20 %	0.0218	0.0131	0.0152

Table 23: Comparison strain estimates from FEA and Models (ΔT = 180°C)

Pad Width	2512 Resistor			1210 Resistor		
	FEA	First Principles	Preliminary Modification	FEA	First Principles	Preliminary Modification
100 %	0.023	0.0122	0.0179	0.0154	0.0090	0.0093
60 %	0.03	0.0200	0.0298	0.01905	0.0144	0.0155
50%	0.0315	0.0237	0.0358	0.0193	0.0170	0.0186
40 %	0.0324	0.0292	0.0448	0.0196	0.0207	0.0233
20 %	0.0402	0.0547	0.0895	0.0233	0.0369	0.0465

Table 24: Comparison strain estimates from FEA and Models ($\Delta T = 140^oC$)

Pad Width	2512 Resistor			1210 Resistor		
	FEA	First Principles	Preliminary Modification	FEA	First Principles	Preliminary Modification
100 %	0.0151	0.0095	0.0139	0.0098	0.0070	0.0072
60 %	0.0207	0.0155	0.0232	0.0121	0.0112	0.0120
50%	0.021	0.0185	0.0278	0.0122	0.0132	0.0144
40 %	0.0215	0.0227	0.0348	0.0124	0.0161	0.0180
20 %	0.0269	0.0425	0.0695	0.0149	0.0287	0.0360

Appendix B: External Patents on Canary Devices

- U.S. Patent No. 6,012,495: Corrosion Protection for Subsea Lines. Date of Patent: Jan 11, 2000. Assignee: Alcatel, Paris, France
  - Steel tubes are used as undersea pipe lines for a variety of applications.
  - This patent involves using a sacrificial tube made of material that will corrode at a faster rate placed over the actual steel tubes.
- U.S. Patent No. 7,089,138 B1: Canary Device for Failure Analysis: Date of Patent: Aug 8, 2006. Assignee: IBM, NY, USA
  - This patent deals with a diagnostic method to test integrated circuits during fabrication. The diagnostic system is located in the "kerf area" on the silicon wafer.
  - The system has one IC with a known electrical signature, one other intentional mis-designed IC circuit and a comparator to compare the signatures of both the circuits.
  - If the signals from first circuit matches that of the intentional mis-designed circuit then it is determined that the actual IC is mis-designed.
- U.S. Patent No. 8,018,271 B2: Semiconductor Integrated Circuit. Date of Patent: Sept 13, 2011. Assignee: Panasonic Corp., Osaka, Japan
  - This patent deals with a semiconductor IC design so as to control the voltage applied to the IC.

- The described technique uses multiple flip-flops in a delay circuit formation.
- By comparing the delay times, the control circuit can determine whether to raise, hold or lower the voltage.

- U.S. Patent No. 8,111,577 B2: System Comprising a State-Monitoring Memory Element. Date of Patent: Feb 7, 2012. Assignee: Cypress Semiconductor Corp., San Jose, CA, USA
  - This patent involves using a state-monitoring memory element with a reduced ability to retain the logic state compared to a normal memory element.
  - Loss of state of the state-monitoring element indicates that the IC state retention is in jeopardy.
  - Corrective actions can be taken by a voltage control unit.
- U.S Patent No. 8,030, 943 B2: Circuit for Detection of Solder-Joint Failures in Digital Electronic Package. Date: Oct 4, 2011, Assignee: Ridgetop Group Inc., Tucson, AZ, USA
  - This patent involves identification of solder joint failure in ball grid array packages.
  - The technique described needs a internally connected I/O buffer on the silicon die in the package and solder connection inside the package and between the package and printed circuit board.

- This involves a built-in-test and logic unit in the silicon die, and an external capacitor is connected to the BGA.
- The BIT unit is programed to apply a time varying voltage through the solder joints to charge the capacitor.
- By monitoring the voltage in the capacitor an estimate of the solder joint degradation is made as a measure of the resistance of the solder joint.

Bibliography

1. M. Pecht, Prognostics and Health Management of Electronics, Wiley-Interscience, New York, NY, August 2008.

2. Mathew, S., Das, D., Osterman, M., Pecht, M., and Ferebee, R., "Prognostics assessment of aluminum support structure on a printed circuit board", ASME Journal of Electronic Packaging, Vol. 128, No. 4, pp. 339-345, December 2006.

3. Dasgupta, A., Doraiswami, R., Azarian, M., Osterman, M., Mathew , S., and Pecht, M., "The Use of Canaries for Adaptive Health Management of Electronic Systems", ADAPTIVE 2010, IARIA Conference, Lisbon Portugal, Nov 21-26, 2010.

4. Chauhan, P., Mathew, S., Osterman, M., and Pecht, M., "In-situ interconnect failure prediction using canaries," IEEE Transactions On Device and Materials Reliability, Vol. 14, No. 3, pp 826-832, September 2014.

5. Chauhan, P., Osterman, M., and Pecht, M., "Canary Approach for Monitoring BGA Interconnect Reliability under Temperature Cycling", The Machinery Failure Prevention Technology (MFPT) 2012 Proceedings, 24-26 April, 2012.

6. Lee, W. W., Nguyen, L. T., and Selvaduray, G. S., "Solder joint fatigue models: Review and applicability to chip scale packages," Microelectronics Reliability, Vol. 40, No. 2, pp. 231–244, Feb. 2000.

7. Manson, S.S., Thermal Stress and Low Cycle Fatigue, McGraw-Hill, New York, NY, 1966.

8. Engelmaier, W., “Fatigue life of leadless chip carrier solder joints during power cycling,” IEEE Transactions on Components, Hybrids, and Manufacturing Technology, Vol. CHMT-6, No. 3, pp. 232–237, 1983.

9. Engelmaier, W., “The use environments of electronic assemblies and their Impact on surface mount solder attachment reliability,” IEEE Transactions on Components, Hybrids, and Manufacturing Technology, Vol. 13, No. 4, pp. 903–908, Dec. 1990.

10. Timoshenko, S., “Bending and Buckling of Bimetallic Strips”, J. Optical Soc. of America, Vol. 11, p.233, 1925.

11. Steinberg, D.S., Cooling Techniques for Electronic Equipment, Wiley-Interscience, New York, NY 1991.

12. IPC Association Connecting Electronics Industries, Standard 610, Acceptability of Electronic Assemblies: IPC –A-610- Revision E-2010, Northbrook, IL, April 2010.

13. IPC Association Connecting Electronics Industries, Standard 9701: “Performance Test Methods and Qualification Requirements for Surface Mount Solder Attachments,” Northbrook, IL, January 2002.

14. Rosunally, Y. Z., Stoyanov, S., Bailey, C., Mason, P., Campbell, S., Monger, G., and Bell, I., “Fusion Approach for Prognostics Framework of Heritage Structure”, IEEE Transactions on Reliability, Vol. 60, No. 1, pp: 3 - 13, 2011.

15. Han, D. K., Pecht, M. G., Anand, D. K., and Kavetsky, R., "Energetic Material/Systems Prognostics," 53rd Annual Reliability & Maintainability Symposium (RAMS), 2007.

16. Shea, H.R, Gasparyan, A., Chan, H.B., Arney, S., Frahm, R.E., López D., Jin, S., and McConnell R.P., "Effects of Electrical Leakage Currents on MEMS Reliability and Performance", IEEE Transactions on Device and Materials Reliability, Vol. 4, No. 2, June 2004.

17. Otsuka, Y., Sato, T., Yoshiki, T., and Hayashida, T., "Multicore energy reduction utilizing canary FF", IEEE 2010 International Symposium on Communications and Information Technologies (ISCIT), Tokyo, pp: 922 - 927, 26-29, Oct. 2010.

18. Calhoun, B.H. and Chandrakasan, A., "Standby Power Reduction Using Dynamic Voltage Scaling and Canary Flip-Flop Structures," IEEE J. Solid State Circuits, Vol. 39, No. 9, Sept. 2004

19. Wang J., Hoefler A., and Calhoun B.H., "An Enhanced Canary-Based System With BIST for Standby Power Reduction", IEEE Transactions on Very Large Scale Integration (VLSI) Systems, Vol.19, No. 5, 2011.

20. Ridgetop Group Inc., Ridgetop Products, www.ridgetopgroup.com/products, Accessed Feb 22, 2011.

21. Goodman D., Vermeire B., Ralston-Good J., and Graves R., "A Board-Level Prognostic Monitor for MOSFET TDDB," IEEE Aerospace Conference, March 2006.

22. Keese, C. R.; Giaever, I., "A Biosensor that Monitors Cell Morphology with Electrical Field", IEEE Eng. Med. Biol. Vol.13, pp: 402–408, 1994.

23. Petrovick, M.S., Harper, J. D., Nargi, F. E., Schwoebel, E.D., Hennessy, M.C., Rider, T. H., and Hollis M.A., "Rapid Sensors for Biological-Agent Identification", Lincoln Laboratory Journal, Special Issue: Chemical and Biological Defense, Vol. 17, No. 1, pp: 63- 84, 2007.

24. Lall, P., Islam,N., Rahim,K., Suhling,J., and Gale, S., "Leading Indicators-of-Failure for Prognosis of Electronic and MEMS Packaging", Proceedings of 54th Electronic Components & Technology Conference 2004., pp. 1570-1578, Las Vegas, NV, Jun 1-4, 2004.

25. Lall, P., Islam, M. N., and Suhling, J. C., "Damage Mechanics of Electronics on Metal-Backed Substrates in Harsh Environments", IEEE Transactions on Components and Packaging Technologies., Vol. 29, No. 1, pp. 204-212, March, 2006.

26. Lall, P., Hande. M., Bhat, C., Islam, N., Suhling, J., and Lee, J., "Feature Extraction and Damage-Precursors for Prognostication of Lead-Free Electronics", Proceedings of 56th Electronic Components & Technology Conference 2006., pp. 718-727, San Diego, CA, May 30 - Jun 2, 2006.

27. Lall, P., Islam, M. N., Rahim, K., and Suhling, J. C., "Prognostics and Health Management of Electronic Packaging", IEEE Transactions on Components and Packaging Technologies, Vol. 29, No.3 pp. 666-677, September, 2006.

28. Lall, P., Hande, M., Bhat, C., Islam, M., Suhling, J., and Lee, J., “Feature Extraction and Damage-Precursors for Prognostication of Lead-Free Electronics”, Microelectronics Reliability, Vol. 47, pp. 1907-1920, April, 2007.

29. Lall, M., Hande, M., Bhat, C., Suhling, J., and Lee, J., “Prognostics Health Monitoring (PHM) for Prior-Damage Assessment in Electronics Equipment under Thermo-Mechanical Loads”, Proceedings of 57th Electronic Components & Technology Conference 2007., pp. 1097-1111, Reno, NV, May 29 - Jun 1, 2007.

30. Lall, P., Hande, M., Bhat, C., More, V., Vaidya, R., and Suhling, J., “Algorithms For Prognostication Of Prior Damage And Residual Life In Lead-Free Electronics Subjected To Thermo-Mechanical Loads”, Proceedings of ITHERM 2008., pp. 638-651, Orlando, FL, May 28-31, 2008.

31. Lall, P., Bhat, C., Hande, M., More, V., Vaidya, R., Pandher, R., Suhling, J., and Goebel, K., “Interrogation of System State for Damage Assessment in Lead-free Electronics”, Proceedings of 58th Electronic Components & Technology Conference 2008., pp. 918-929, Orlando, FL, May 27-30, 2008.

32. Lall P., Vaidya R., More V., Goebel K., and Suhling J., “PHM-Based Residual Life Computation of Electronics Subjected to a Combination of Multiple Cyclic-Thermal Environments”, Proceedings of ITHERM 2010., Las Vegas, NV, June 2-5, 2010.

33. Lall, P., Bhat, C., Hande, M., More, V., Vaidya, R., and Goebel, K., “Prognostication of Residual Life and Latent Damage Assessment in Lead-Free

Electronics Under Thermo-mechanical Loads”, IEEE Transactions On Industrial Electronics, Vol. 58, No. 7, July 2011.

34. Ganesan, S., Eveloy, V., Das, D., and Pecht, M. “Identification and utilization of failure mechanisms to enhance FMEA and FMECA”. Proceedings of the IEEE Workshop on Accelerated Stress Testing & Reliability (ASTR), Austin, Texas, October 2–5, 2005.

35. Mathew, S., Alam, M., and Pecht, M., “Identification of Failure Mechanisms to Enhance Prognostics Outcomes”, ASM Journal of Failure Analysis and Prevention, Vol. 12, No. 1, pp: 66-73, 2012.

36. IPC Association Connecting Electronics Industries, IPC-D-279, “Design Guidelines for Reliable Surface Mount Technology Printed board Assemblies”, Northbrook, IL, July 1996.